CHARACTERIZATION OF DYNAMIC THERMAL CONTROL SCHEMES AND

HEAT TRANSFER PATHWAYS FOR INCORPORATING VARIABLE

EMISSIVITY ELECTROCHROMIC MATERIALS INTO A SPACE SUIT HEAT

REJECTION SYSTEM

by

CHRISTOPHER JAMES MASSINA

B.S., University of Northern Iowa, 2009

B.S., Iowa State University, 2009

M.S., University of Colorado, 2012

A thesis submitted to the

Faculty of the Graduate School of the

University of Colorado in partial fulfillment

of the requirement for the degree of

Doctor of Philosophy

Department of Aerospace Engineering Sciences

2016

This thesis entitled:

Characterization of Dynamic Thermal Control Schemes and Heat Transfer Pathways for

Incorporating Variable Emissivity Electrochromic Materials into a Space Suit Heat Rejection

System

written by Christopher James Massina

has been approved for the Department of Aerospace Engineering Sciences

_____

David M. Klaus, Ph.D.

_____

James A. Nabity, Ph.D.

Date_____

The final copy of this thesis has been examined by the signatories, and we

Find that both the content and the form meet acceptable presentation standards

Of scholarly work in the above mentioned discipline.

Massina, Christopher James (Ph.D., Aerospace Engineering Sciences)

Characterization of Dynamic Thermal Control Schemes and Heat Transfer

Pathways for Incorporating Variable Emissivity Electrochromic Materials into a

Space Suit Heat Rejection System

Thesis directed by Professor David M. Klaus

The feasibility of conducting long duration human spaceflight missions is largely dependent on the provision of consumables such as oxygen, water, and food. In addition to meeting crew metabolic needs, water sublimation has long served as the primary heat rejection mechanism in space suits during extravehicular activity (EVA). During a single eight hour EVA, approximately 3.6 kg (8 lbm) of water is lost from the current suit. Reducing the amount of expended water during EVA is a long standing goal of space suit life support systems designers; but to date, no alternate thermal control mechanism has demonstrated the ability to completely eliminate the loss. One proposed concept is to convert the majority of a space suit's surface area into a radiator such that the local environment can be used as a radiative thermal sink for rejecting heat without mass loss. Due to natural variations in both internal (metabolic) loads and external (environmental) sink temperatures, radiative transport must be actively modulated in order to maintain an acceptable thermal balance. Here, variable emissivity electrochromic devices are examined as the primary mechanism for enabling variable heat rejection. This dissertation focuses on theoretical and empirical evaluations performed to determine the feasibility of using a full suit, variable emissivity radiator architecture for space suit thermal control. Operational envelopes are described that show where a given environment and/or metabolic load combination may or may not be supported by the evaluated thermal architecture. Key integration considerations and guidelines include determining allowable thermal environments, defining skin-to-radiator heat transfer properties, and evaluating required electrochromic performance properties. Analysis also considered the impacts of dynamic environmental changes and the architecture's extensibility to EVA on the Martian surface. At the conclusion of this work, the full suit, variable emissivity radiator architecture is considered to be at a technology readiness level of 3/4, indicating that analytical proof-of-concept and component level validation in a laboratory environment have been completed. While this is not a numeric increase from previous investigations, these contributions are a significant iteration within those levels. These results improve the understanding of the capabilities provided by the full suit, variable emissivity architecture.

This thesis is dedicated to my Mom and Dad, for always encouraging me to do more

Also to my Wife and Boys, for providing their unwavering support

ACKNOWLEDGEMENTS

CONTENTS

FIGURES

TABLES

NOMENCLATURE

Acronyms

BHS	body heat storage
EMU	extravehicular mobility unit
EVA	extravehicular activity (spacewalks)
HIDH	Human Integration Design Handbook
HST	Hubble Space Telescope
IR	infrared
LST	local solar time
MLI	multi-layer insulation
NASA	National Aeronautics and Space Administration
NIAC	NASA Institute for Advanced Concepts
PCM	phase change material
PLSS	portable [primary] life support system
TCS	thermal control system
TRL	technology readiness level

Symbols

A area, m^2

c_p specific heat, $kJ/(kg \cdot K)]$

D diameter, m

d disturbance matrix

F view factor

f function designation

H height, m

h convection heat transfer coefficient, W/m^2K

IR total incident infrared heat flux, W/m^2

Ls solar longitude

m mass, kg

$\dot{m}$ mass flow rate, kg/sec

Nu   Nusselt number

Pr   Prandtl number

Q heat, J

ΔQ change in heat from nominal, $W \cdot hr$

q heat rate, W

q'' heat flux, W/m^2

R	Resistance (thermal), K/W
	Resistance (electrical), ohm
Ra	Rayleigh number
Re	Reynolds number
S	total incident solar flux, W/m^2
T	temperature, K $(°F)$
t	time, sec
thk	thickness, m
u	input matrix
V	voltage, V
VF	view factor
x	state matrix
	distance between nodes (thermal model)
$\dot{x}$	state matrix derivative

Greek Characters

α	Absorptivity (absorptance), fraction solar spectrum energy absorbed
β	solar incidence angle, ° (deg)
ϵ	Emissivity (emittance), fraction infrared spectrum energy absorbed or emitted
λ	wavelength

σ Stefan-Boltzmann constant, $5.67 \times 10^{-8}\,\text{W/m}^2\,\text{K}^4$

Subscripts

1m	atmospheric properties at 1 meter
b	blood
basal	basal metabolic rate
c	core
high	high limit
HRL	heat recovery layer
i	i'th pixel position, heat source designator, or thermal compartment designation (initial sunlit or shaded)
IR	infrared spectrum energy
j	j'th element, thermal node within compartment identifier (core, muscle/fat, skin)
k	Parametric iteration designator
lim	limit
low	low limit
m,f	muscle/fat
MR	metabolic rate
net	net heat rejection net emissivity

rad	radiator
shroud	cold shroud property (temperature)
sink	environmental sink temperature
skin	skin property (generally in reference to temperature)
sol	solar
stored	stored energy
suit	space suit surface property
sup	supplemental (non-radiative)
surface	surface property (temperature)
thk	thickness property (cross-sectional area)

CHAPTER 1

Research Motivation and Objectives

1.1. Motivation

Extravehicular activity (EVA) will continue to play a pivotal role in mission design and operations as humans continue to explore our solar system. To enable these EVAs, a space suit is donned to "support human life and enable functionality" of the astronaut while working in an otherwise inhospitable environment (Klaus et al., 2006). The thermal control subsystem provides one of the most important functions of the space suit and is responsible for maintaining the astronaut's thermal balance such that physical and mental performance is not impaired (Buckey, 2006).

Traditionally, ice water sublimation has served as the primary heat sink in space suit thermal control (Larson and Pranke, 1999; Harris, 2001). Although the sublimator system has performed well since the early days of EVA, several drawbacks exist for its continued use in future missions. Alternative EVA thermal control architectures that reduce or eliminate vented water also decrease the potential for contamination of scientific instruments and the local exploration environment (Hedgeland et al., 1994; Conley and Rummel, 2008; Nabity et al., 2009). Motivated by the desire to reduce the consumable burden of EVA, this work evaluates a novel thermal control system capable of achieving this goal in Lunar and Martian environments.

1.2. Overview of Objectives

This dissertation investigated an innovative means of providing thermal control in EVA space suits. The evaluated concept converts the majority of a suit's surface area into a radiator that allows the local environment to serve as the primary heat sink. Variable infrared (IR) emissivity[1] electrochromic devices were included on radiator surfaces and provide the active variable heat rejection mechanism required to maintain equilibrium during dynamic metabolic and external environment thermal loading. Analytical modeling and concept verification testing were used to generate first-order integration guidelines for the use of the full surface, variable emissivity radiator architecture.

The primary objectives of this research were as follows:

1. Analytically characterize the steady-state performance envelope and contamination impacts for utilizing flexible radiators in the lunar surface environment

2. Analytically assess the impact of emissivity modulation on sink (equilibrium) temperature

3. Provide a first-order electrochromic pixel resolution metric based on analysis and testing for thermal control in a lunar environment

---

[1] In the literature *emissivity* and *emittance* are often used interchangeably. Throughout this dissertation the term *infrared emissivity* is used to describe the broadband infrared spectrum (wavelengths $\geq 5\mu m$) emissive potential of the devices. Unless otherwise noted, *emissivity* in this context is synonymous with the material's *emittance*, or the integrated broadband IR emissive state.

4. Assess transient impacts of flexible/electrochromic radiator performance on human thermal comfort in a dynamic environment

5. Evaluate integration extensibility potential for Martian surface EVA

1.3. Dissertation Overview

Chapter 2 provides additional introductory and background information necessary to evaluate the EVA thermal control problem. Chapter 3 addresses research objectives 1 and 2, and focuses on concept evaluation using a flat plate approximation. Chapter 4 addresses research objective 3, and focuses on key considerations for establishing a pixilated radiator surface in a lunar environment. Chapter 5 includes the results of an empirical and analytical evaluation that provide proof-of-concept for the pixilation considerations established in Chapter 4. Chapter 6 addresses research objective 4, and provides a first-order analysis of allowable thermal transient characteristics for the architecture's integration in a lunar environment. Chapter 7 addresses objective 5, and provides an evaluation of the architecture's extensibility to EVA on the Martian surface. Finally, chapter 8 summarizes this work, discusses the larger impact of this dissertation, and outlines recommendations for future investigation.

CHAPTER 2

Investigation Rationale and Background

2.1. Introduction

As humans continue further into space, emphasis on extravehicular activity (EVA) will remain a central part of exploration (Chappell et al., 2010). To accommodate the demands presented by diverse exploration destinations such as Mars, the Moon and Near Earth Asteroids; the next generation of EVA systems must become more robust than their contemporary counterparts (Olson et al., 2011). The development of innovative EVA technologies and strategies that enable scientific discovery and exploration of the solar system is imperative to the success of future missions (Obama, 2010; Peck et al., 2012).

The development of new space suit systems and their components will focus on technologies that maximize crew health and safety (Gernhardt et al., 2009). These technologies will include those that provide the necessary thermal conditions for suited astronauts, while also reducing the loss of thermal control water (Hurlbert et al., 2012).

The thermal control system (TCS) of both modern and historic space suits utilized ice water sublimation to vacuum as their primary heat sink (Larson and Pranke, 1999; Harris, 2001; Young, 2009). However, similar systems that rely on ventilation processes result in an undesirable cumulative loss of a consumable and introduce the potential to contaminate scientific instruments or the local exploration environment (Hedgeland et al., 1994; Race et al., 2003; Nabity et al.,

2009). Several methods may be adopted to reduce or eliminate the water mass expended during EVA; among the most intriguing are those that fully utilize the external environment as a component of the thermal control system. Converting the majority of the suit's surface area into a functional radiator allows the external environment to serve as the primary heat sink for the TCS without introducing a mass consumable loss.

2.1.1. Problem Statement

Before man stepped foot on the moon in 1969, it was recognized that an extravehicular space suit capable achieving closed-loop life support functions would be advantageous for future missions. Among the earliest of these investigations was a 1965 study commissioned by the Air Force that investigated suit requirements for passive [radiative] thermal control in low earth orbit (LEO) (Richardson, 1965). Since this time, researchers have continued to examine a multitude of potential mechanisms for reducing consumable losses and achieving closed-loop EVA thermal control in a variety of destination environments.[2] Within these investigations the fundamental goal of EVA thermal control has remained constant. Energy generated within the suit or deposited by the external environment must be stored or expelled via some means in order to maintain thermal equilibrium of the suited astronaut.

---

[2] The list of examples is extensive. The following is a subset of investigations into closed-loop EVA thermal control over the years: Ephrath, 1971; Williams et al., 1972; Kuznetz, 1990; Crawford et al., 2000; Harris, 2001; Mays et al., 2001; Pitts et al., 2001; Hodgson, 2001; Hodgson et al., 2004; Trevino et al., 2004; Izenson et al., 2005; Ochoa et al., 2006; Nabity et al., 2007; Sompayrac et al., 2009; Izenson et al., 2011; Metts et al., 2011; Metts & Klaus; 2012; Bue et al., 2013.

Despite these investigations, to date, no technology for closed-loop EVA thermal control has been fully integrated into a space suit and tested outside of earth based laboratories. As such, NASA has maintained the goal of achieving closed-loop EVA heat rejection with zero consumable usage. By advancing enabling technologies to the point in which a TRL-6 [Technology Readiness Level] component ground demo can occur by 2020 (Hurlbert et al., 2012).

The complexity of the dynamic internal and external environments experienced during EVA dictates the availability of variable heat rejection to actively maintain the astronaut's thermal equilibrium. Variable heat rejection systems also have applications to vehicle level integration where they are expected to provide a reduction in system mass and complexity in a variety of mission profiles (Hill et al., 2012). While the investigations completed in this dissertation consider only EVA conditions, results provide additional fodder for consideration at the vehicle level.

The overarching goal of this research was to investigate a novel technology and techniques for achieving closed-loop thermal control in EVA space suits. This was realized by demonstrating through analytical modeling that astronaut thermal equilibrium can be maintained in complex EVA environments when incorporating flexible radiators and variable emissivity electrochromic devices into the space suit's TCS. Coupon level testing provided partial proof-of-concept validation of key concepts that resulted from analytical modeling.

2.1.2. History of the Investigated Concept

The Chameleon Suit concept was developed by Edward Hodgson and a team at then Hamilton Sundstrand Space Systems International over Phase I and Phase II NIAC [NASA Institute for Advanced Concepts] contracts completed in 2001 and 2004 respectively. The Chameleon Suit proposed the development of several emerging technologies that together facilitated the integration of the EVA crew member and their environment for nearly all required suit functions.

The Chameleon Suit's TCS strove to selectively couple the crew member to the external environment through active control of the suit garment's properties. The TCS concept primarily leveraged controllable layering, capable of varying conduction from the skin surface to the outer surface [radiator] of the suit. Variable IR emissivity electrochromics were included within the insulation layup to further regulate radiation heat transfer **between** layers but were not used directly to modulate the interaction with the external environment. The outermost layer of the chameleon suit's layup included MEMS (micro-electro-mechanical system) louvers over a flexible radiator with static properties to further expand the operational environment by shielding unfavorable thermal fluxes (Hodgson et al., 2004).

A derivative of the Chameleon Suit's full surface radiator concept that incorporated electrochromic devices on radiator's surface was shown to be a viable TCS candidate through several analyses (Metts and Klaus, 2009; Metts and Klaus, 2011; Metts et al., 2011; Metts and Klaus, 2012). The full suit, electrochromic radiator scheme was envisioned to occur through one of three integration concepts.

The first concept had the same basic layup as the Extravehicular Mobility Unit (EMU – gas pressure suit with metabolic loads removed via a liquid-cooling and ventilation garment) and included a secondary fluid loop or heat spreader capable of directing some portion of the internal heat load to the radiator's surface, external to all multi-layer insulation (MLI). The second concept replaced traditional MLI with a thermally transparent restraint to micrometeoroid protection layer where heat loads were allowed to transfer directly from the skin to the suit surface. The third concept utilized the mechanical counter pressure suit concept, currently under development in MIT's Man Vehicle Laboratory under the supervision of Prof. Dava Newman, who is currently on leave as NASA's Deputy Administrator (Pitts et al., 2001), where the suit walls supply the pressure required for human physiology and also function as a radiator (Metts & Klaus., 2009).

Analysis on the full suit, electrochromic radiator concept showed that the architecture could have significantly reduced water lost via sublimation (Metts et al., 2011). Using metabolic profiles from the Apollo lunar missions, analysis showed that the architecture could have reduced sublimated water losses by 69.0%, or 68.5kg, across the entire program (Metts & Klaus, 2012). At the conclusion of the Metts' work (Metts, 2010), the full-suit/electrochromic radiator thermal control architecture was said to be at a TRL-3/4 as described by Mankins (1995), indicating that analytical proof-of-concept and preliminary component laboratory testing had been completed.

2.2. Background

2.2.1. EVA Thermal Control

This section provides an overview of the considerations that influence the development and implementation of an EVA thermal control system. First, the fundamental thermal balance for a shirt-sleeve and a suited human is introduced. Second, the function of contemporary space suit thermal control systems is described. Third, an overview of the drawbacks associated with the current implementation is provided.

The human thermal balance is a function of many variables. Fundamentally, heat is generated within the body and is rejected to the environment via several different processes. The overall human thermal balance in a terrestrial shirt-sleeve environment is represented by Fig. 2.1; its analytic counterpart is found in Eq. 2.1 (Ephrath, 1971; Havenith, 1999). A body heat storage (BHS) term is included as the difference in heat inputs and outputs. True thermal neutrality occurs when BHS is zero, indicating that all generated and incident heat loads are dissipated in some way. Throughout the calculations of this dissertation, the difference between metabolic load and external work (physical movements) are considered as the provided net metabolic rate that must be rejected by the suit's thermal control system.
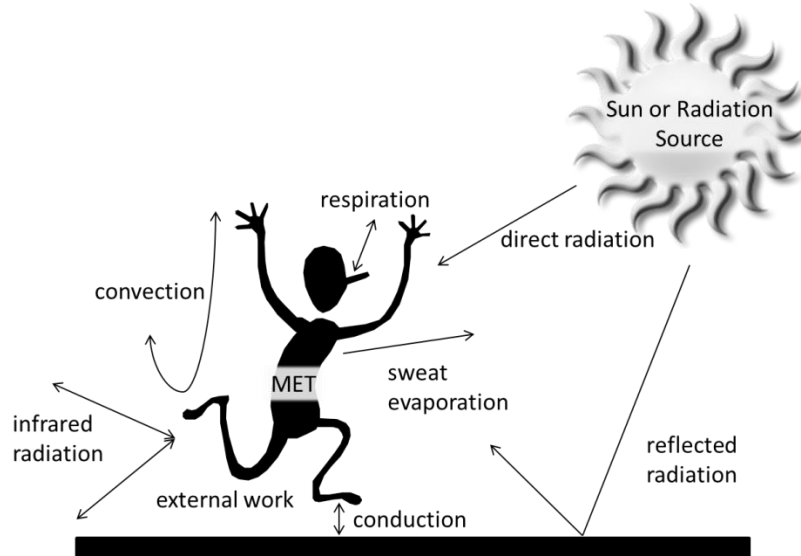
Figure 2.1. Human thermal balance in a shirt-sleeve environment (adapted from Havenith, 1999)

$$Body\ Heat\ Storage = (Metabolic\ Load - External\ Work) - (Conduction +$$

$$Radiation + Convection + Evaporation + Respiration) \qquad (2.1)$$

When a suit is donned to protect an astronaut from the extremes of the EVA environment, all of the heat fluxes in Fig. 2.1 can still be encountered either inside or outside of the suit. Assuming the suit's exterior surfaces serve as the analysis boundary condition, the overall space suit thermal balance is found in Fig. 2.2 and is governed by Eq. 2.2. Depending on the environment under evaluation, the heat transfer mechanisms depicted may not be included in the balance. For example, external convection will not occur in vacuum environments but is significant on the Martian surface (Crawford et al., 2000). Space suits may also be designed to utilize conduction to surfaces (planetary or otherwise) as a means of heat dissipation

10

(Kuznetz, 1990; Harris, 2001). A *supplemental* heat rejection load was also included

to account for heat dissipation from mechanism(s) not already explicitly considered

(e.g. sublimator, evaporator, and phase change materials). However, throughout

this dissertation radiation was considered the primary mechanism of suit thermal

control unless otherwise noted. The inability for the radiator architecture to provide

a balancing heat rejection rate corresponds to a change in the total energy stored by

the system, and ultimately an undesirable change in the astronaut's thermal

condition.
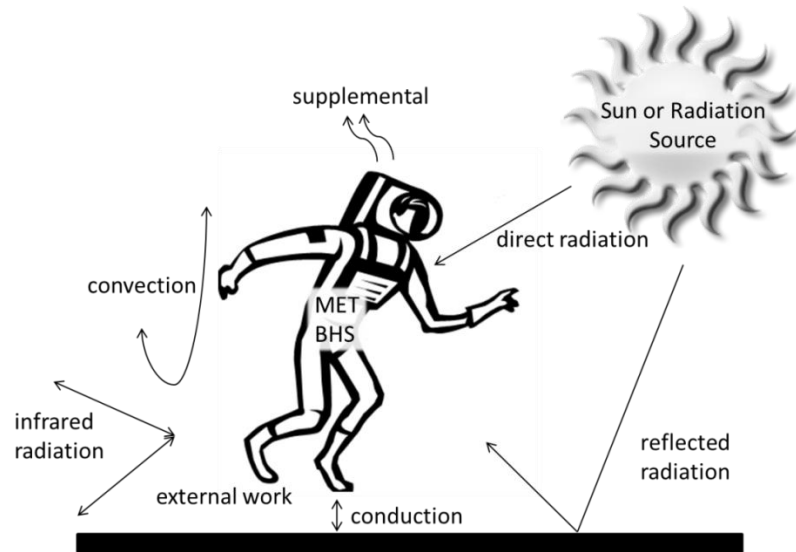
Figure 2.2. Thermal balance in a suited environment

$$Environmental\ Loads + Internal\ Loads = Radiated\ Energy + Convection +$$

$$Conduction + Supplemental\ Cooling + Body\ Heat\ Storage \qquad (2.2)$$

Depending on the local environment and properties of the space suit's

surfaces, some inherent heat leak into or out of the system may also occur (Mays et

al., 2001; Sompayrac et al., 2009). Uncontrolled heat leak has the potential to significantly impact the ability to maintain the astronaut's thermal balance. For example, the lunar surface temperature can increase from ~110K at dawn to up to ~390K at lunar noon (Heiken et al., 1991). Many of the hot cases are considered unsuitable for EVA [No-Go cases] due to the resulting excessively high sink temperatures.

The current philosophy of space suit TCS construction is to isolate the astronaut from the local environment and release heat from a single location. To do this, several layers of multi-layer insulation (MLI) are used in the suit's garment construction to thermally decouple the human and their surroundings (Larson and Pranke, 1999; Harris, 2001; Farrington et al., 2005; Young, 2009). Heat loads generated by astronauts are confined to the suit and collected by a liquid-cooling and ventilation garment (LCVG). Human generated loads are then combined with the remaining space suit loads (e.g. avionics) and directed to a porous plate ice water sublimator located in the portable [primary] life support system (PLSS) backpack. The sublimator then acts as the suit's primary heat sink, and provides the active cooling mechanism needed to maintain the thermal balance of the astronaut and suit system (Larson and Pranke, 1999).

The following discussion provides a more complete description of the current system and its function. The sublimator has been the primary means of EVA heat rejection since astronauts were disconnected from their vehicles during the Apollo program (Harris, 2001; Young, 2009). In the sublimator apparatus, feed water is

forced between two metal plates, one of which is porous and exposed to the vacuum of space. The water evaporates through the pores, resulting in a plate temperature drop to the freezing point of water that causes the remaining water to freeze before escaping. The frozen mass then acts as the heat sink to the solid plate that receives loads directly from the suit's cooling circuit and transfers the heat loads to space via sublimation [solid to vapor phase transition] (Harris, 2001). The Russian's Orlan space suit also utilizes a similar sublimator/heat exchanger to provide the thermal sink for an EVA cosmonaut (Barer, 1991; Newman & Barratt, 1997).

The cooling circuit's primary interface for providing the crew member thermal comfort comes from the LCVG, which is used by both Russian and U.S. space programs. The LCVG is worn above a long underwear type comfort garment and provides thermal control by circulating water through several flexible tubes woven into the garment – this is the liquid-cooling component of the garment. Flexible ducts with openings along arms and legs reduce perspiration by concentrating airflow in these areas and serve as the gas flow return inlets to the PLSS – this is the ventilation component of the garment (Newman & Barratt, 1997; Larson & Pranke, 1999; Harris, 2001).[3]

During Apollo lunar surface EVAs, suit temperature was manually controlled by a three-position valve that discretely varied the LCG coolant temperature by diverting a portion of the water circuit flow around the sublimator. During Apollo

---

[3] Cooling by the ventilation loop accounts for ~25% of total cooling, the majority of which is from around the head (Larson & Pranke. 1999).

11, 12 and 14 available LCG temperatures were 21°C (294 K), 15°C (288 K) and 7°C (280 K); only one of the six crewmen to fly with this configuration frequently used the maximum cooling position. For Apollo 15, 16 and 17 the LCG temperatures were set to 27°C (300 K), 18°C (291 K) and 7°C (280 K); the higher temperatures were provided to avoid overcooling during lunar roving vehicle rides (Waligora & Horrigan, 1975b). Evolution of the discretized Apollo system lead to the continuously variable EMU valve design that is capable of matching metabolic rates within the design envelope and provides LCG water temperatures from 16°C to 33°C [289 K – 306 K] (Newman & Barratt, 1997; Larson & Pranke, 1999).

The continued use of a sublimator type system has several drawbacks that include potential contamination of sensitive hardware, potential contamination of the local environment, and the loss of an otherwise useful or costly consumable. For example, hardware developers of the Hubble Space Telescope (HST) were concerned that the thermal control exhaust [the sublimated water] of the extravehicular mobility unit (EMU) could contaminate sensitive instrumentation before the initial service mission. Through analysis it was determined that materials vented by the EMU would not significantly impact HST (Hedgeland et al., 1994). Additionally, forward contamination, or solar system body contamination from Earth originating materials, is increasingly likely with TCSs that require venting. The development of "minimal-release" space suit TCSs has been identified as one means of mitigating forward contamination during future exploration missions (Race et al., 2003; Conley & Rummel, 2008; Conley & Rummel, 2010).

Consumable losses encountered during EVA operations come in many forms, for a variety of different reasons. Some amount of vehicle atmosphere is lost to space and power is consumed with each air-lock egress and ingress (Fullerton, 2001; Trevino & Lafuse, 2008). However, the single largest consumable loss encountered during an eight-hour EVA is water. Typically, 3.6 kg (8 lbm) of water mass is sublimated during an 8 hour EVA (Nabity et al., 2009; Bue et al., 2013).[4] Consumable losses can also have major impacts on vehicle systems. Any un-recoverable material that has a use throughout the remainder of a mission must be additionally accounted for in the initial launch or harvested from in-situ resources. In either case, regenerable and non-venting EVA life support systems have the potential to reduce upfront expendable transport and logistics penalties (Eckart, 1996).

The Space Evaporator-Absorber-Radiator (SEAR) concept is among the leading candidates for replacing the current sublimator system and achieving a non-venting EVA thermal control mechanism. SEAR replaces the traditional porous plate sublimator with a hollow fiber Spacesuit Water Membrane Evaporator (SWME) and adds a lithium chloride absorber radiator (LCAR) to the system. Essentially, heat loads generated within the suit by the human and avionics are

---

[4] Different sources have several values for total feedwater loaded into the thermal control system; for instance Wilde et al. (1993) presents that an EMU feedwater recharge is 4.1 kg or 9.8 lb. The Life Support Systems text by Eckart (2006), states that for an 8 hour EVA 3.5-5.4 kg (7.7-11.9 lb) of water will be consumed for EVA cooling. Up to ~0.9 kg of this feedwater also consists of condensate from breathing, perspiration and LiOH reaction (Larson & Pranke, 1999). For analysis and comparison purposes it's more appropriate to estimate expended mass based on some metabolic profile being analyzed.

directed to SWME. Those loads drive the evaporation of water in SWME, and the product water vapor is directed to the LCAR where the majority is absorbed. The resulting lithium chloride and water reaction acts as a chemical heat pump, increasing the temperature of the radiator's surface. The increased temperature leads to an increase in radiator power dissipation capacity, and the internal loads are finally radiated to the environment (Hodgson et al., 2012). SEAR is nearly capable of achieving closed-loop performance; however, buildup of non-condensable gases can lead to performance inefficiencies so periodic venting of these gases is required (Bue et al., 2013). Additionally, LCAR regeneration is currently achieved by heating the unit to 120 °C for 4 hours under vacuum (Izenson et al., 2014). This post EVA processing procedure would be highly energy intensive for the spacecraft. Finally, the SEAR system provides little apparent on-back mass relief, as carried water mass will be approximately the same as for a sublimator.

2.3. Space Suits and Electrochromic Devices in Radiative Heat Transfer

The general governing equation of radiation heat transfer is the Stefan-Boltzmann Equation, found in Eq. 2.3 (Siegel & Howell, 2002; Incropera et al., 2007). With the exception of the Stefan-Boltzmann constant, the other variables are driven by the suited astronaut's physical properties, the space suit's design, and the properties of the external environment (Massina et al., 2014). A brief description of how a space suit might encounter variable radiation properties is provided below.

$$q = A\sigma\epsilon\left(T_{surface}^4 - T_{sink}^4\right) \tag{2.3}$$

Without the inclusion of some additional area (e.g. a deployable radiator), the total available radiating area is limited to existing suit surfaces that actively participate in heat exchange with the environment. As such, when defining the effective radiating area, the suit total available area, configuration factor,[5] and view factor to the environment should all be considered (Guibert & Taylor, 1952; HIDH, 2010; Tepper et al., 1991; Howell, 2014).

The surface [radiator] temperature of the suit is ultimately driven by the temperature potential provided by the suited astronaut's skin (Hodgson, 2001; Hodgson et al., 2004). Therefore, heat transfer properties between skin surfaces and radiator surfaces define the dynamic interaction of the crew member and the external environment. Additionally, the desirable astronaut skin temperature state is variable with the amount of work being done. One characterization of mean skin temperature trends was established for space suit applications by Alan Chambers (1970) and is provided in Fig. 2.3. In short, as metabolic rates increase the ideal mean skin temperature will decrease. This is the result of an approximately constant thermal resistance between the person's core (heat generation site) and skin surface (heat removal), indicating that as metabolic heat generation increases the temperature drop from the core to skin also increases.

---

[5] A configuration factor is used to quantify the ratio of total available area to area interacting with the external environment. In general, some amount of a person's surface area will interact mainly with other body surfaces and not the environment – between legs and under arms are good examples. The configuration factor is a function of body posture; a crouched person will have a lower factor than one standing erect (Guibert & Taylor, 1952).
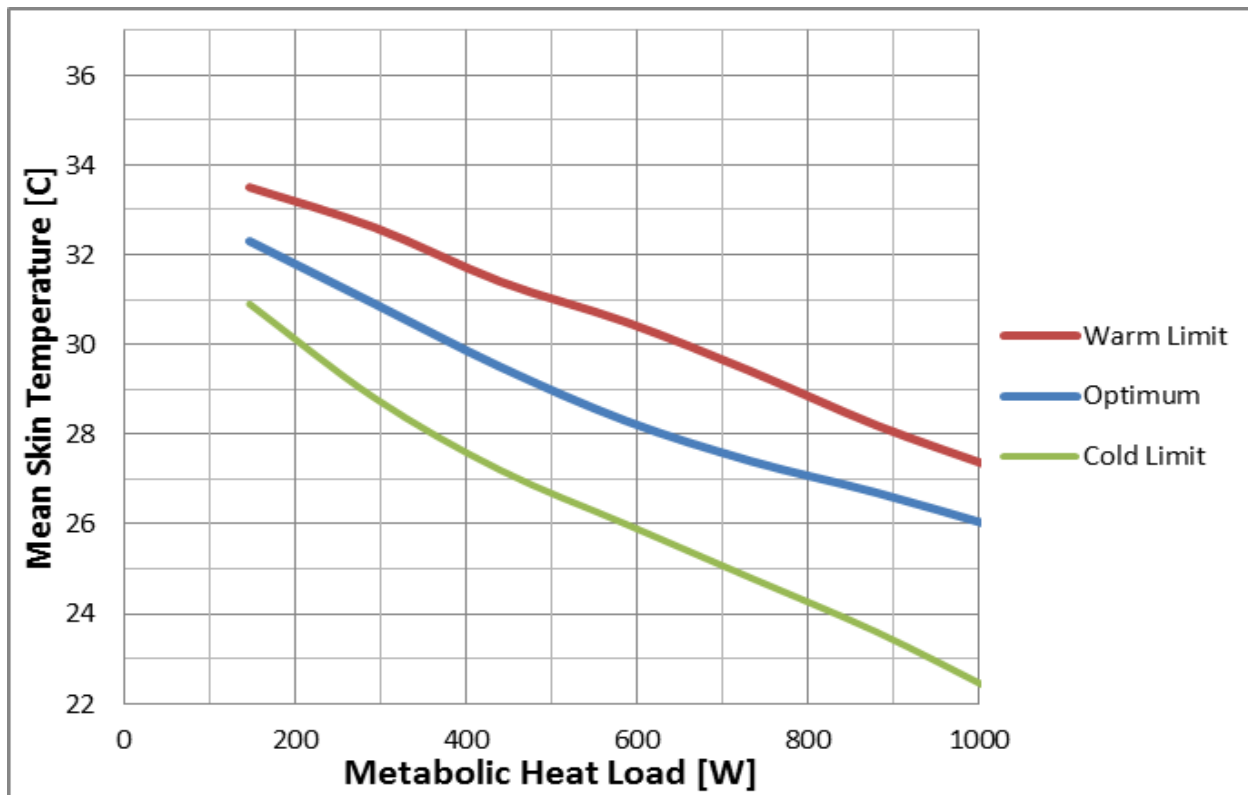
Figure 2.3. Mean skin temperature comfort curves for various metabolic loads (modified from Chambers, 1970).

Including electrochromic devices allows the emissivity of the surface to be selected by system designers and suited astronauts. Traditionally, thermal control designers choose a set of static surface properties appropriate for the operation environment and radiator size (Gilmore, 2002). Integration of variable IR electrochromics allows for the intelligent selection of interaction with the environment to dissipate the appropriate metabolic rate and internal load (Metts et al., 2011; Metts & Klaus, 2012). Electrochromism is achieved when a voltage is applied across a material and induces a change in optical properties. While electrochromic device formulation, deposition techniques and fundamental construction may vary across developers, the most practical device arrangement can

be found in Fig. 2.4. The application of an electric field causes ions to move into or out of the electrochromic material, and the ensuing charge-balancing counter-flow in the circuit results in a difference in electron density in the material and causes the variation in optical properties (Granqvist, 1995). The potential for integration into a full-suit radiator system has been made possible through advances in electrochromic deposition onto flexible substrates that show little performance degradation over multiple flexion cycles (Chandrasekhar et al., 2002; Bessière et al., 2002; Kislov et al., 2003).[6] Additionally, electrochromic-based systems require very little power to operate relative to the mass savings the architecture provides (Metts, 2010). At a watt density of ~0.4 W/m^2 the entire surface of the space suit could be controlled with 1.5 W of power or less, applied in periodic pulses only when a state change or state maintenance is needed (Ashwin-Ushas Corp.).

---

[6] Electrochromic provider Ashwin-Ushas Corp. (www.ashwin-ushas.com) advertises their electrochromics as suitable for deposition on highly flexible substrates. One such substrate is a 3M adhesive that provides both physical flexibility and the ability to mount to non-flat surfaces. This is the configuration of the IR electrochromics tested at NASA JSC.
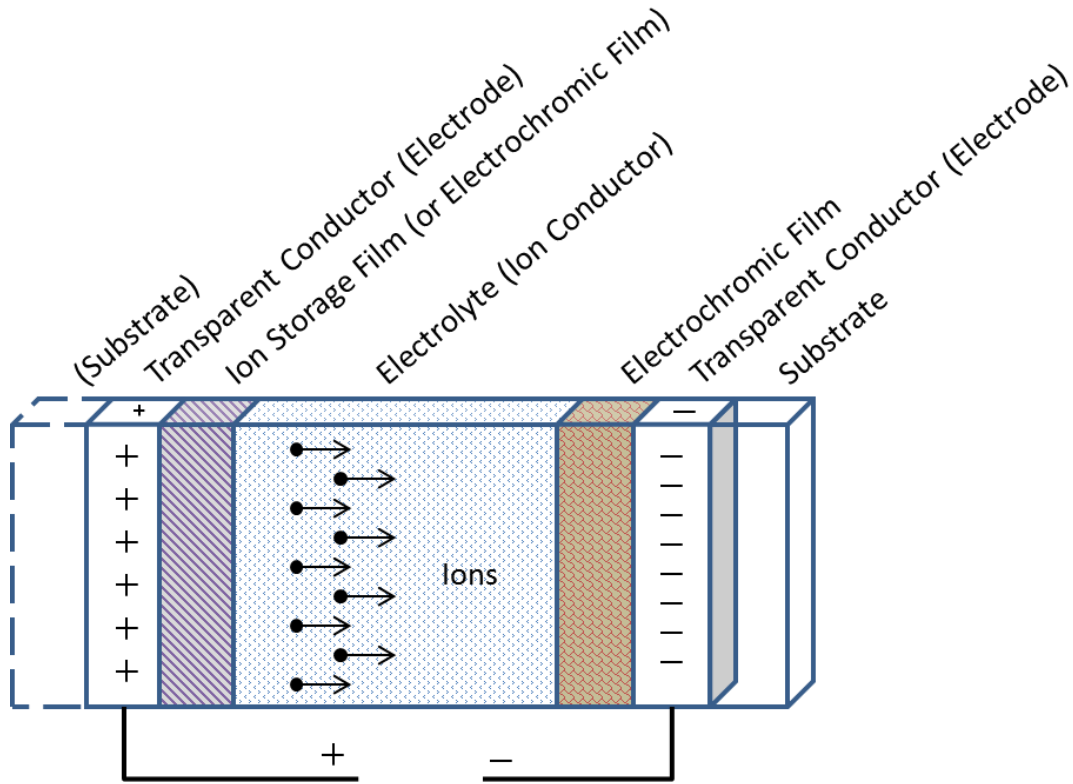
Figure 2.4. Basic design of an electrochromic device. Transport of positive ions dictated by imposed electric field. (Adapted from Granqvist, 1995)

One result of using variable infrared emissivity materials is a continuously variable sink temperature when the surface is exposed to solar spectrum energy and has a non-zero solar absorptivity. The sink temperature of a body in a purely radiative environment is found in Eq. 2.4 (Larson & Pranke, 1999; Clark & Conger, 2000). The wavelength dependence of electromagnetic energy lends itself to separation of solar (visible) and IR heat fluxes, which is a common and necessary practice in spacecraft thermal control analysis (Gilmore, 2002). The spectral differentiation phenomenon is represented graphically in Fig. 2.5. The term *absorptivity* is used to describe *solar absorptivity*, α, and *emissivity*, ε, is used to describe *infrared emissivity*. Due to Kirchoff's Law of radiation, emissivity and

absorptivity are equal for a given wavelength ($\epsilon_\lambda = \alpha_\lambda$), so the term *emissivity* is also used to describe the *infrared absorptivity* of a surface (Glimore, 2002; Incropera et al., 2007).

$$T_{sink} = \left(\frac{1}{\sigma} \left(\frac{\alpha}{\epsilon} (q''_{solar}) + q''_{IR} \right) \right)^{\frac{1}{4}} \tag{2.4}$$
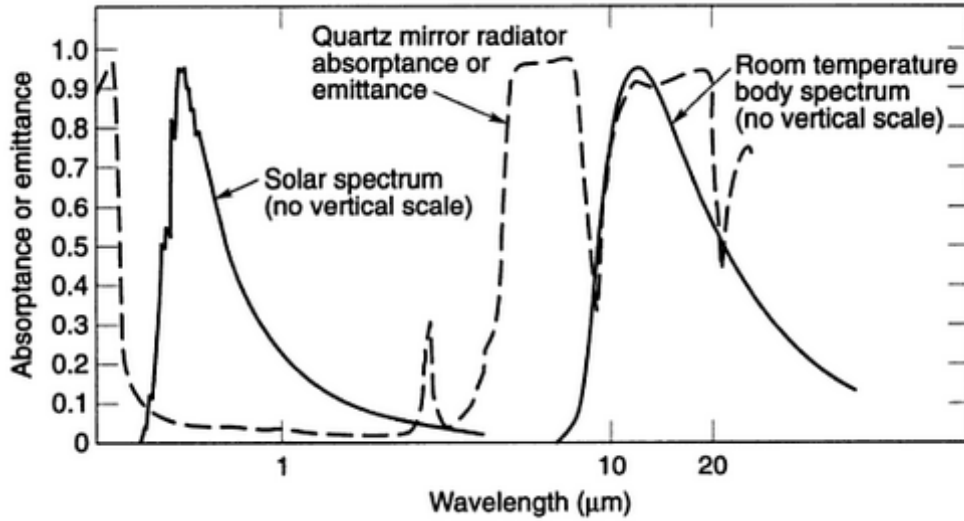
Figure 2.5. Solar and room temperature spectral distributions (from Gilmore, 2002)

The result of Eq. 2.4 is that in an otherwise constant flux environment that includes solar spectrum energy, the sink temperature will vary as α/ϵ with a non-zero solar absorptivity. In this respect, the sink temperature can also be referred to as an equilibrium temperature. Two bodies with different α/ϵ ratios will equilibrate to two different temperatures in the same steady-state flux environment consisting of both solar and IR spectral energy. Therefore, non-zero solar absorptivity values should be considered in parallel with the IR emissivity variation provided by the electrochromic devices. This is because changes in an emissivity set point will change the effective sink temperature of the radiator.

CHAPTER 3

Evaluation of a Full Suit Radiator for Lunar EVA

3.1. Abstract

Traditionally, thermoregulation of spacewalking astronauts has been achieved by the sublimation of water to the vacuum of space. Future missions call for the need to achieve robust closed-loop thermal control to reduce or eliminate extravehicular activity (EVA) burden on consumables. The current leading concept to achieve closed-loop thermal control is the Space Evaporator-Absorber-Radiator (SEAR). The SEAR is nearly capable of achieving the desired non-venting capability; however, carried water mass for evaporation will still be comparable to a sublimator-based system. Evolution from systems that leverage sublimation or evaporation of water as the primary heat rejection mechanism to a system that directly leverages the local radiation environment may provide another means of achieving robust closed-loop space suit thermal control at a reduced system mass. Previous EVA thermal control investigations that utilize radiation have generally limited radiator surface area to the available size of the portable life support system backpack: about 0.85 m². The utilization of a full suit flexible radiator increases this area by a factor of ~4 for traditional gas pressure suits and ~2 for the advanced mechanical counter pressure suit concept. Radiator heat dissipation capacity is also dictated by radiator temperature, radiator surface properties (e.g. emissivity, absorptivity) and the local thermal environment. As such, suit radiator surface temperature should be maximized to the extent possible for the flexible radiator

architecture to be feasible under most circumstances. Here we present radiator surface temperature guidelines for the full suit flexible radiator architecture in steady-state environments. Results identify favorable thermal environments in which a full suit flexible radiator can reject a nominal 300 W metabolic heat load produced within a space suit.

3.2. Introduction

The expulsion of water mass is a well-documented concern for the reasons described in Chapter 2 and is noted specifically in NASA's Space Technology Roadmaps. Technology Area 6 maintains the stated goal of providing EVA heat rejection with no consumable usage (Hurlbert et al., 2012). Among the many ways to achieve this goal, radiation offers perhaps the most convenient approach, as bulky support hardware can be reduced, distributed or eliminated. Several PLSS backpack mounted radiator concepts have been investigated previously for potential integration in the lunar environment. These PLSS mounted systems are inherently limited in surface area, to approximately 0.85 m² (9.2 ft²), which significantly restricts radiator heat rejection potential (Sompayrac et al., 2009).

Richardson (1965) provided one of the earliest investigations of the full suit flexible radiator concept under the assumption of a 556 km Earth orbit without the presence of the supporting space vehicle. It was concluded that passive radiative thermal control could not provide the necessary thermal control by selection of solar absorptivity and infrared emissivity properties for internal heat loads greater than 440 W (1500 Btu/hr). By including a variable conductance suit wall, however,

23

internal heat loads up to 586 W (2000 Btu/hr) were achievable given that the exterior suit surface had a solar absorptivity of 0.17 and infrared emissivity of 0.85 (Richardson, 1965). These radiative properties, somewhat coincidentally, are consistent with the optical properties of the EMU.

In the investigations of both Hodgson (2001, 2004) and Metts, the suit radiator surface temperature was assumed to be a constant 300 K regardless of the astronaut's metabolic heat expenditure. This was considered a reasonable differential from the mean skin temperature, and adequate to facilitate the necessary heat transfer to the radiator surface. Special consideration of variations in desirable mean skin temperatures at various metabolic loads, as provided in Fig. 2.3, and differences in heat transfer mechanisms between the skin and radiator, however, were not addressed in significant detail.

Based on results from these earlier studies, the full suit flexible radiator concept appears to have the potential to provide thermal control across a range of operational scenarios and to mitigate water consumable losses that would otherwise be incurred from sublimation during EVA. Here we further elaborate on those previous works to provide guidelines for incorporating a full suit flexible radiator into a space suit thermal control system. Namely, guidelines are established for desirable radiator surface temperatures to provide meaningful heat dissipation capacity. Temperature guidelines are used to establish first-order estimates where destination environments would restrict use should the full suit radiator architecture ultimately be adopted.

3.3. Background

Spacesuit thermal control can be very dynamic in terms of both external environments and internal heat loads. As one may expect, environmental fluctuations are highly dependent on mission scenario. A low-earth orbit EVA will pass in and out of earth's shadow every 90 minutes. On the lunar surface, local temperatures may be mostly constant or have large fluctuations due to contributions from nearby surface features (e.g. boulders, craters and mountain ranges) depending on the path taken by an EVA astronaut. Additionally, internal variations from crew metabolic loads must be considered. Baseline minimum, average and maximum metabolic rates for different operational scenarios as defined by NASA's Human Integration Design Handbook (HIDH) are provided in Table 3.1. In practice, real time variations in both internal and external environments must be managed so thermal equilibrium is maintained within specified tolerances.

Table 3.1.   EVA Metabolic Rates for Suited Operations (from HIDH, 2010).

Data Source	Minimum	Average	15-min Maximum
μ Gravity EVA (ISS & Shuttle)	160 W (545 Btu/hr)	264 W (900 Btu/hr)	645 W (2200 Btu/hr)
Apollo Lunar Surface **EVA**	144 W (490 Btu/hr)	287 W (980 Btu/hr)	724 W (2471 Btu/hr)
Advanced Walk Back Test	491 W (1675 Btu/hr)	696 W (2374 Btu/hr)	880 W (3002 Btu/hr)

Depending on the metabolic rate of the astronaut, the heat load associated with avionics and PLSS systems will vary in significance. A modest system heat load of 100 W is ~40% of the total heat load when added to the minimum Apollo

EVA metabolic rate and reduces to ~12% when added to the Apollo peak maximum rate. Depending on the thermal control architecture capabilities, it can be difficult to assess how these loads will be handled by the system. As such, for this first-order analysis, dissipation of non-metabolic suit heat loads is not considered.

For the purposes of this assessment, it's also prudent to define a reasonable success criterion for heat dissipation potential to the local environment. Here we define this criterion as the ability of the radiative system to reject a metabolic load of 300 W (1024 Btu/hr). In terms of approximate mass savings, this capability offsets ~2.3 kg of otherwise sublimated water during one six hour EVA (~3 kg for an eight hour EVA). This assumption dictates that periods of higher heat loads be offset by some supplemental mechanism in the event that the radiating system cannot vary its properties to meet the demand and the thermal mass of the system cannot buffer these intervals.

The lunar surface is used throughout the analysis as the baseline EVA environment. With a relatively high solar absorption of ~0.92 and the lack of an atmosphere, the moon's surface has a very large temperature distribution that reduces as a cosine function from the subsolar point. Surface temperatures can range from ~120°C at the subsolar point to ~-180°C on the dark side. While these temperatures dictate infrared (IR) heat loads, non-shaded EVA environments also contain solar spectra energy in the form of direct solar and/or albedo (Gilmore, 2002; Heiken et al., 1991).

Net heat dissipation via radiation is governed by the Stefan-Boltzmann law provided in Eq. 2.3. With the exception of the Stefan-Boltzmann constant, the other parameters are defined by the spacesuit and environmental properties. In many ways, surface area is the most straight-forward of these parameters; however, several concepts have been evaluated in the context of variable heat rejection for lunar landing vehicles that leverage an effective area variability to modulate the heat rejection rate (Bannon et al., 2010a; Sunada et al., 2010). While these concepts could potentially extrapolate to space suit thermal control, the definition of the maximum potential radiating area is also important. Without designing in extra radiating area beyond existing suit surfaces, e.g. a deployable radiator, available area is limited to either the PLSS structure alone or the entire exterior surface area of the suit and PLSS. A radiating area of ~0.85 m^2 is representative of previous PLSS mounted radiator studies (Sompayrac et al., 2009). For MCP-suit integration, the full suit radiating area is approximated as the skin surface area of a nude crewmember. The projected astronaut population is expected to have a body surface area distribution from 1.53 m^2 to 2.28 m^2, a 5th percentile female to a 95th percentile male (HIDH, 2010). For gas pressure type suit integration, the approximate total surface area is based on previous Extravehicular Mobility Unit (EMU) evaluations which found this area to be 3.9 m^2 for the suit utilized (Tepper et al., 1991). In either case, the total area is not necessarily representative of the area radiating to the environment (e.g. arm pit sections don't readily see the external environment). A radiating area factor (f_R), that varies with body posture, is introduced as a scaling

factor for this reason. Guibert and Taylor found a maximum f_R of 0.88 for clothed subjects standing erect in their studies. Mean variations of f_R from 0.77 to 0.65 were provided for erect to crouched postured subjects (Guibert and Taylor, 1952). The radiating area factor used in the EMU study was 0.92. For the purposes of this study a maximum mean $f_R = 0.86$ is used as a first approximation to this variable. This is done with the understanding that EVAs are not conducted in a purely erect posture and other scaling factors may be appropriate depending on activity. Additional scaling could also be done to account for suit surface areas undesirable for radiator integration, such as a display and control module.

The definition of a radiating suit's surface properties is coupled to the degree that the suit is allowed to interact with the environment. In purely radiative heat transfer, T_{sink} is the temperature that a body/suit with a given solar absorptivity (α) and IR emissivity (ϵ) will equilibrate to in a radiative flux environment. The sink temperature is defined in Eq. 2.4.[7] Where, solar spectrum (q''_{solar}) fluxes are differentiated by direct solar (q''_{sun}) and reflected solar/albedo (q''_{Alb}) and all infrared heat fluxes are included as q''_{IR}. Several system concepts have been suggested that allow sink temperature manipulation through intelligent selection of surface properties and environment interaction. Ochoa and Hodgson have both suggested using surface geometry manipulation through louver type systems that essentially block lunar surface IR heat loads from interacting with the radiator (Hodgson et al.,

[7] Clark, Craig and Conger, Bruce, "Thermal Analysis Basics and Design Guidelines". Unpublished Presentation, Created May, 2000.

2004; Ochoa, et al., 2008). Electrochromic materials, with IR emissivity modulation potential, have also been suggested as a means for varying interactions with the local environment in both vehicle and space suit applications (Metts et al., 2011; Bannon et al., 2010b). The exterior surface of the currently used EVA space suit, the EMU, is designed such that the emissivity is maximized and solar absorptivity is minimized; $\epsilon = 0.84$ and $\alpha = 0.18$ (Sompayrac et al., 2009; Larson and Pranke, 1999). These properties mitigate the thermal influence of the sun while allowing the suit some heat leak. However, additional aluminized Mylar insulation layers are included to further decouple the crewmember from the environment and limit heat leak.

Definition of a radiator surface temperature can likewise be difficult to establish in this context. Metabolic loads generated within the body are directed to the skin in the form of heat that is then transferred to the local environment. If the heat loads are not adequately handled by the thermal control system, core temperature will shift from the nominal and increase the potential for degraded performance and injury (Buckey, 2006). The skin surface provides the primary interface between metabolic loads, core temperature, and the thermal control mechanism. By extension, the skin surface also provides the primary temperature potential to the thermal control system and thereby drives radiator surface temperatures. For the purposes of this evaluation, the threshold for maximum skin temperature is defined as 37°C (310K), the nominal body core temperature. However, mean skin temperatures will generally be lower since 37°C (310K) at the

skin surface would suggest the astronaut is approaching hyperthermia [heat stroke] (HIDH, 2010; Buckey, 2006).

Mean skin temperature is a commonly used metric for simplifying the nominal range of distributed skin temperatures. For persons at rest (low metabolic rates) a mean skin temperature of ~306 K (33°C) is considered near optimum (Nunneley, 1970). As metabolic rates increase the desired mean skin temperature actually decreases, indicating that metabolic loads are adequately being removed from the astronaut and thermal stress is being avoided. This trend was characterized by Chambers and is illustrated in Fig. 2.3 (Chambers, 1970). At a high end metabolic rate of 800 W the optimum mean skin temperature is ~300 K (27°C). While this 6 K drop in mean skin temperature seems modest, the result is a 7.6% reduction in total radiating flux potential before accounting for other performance modifiers or heat transfer losses. Additionally, the constant 300 K radiator surface temperature assumption made by both Hodgson and Metts would require heat transfer without a temperature difference from the skin surface to the radiator surface during periods of high metabolic loads. The optimum temperature line from Fig. 2.3 is considered the baseline mean skin temperature for the calculations in this assessment.

3.4. Methods

This investigation utilized the following methods to establish radiating temperature guidelines for evaluating flexible radiator performance in the lunar environment. First, the desired net heat dissipation potential (q_{rad} = 300W) was

used to establish mean radiator surface temperature as a function of angle from the subsolar point. This was complemented by assessing the impact of varying radiator surface properties (absorptivity and emissivity) on net flux potential and resulting radiating temperature guidelines. These results were used to establish a first-order interaction between the suit and environment and to define the threshold operating environment for feasibility of use. After establishing minimum operating temperatures, required overall heat transfer effectiveness guidelines were determined based on the optimum mean skin temperature. The following sections describe the analytic methods used to perform these evaluations.

3.4.1. Definition of Suit Interaction with the Environment and Minimum Radiator Surface Temperature

The expected thermal environment of the moon must be characterized before meaningful operational results can be collected. Figure 3.1 illustrates the primary radiation flux sources experienced during a lunar surface EVA. Conduction of heat to the lunar surface is considered negligible for these investigations and is not included in the analysis. Heat flux out, σT_{surf}^4, is representative of the maximum flux potential before scaling by the surface emissivity value. Metabolic rate is included as the desired net heat dissipation target for the thermal control system. This initial study approximates the entire lunar surface as a flat plane (e.g. featureless). The local area of the EVA is considered an infinite plane with a constant external flux environment based on the location's angle from the subsolar point, as was done for previous similar investigations (Ochoa et al., 2006). The space

suit is approximated as a flat plate where each side "sees" a different effective flux environment; one side is effectively shaded by the other and will have no direct solar contribution. Combined, these approximations allow a simple view factor (VF) for each radiating surface to be calculated as 0.5 to both the lunar surface and space environment. The view factor equation associated with Fig. 3.2 is found in Eq. 3.1; it is evaluated as if the astronaut is in a fully erect posture, resulting in a constant $\eta = 90\ deg$ (Howell).
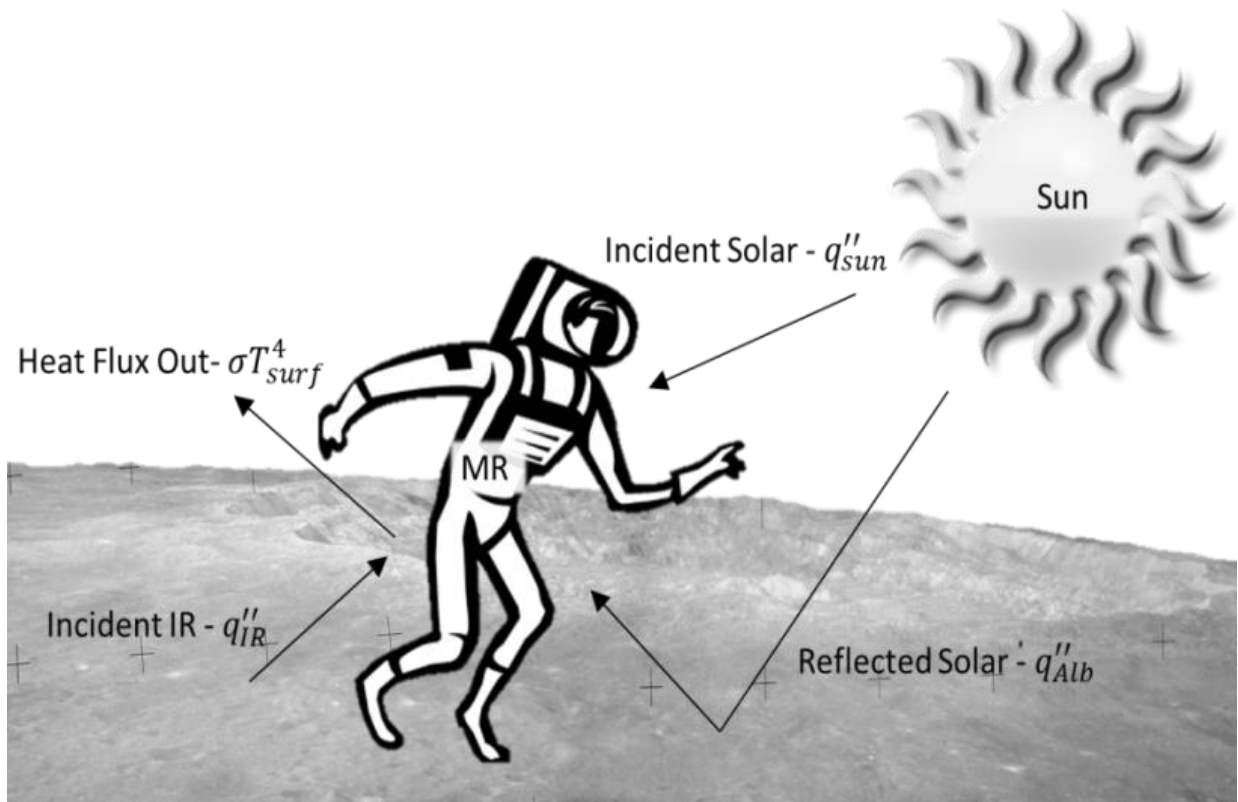
Figure 3.1. Radiative heat fluxes during lunar EVA
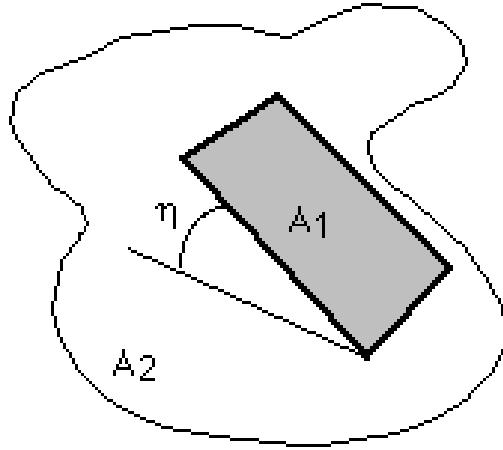
Figure 3.2. View factor approximation (from Howell).

Net steady state flux environments are calculated via Eq. 3.2 for each radiator surface based on a mean incident solar flux (S) of 1368 W/m^2, an approximate lunar albedo coefficient of 0.08 (lunar surface solar absorptivity, $\alpha_{Lunar} = 0.92$) at some angle from the subsolar point θ. The 90°, lunar pole, case is assumed to have a constant IR heat flux of 5.2 W/m^2 (Gilmore, 2002). Radiating temperature is shown as a mean surface temperature$(\bar{T}_{surf})$. Here, $\bar{T}_{surf}$ is considered constant over the entire flexible radiator surface despite potentially variable internal and external environment conditions. As previously established, two equal radiating areas are considered throughout this analysis. The nude body surface area is approximated as the mean of the extreme surface areas provided in the previous section, 1.91 m². The pressure suit surface area of 3.90 m² was taken directly from the previous investigation (Tepper et al., 1991). After applying a radiating area factor (f_R) of 0.86, radiating surface areas are assumed to be 1.64 m² and 3.35 m² for the mechanical counter pressure and pressurized suits, respectively. In cases with non-zero solar absorptivity, radiating area is considered to be split

equally between sun facing and shaded sides of the suit and the net heat dissipation potential (q_{rad}) is calculated from Eq. 3.3. Flux contributions of infrared heat loads, direct solar and albedo are provided in Eqs. 3.4, 3.5 and 3.6, respectively. Again, note that q''_{sun} is zero on the shaded side.

$$VF = F_{1 \to 2} = \frac{1 - cos\eta}{2} \tag{3.1}$$

$$q''_{rad} = \epsilon\left(\sigma \bar{T}^4_{surf} - q''_{IR}\right) - \alpha(q''_{sun} + q''_{Alb}) \tag{3.2}$$

$$q_{rad} = \Sigma \frac{A}{2} q''_{rad} = \frac{A}{2}\left(2\epsilon\left(\sigma \bar{T}^4_{surf} - q''_{IR}\right) - \alpha(q''_{sun} + 2q''_{Alb})\right) \tag{3.3}$$

$$q''_{IR} = cos\theta * VF * S\alpha_{Lunar} \tag{3.4}$$

$$q''_{sun} = VF * S \; or \; 0 \tag{3.5}$$

$$q''_{Alb} = cos\theta * VF * S(1 - \alpha_{Lunar}) \tag{3.6}$$

By defining the first-order flux environment in this way, one can solve Eq. 3.3 for $\bar{T}_{surf}$ and establish the required temperature to provide a nominal heat dissipation rate of 300 W. Threshold limits are identified as regions where body temperatures cannot drive radiator temperatures to the required degree without some heat pumping mechanism. Results of varying absorptivity and emissivity surface properties are also provided.

3.4.2. Evaluation of Heat Transfer Effectiveness (UA)

Additional insight into the potential difficulty associated with the integration of a full suit flexible radiator into a space suit thermal control system can be gained

by examining the allowable overall heat transfer effectiveness coefficient (UA). This commonly used metric essentially tells a system designer how good the heat transfer mechanism from the skin to the radiator surface must be. UA in its most general form is calculated from Eq. 3.7, where ΔT is the difference in mean skin temperature and mean radiator surface temperature for the given amount of energy being rejected in some operating environment (Incropera et al., 2007). UA is also described as the inverse of the total thermal resistance (R_{total}) of the system. No threshold UA is suggested in this evaluation; however, a negative or an infinite UA represents a negative temperature difference (heat pumping) or zero temperature difference, neither of which represents a feasible solution.

$$UA = \frac{q}{\Delta T} = \frac{1}{R_{total}} \tag{3.7}$$

For the purposes of this investigation, UA and R_{total} are used only to illustrate the potential difficulty of achieving a low temperature drop from skin to radiator surfaces. The thermal resistance formulation for one-dimensional steady-state conduction is found in Eq. 3.8, where k is the material's thermal conductivity, thk is the thickness of the material and A is the area across which energy is distributed. Similar relationships exist for both convection and radiation, although neither were used in this evaluation (Incropera et al., 2007).

$$R_{total} = \frac{thk}{kA} \tag{3.8}$$

3.5. Results & Discussion

The highly variable nature of heat loads on the lunar surface makes it difficult to accommodate all operating environments without the addition of some surface IR shielding mechanism. However, a first-order feasibility of implementing the flexible radiator architecture, without such a mechanism, can be gleaned from solving Eq. 3.3 for the mean surface temperature required to dissipate a prescribed thermal load. Figure 3.3 was produced in this fashion for EMU and MCP-Suit characteristic radiating areas based on the described approximation of the lunar surface and different uniform radiator surface properties.

Four surface property sets were chosen to represent a range of radiator conditions. The $\alpha = 0$, $\epsilon = 1$ case represents an ideal blackbody radiator free from the influence of solar spectrum energy. This blackbody case is essentially the theoretical low temperature limit without additional intervention to block lunar surface IR fluxes or increasing radiating area. The $\alpha = 0.18$, $\epsilon = 0.84$ case represents integration with a radiator that has equivalent surface properties to the EMU outer layer (ortho fabric). The $\alpha = 0.15$, $\epsilon = 0.89$ case represents the best case surface properties of an electrochromic radiator as provided by Ashwin-Ushas Corp.[8] The $\alpha = 0.5$, $\epsilon = 0.9$ case is intended to represent an arbitrary degradation of surface properties due to the collection of lunar dust on the radiator surface (Campbell, 1999).

---

[8] URL: http://www.ashwin-ushas.com/ Retrieved Jan. 31, 2014.

The required $\overline{T}_{surf}$ guidelines provided in Fig. 3.3 can also be used to assess long duration exploration site feasibility, should the full suit flexible radiator architecture be adopted for EVA thermal control. Figure 3.4 uses these results to illustrate destination restrictions for a particular test case, where changes in chart color represent where different combinations of the suit properties examined are or are not acceptable. The inclination of the moon's equator to the ecliptic is ~1.53° (Heiken et al., 1991). This condition dictates that deviations of the subsolar point from the lunar equator are small throughout the year (Hager, 2013).[9] As such, mission sites are essentially limited to latitudes that support the required heat dissipation for realistic radiator mean surface temperatures. Small seasonal variations are not included. Also note in Fig. 3.3 that variations in radiator surface properties change the effective sink temperature and limit heat dissipation capability, driving up required radiator temperatures and additionally restricting exploration area. With the surface properties of the EMU and best case electrochromic radiator being similar, the required surface temperature profiles of each are very close to the same.

Assuming a maximum mean temperature threshold of 310 K (e.g. human core temperature) and radiator-only heat rejection, long term exploration sites are absolutely restricted to latitudes greater than ~46° for EMU and ~57° for MCP-Suit characteristic radiating areas. This upper limit assumes perfect transmission of ideal core temperatures to the surface of the space suit. A more realistic surface

---

[9] The result is nearly no "seasonal" variation in solar angle with respect to the moon's equator.

temperature would be closer to 290 K. The 290 K (17 °C) value was chosen as it's near the Shuttle/Station EMU minimum liquid cooling garment water temperature (16 °C) (Larson and Pranke, 1999). This radiator surface temperature is ultimately dependent on the actual suit cooling system architecture and could be higher or lower.
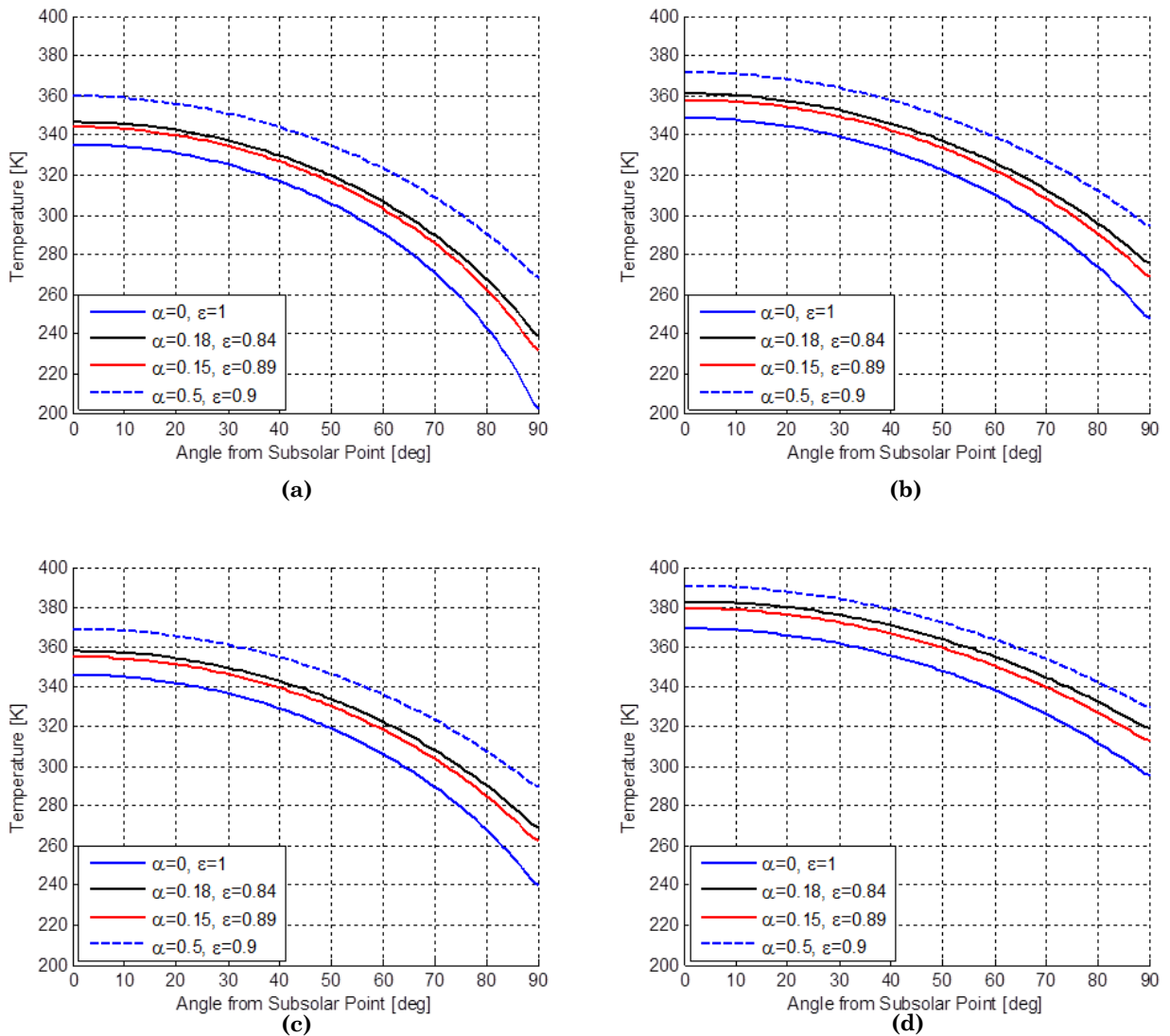
Figure 3.3. Mean radiator temperature requirement for given dissipation rate: (a) EMU at 300 W, (b) EMU at 700 W, (c) MCP-Suit at 300 W, (d) MCP-Suit at 700 W.
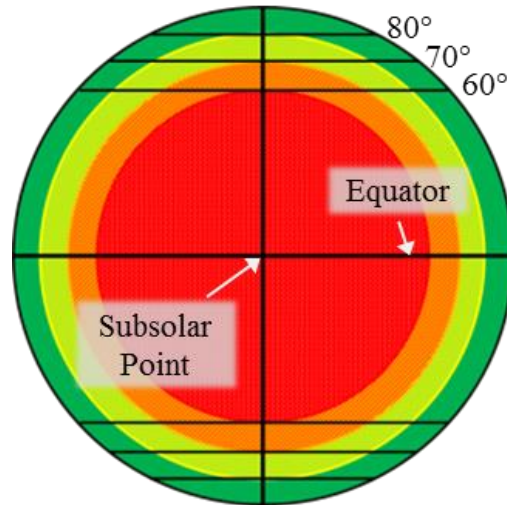
Figure 3.4. Exploration restriction with angle from subsolar point. 300 W of dissipation, EMU area at 290 K.

Minimum threshold angles from the subsolar point at mean radiating temperatures of 310 K and 290 K for blackbody, EMU and degraded radiator surface properties are provided in Table 3.2. The single EVA angular restriction for both 300 W and 700 W of metabolic heat dissipation are provided. These two rejection cases are provided to establish where the success criterion of 300 W dissipation could be met and to determine if the system is capable of handling peak metabolic rates of up to 700 W. Cases in Table 3.2 that do not exist (DNE) are where the architecture cannot provide the prescribed level of heat rejection at the chosen radiator temperature. All anticipated heat loads need to be managed by the thermal control system in some way; this includes the ability to accommodate metabolic rates associated with contingency walkback scenarios. The inability of the radiative system to accommodate these scenarios implies that the addition of some type of supplemental thermal control mechanism will be required in the PLSS architecture.

Table 3.2. Threshold angles from subsolar point for 310 K and 290 K mean radiator surface temperatures. BB: Black Body, Deg: Degraded, DNE: Does Not Exist.

	BB 310 K	BB 290 K	EMU 310 K	EMU 290 K	Deg. 310 K	Deg. 290 K
EMU Area 300 W Rejection	46°	60°	58°	70°	69°	80°
EMU Area 700 W Rejection	60°	72°	72°	83°	81°	DNE
MCP-Suit Area 300 W Rejection	57°	70°	69°	80°	79°	90°
MCP-Suit Area 700 W Rejection	81°	DNE	DNE	DNE	DNE	DNE

For a true long duration mission with EVA to be feasible, perhaps the most telling restriction arises from degraded radiator performance. In either case (EMU or MCP-Suit area), the 700 W peak metabolic rate cannot be fully dissipated at 290 K radiating temperatures. In order to meet the 300 W integration standard, destination environments are essentially restricted to polar regions of the lunar surface. Figure 3.4 illustrates this point by distinguishing the threshold angle zones for 300 W of heat dissipation for a flexible radiator with the approximated EMU area at 290 K. Threshold angles from Table 3.2 of 60°, 70° and 80° are represented by variations in color for radiators with ideal blackbody, EMU and degraded radiative surface properties. In order for this heat rejection mechanism to be feasible, the EVA must be conducted outside (greater than) of the threshold angle corresponding to the radiator's current surface property state. Horizontal separation lines represent threshold latitudes for long duration missions, those missions occurring over multiple lunar days. Transition into areas below these threshold limits would result in some fraction of a lunar day where EVAs utilizing

the flexible radiator architecture can no longer meet the 300 W dissipation success criteria based on this analysis.

In the unfavorably hot EVA cases, the feasibility of reaching these destinations could be increased by including some IR shielding scheme or heat pumping mechanism to increase the radiator's potential. In the coldest EVA cases, such as the lunar poles or dark side, excess heat dissipation may be an issue. The more traditional approach of astronaut insulation in combination with heaters could be implemented if desirable. Alternatively, variable heat rejection mechanisms or strategies could be implemented to modulate the interaction with the cold environment. One example would be the integration of IR electrochromics, whereby a controlled reduction of the IR emissivity reduces the net heat flux out of the suit system. The benefit of the cold environment is that the temperature drop from the skin to radiator surface can be large while still providing the same amount of heat rejection. This essentially makes it easier for the architecture to be integrated in a meaningful capacity.

In order to better project the feasibility of attaining the target surface temperatures in a flexible radiator based EVA thermal control scheme, the optimum skin comfort curve of Fig. 2.3 is used. From that projection, an astronaut with a metabolic rate of 300 W has an optimum mean skin temperature of ~304 K (31°C) while a metabolic rate of 700 W corresponds to a mean skin temperature of ~301 K (28°C). From Eq. 3.7, the minimum UA required to attain a 290 K mean radiator temperature is 21.4 W/K (13.1 W/m²K) for 300 W of heat dissipation and

63.5 W/K (30.5 W/m²K) for 700 W of dissipation. These UAs correspond to maximum total thermal resistances between skin and radiator surfaces of 0.0467 K/W and 0.0157 K/W for 300 W and 700 W of heat transfer, respectively.

To put these resistances into perspective, the thickness of a cotton garment covering the entire surface area of the *average* astronaut is used. Eq. 3.8 is used to make this prediction, where the thermal conductivity (k) of the cotton garment is 0.06 $W/m \cdot K$ (Incropera et al., 2007). In order to have an exterior surface temperature of 290 K while at a metabolic rate of 300 W, the cotton garment can be up to 5.35 mm (0.211 in) thick or approximately the thickness of a sweatshirt. For the same surface temperature at a metabolic rate of 700 W, the cotton garment is additionally restricted to a maximum thickness of 1.80 mm (0.071 in) or similar to that of a T-shirt. While these results do not support or reject any particular heat transfer mechanism, this completely dissimilar use case illustrates the inherent difficulty associated with maximizing radiator surface temperatures.

3.6. Conclusions

The analysis described here was used to determine a set of baseline temperature requirements capable of dissipating a nominal metabolic rate of 300 W to the local environment using a full suit flexible radiator during EVA. Variations in surface radiating properties (absorptivity and emissivity) were included to bound operational temperature requirements. These properties ranged from an ideal emitter with no solar spectrum influence to a radiator representative of one which has been degraded from use on the lunar surface. Two radiating areas were used in

the evaluation and are considered to be representative of application for a gas pressure or mechanical counter pressure type garment. First-order radiating temperatures were chosen to assess threshold latitudes on the lunar surface for long duration exploration missions. The degraded surface properties, representative of worst case operational scenarios, essentially limit lunar exploration to polar regions if a full suit flexible radiator scheme were to be adopted as the sole source for cooling. The results provided here can be used to set preliminary design objectives, to be refined with follow on work, should such a thermal control system be considered for future EVA missions.

Related Output Publications:

Massina, C.J. and Klaus, D.M. (2013). Considerations for Incorporating Variable Emissivity Radiators into a Space Suit Heat Rejection System (poster), *AIAA 43rd International Conference on Environmental Systems*, Vail, CO.

Massina, C.J., Klaus, D.M., & Sheth, R.B. (2014). Evaluation of Heat Transfer Strategies to Incorporate a Full Suit Flexible Radiator for Thermal Control in Space Suits*, ICES-2015-89, *44th International Conference on Environmental Systems,* Tucson, AZ.

Hager, P.B., Walter, U., Massina, C.J., and Klaus, D.M. (2015). Characterizing a transient heat flux envelope for lunar surface space suit thermal control applications. *J. Spacecraft and Rockets*, 7(4), pp: 1193-1202, doi: 10.2514/1.A33182.

CHAPTER 4

Defining Electrochromic Pixel Size

4.1. Abstract

Heat rejection for space suit thermal control is typically achieved by sublimating water ice to vacuum. Converting the majority of a space suit's surface area into a radiator may offer an alternative means of heat rejection, thus reducing the undesirable loss of water mass to space. In this work, variable infrared emissivity electrochromic materials are considered and analyzed as a mechanism to actively modulate radiative heat rejection in the proposed full suit radiator architecture. A simplified suit geometry and lunar pole thermal environment is used to provide a first-order estimate of electrochromic performance requirements, including number of individually controllable pixels and the emissivity variation that they must be able to achieve to enable this application. In addition to several implementation considerations, two fundamental integration architecture options are presented – constant temperature and constant heat flux. With constant temperature integration, up to 48 individual pixels with an achievable emissivity range of 0.169 to 0.495 could be used to reject a metabolic load range of 100 W to 500 W. Alternatively, with constant heat flux integration, approximately 400 pixels with an achievable emissivity range of 0.122 to 0.967 are required to reject the same load range in an identical external environment. Overall, the use of variable emissivity electrochromics in this capacity is shown to offer a potentially feasible solution to approach zero consumable loss thermal control in space suits.

4.2. Introduction

A space suit's primary functions are to provide atmosphere and thermal control for the human inside. It's especially challenging to maintain an acceptable thermal balance across the wide range of external environments that are encountered in space (Griffin et al., 1999). In traditional suit designs, the astronaut is largely insulated from these thermal extremes during extravehicular activity (EVA) through the addition of multiple aluminized Mylar layers separated by vacuum in the suit's material layup (Griffin et al., 1999; Harris, 2001; Farrington et al., 2005). While this material scheme provides considerable thermal isolation, some radiation heat leak is still inevitable. The magnitude of the heat leak is driven by a combination of internal (metabolic) and external (environmental) conditions, which can become sufficiently large so as to preclude operations in certain locations on the moon, especially in the hotter regions where excessive environmental heat loads make EVA thermal control particularly difficult (Campbell, 2000; Ochoa et al., 2006).

A derivative of the Hamilton Sundstrand radiative thermal control architecture was later formulated in our lab and an initial feasibility study into using electrochromics on the outside of a full suit radiator was conducted (Metts and Klaus, 2009; Metts et al., 2011; Metts and Klaus, 2012). Adding variable IR emissivity electrochromic material on the suit's surface allows the passive interaction with the environment to be actively modulated by appropriate selection of an applied voltage that alters the IR emissivity surface property.

Several primary design and performance considerations for incorporating a full suit radiator using variable IR emissivity electrochromics have been identified for further analysis. Heat dissipation rate can be adjusted instantaneously or averaged over some appropriate period to maintain an acceptable range of thermal conditions, depending in part on response time of the electrochromic state changes and on the rate of change in environmental sink view factors (Hager et al., 2015). Transferring metabolic heat from the person to the radiator can be accomplished by allowing the heat to 'leak' directly through the entire suit surface area or by collecting it in a centralized plenum and distributing it via a heat exchanger to the radiator surface. In order to maintain adequate thermal equilibrium as suit surfaces face different environmental sink temperatures, it may prove desirable to divide the electrochromic material into individual pixels that can be independently modulated. Concepts for pixilation control range from using a continuous transition of emissivity set points for each pixel to mixing a pattern of individual pixels that can be discretely switched between high/low states in order to create an average (or effective) emissivity over a given surface area.

First-order system requirements are defined and analyzed here for two radiator integration schemes operating in a representative lunar pole environment. The primary goals of this investigation include determining the required emissivity modulation potential of the electrochromics and the number of electrochromic pixels required to maintain defined thermal comfort conditions. While these results are suit geometry and EVA operational environment specific, the rationale and methods

used to generate these first-order guidelines can be adapted to any combination of suit geometry and EVA environment of interest.

4.3. Background

During an EVA, astronauts can expect to encounter large variations in internal and external heat loads. Internal heat sources consist primarily of the astronaut's metabolic expenditure and the avionics required for suit functions (HIDH, 2010; Sompayrac et al., 2009). While avionics heat can be considered mostly constant, actual values will be contingent on the space suit system design. Metabolic loads can vary from ~100 W minimum to ~800 W 15-minute peak maximum; while generally, an average metabolic rate of 300 W is considered a near nominal EVA rate (HIDH, 2010; Sompayrac et al., 2009; Izenson et al., 2011). This investigation accounts only for metabolic heat dissipation since the avionic load is ultimately a function of the future design, and as such, that specific contribution is not yet determined.

Incident external loads can also vary considerably with the local surroundings of the EVA excursion. LEO environments tend to be generally well categorized in terms of contributions from both the Sun and Earth; however, the addition of a spacecraft in the nearby vicinity can considerably complicate the incident thermal loads during an EVA (Gilmore, 2002). The same is true for the lunar environment, where infinite plane approximations can be used for first-order estimates, but high fidelity simulation packages become necessary for characterizing thermal flux interactions between complex surfaces topography

features and detailed geometric objects such as space suits, especially as they randomly move around on the lunar surface (Hager et al., 2015; Massina et al., 2014; Hager, 2013). Maintaining thermal equilibrium under these circumstances requires some degree of active control.

Use of a variable emissivity electrochromic radiator offers one potential means of modulating desired heat rejection to actively balance the environmental thermal sink with the internal heat load of the space suit. Emissivity values change as a result of inducted electrochromic property states when a voltage is applied. The supplied electric field encourages ion migration into or out of the electrochromic material causing a change-balancing counter flow of electrons within the device. The induced change in electron density is physically manifested as a variation in surface properties that alter the emissivity (Granqvist, 1995).

The spectral distribution of incident heat fluxes on the suit dictate the impact of surface property changes of the electrochromic device. For a spacecraft operating in vacuum, the principle heat fluxes generally include direct incident solar energy, reflected solar energy (albedo), and IR energy emitted from local objects. Due to the spectral separation of the solar and IR energies, the surface properties associated with absorption or emission in either spectrum are regarded as independent (Gilmore, 2002). As such, the absorptivity (α) is used in reference only to the fraction of solar spectrum flux absorbed by the surface and the emissivity (ϵ) is used in reference to the fraction of IR flux absorbed or emitted by the surface, per

Kirchhoff's law, where $\alpha = \epsilon$ only for a given spectrum with purely diffuse interactions (Incropera et al., 2007; Siegel and Howell, 2002).

The presented investigation considers electrochromic devices capable of modulating surface properties in the IR spectrum, as demonstrated by several previous studies (Chandrasekhar et al., 2002; Kislov et al., 2003; Hale and Wollam, 1999; Demiryont and Moorehead, 2009; Bannon et al., 2010b). Additionally, we include a constant solar absorptivity of 0.20 throughout the calculations. Note that the value of absorptivity will practically depend on the material selected, but is consistent with NASA's current spacesuit, or Extravehicular Mobility Unit (EMU), value of 0.18 (Griffin et al., 1999). Currently available electrochromic materials have demonstrated a solar absorptivity range of 0.29 to 0.50 (Chandrasekhar et al., 2014), which we consider to be prohibitively high for the evaluated application. However, the inclusion of any non-zero solar absorptivity provides additional insight into the performance potential of the system, since previous investigations of this architecture had assumed ideal solar reflectance (Metts et al., 2011).One implication of the distributed spectra on surface coating selection is that the outermost material must be transparent in the bulk of the IR spectrum. This IR transparency is required in order to fully utilize the emissivity modulation capability of the electrochromic device below the coating.

4.4. Considerations for Technology Infusion

Humans require fine regulation of their thermal condition in order to avoid physical and mental performance degradation (HIDH, 2010; Havenith, 1999; Buckey, 2006). Metabolic heat loads generated in a space suit should be balanced in a nearly one-to-one, real-time manner with heat rejection rates to avoid undesirable fluctuations in body heat storage or depletion, thereby maintaining an acceptable core temperature (HIDH, 2010). In principle, under favorable environments, electrochromic devices are capable of providing this effective load matching capability through active modulation of their emissivity surface properties as described above.

Electrochromics have been previously investigated for their modulation potential (binary high-to-low state emissivity) in spacecraft applications (Demiryont and Moorehead, 2009; Bannon et al., 2010b). These systems were designed and evaluated to accommodate some combination of differences in the external thermal environment and variations in the internal vehicle heat loads, but utilization of intermediate emissivity states has generally not been considered. The dynamic nature of EVA, however, requires a multi-emissivity state architecture capable of dissipating a variable internal load to a dynamic external environment.

Two fundamental heat dissipation control schemes are identified here as potential ways to integrate the full suit electrochromic radiator concept. In the first scheme, electrochromics modulate their surface emissivity to provide steady-state load matching of the current metabolic load to the current local environment flux

conditions. The second control scheme operates through continuous thermal state averaging. In this case, the desired thermal load is rejected as an average of limit high and low dissipation rates. The two thermal control schemes are illustrated in Fig. 4.1. The response to state variation is depicted as being capable of maintaining a constant 300 W of power dissipation and the thermal averaging case cycles between 100 W and 500 W to give a time average 300 W of power dissipation. In either case, the control systems are capable of providing an effective intermediate heat rejection rate that results in near coincident net heat rejection through independent emissivity control schemes.
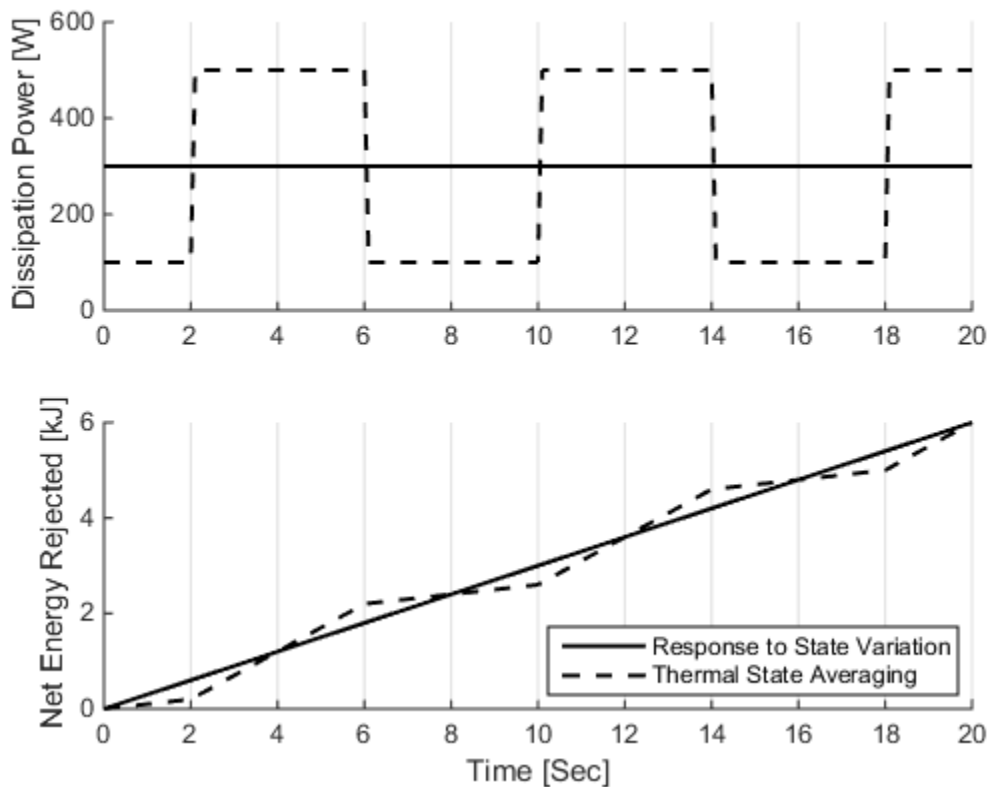
Figure 4.1. Representative response to state variation and continuous thermal state averaging heat dissipation schemes

Two discrete physical integration schemes have been identified for incorporating a full space suit radiator thermal control system, referred to as 'constant temperature' and 'constant flux' options. The nature of the thermal radiation interaction at the suit surface is dictated by the mode of heat delivery. For instance, isolation of the astronaut and the environment can effectively be maintained using a dual-loop architecture. This concept would operate in a similar mode to the current space suit, the EMU, where metabolic loads generated by the crew member are collected within the suit via a Liquid-Cooling and Ventilation Garment (LCVG) worn by the astronaut and directed to the suit's heat rejection mechanism (Harris, 2001). In our case, however, the sublimator would be replaced with a heat exchanger that would then reject the collected thermal load via an external cooling loop to the suit's surface radiator (Metts and Klaus, 2009).

In this case, the LCVG water-loop can be set to a desired comfort temperature, which in turn drives the external-loop radiator temperature. Without defining detailed operational properties of the external radiator loop, a reasonable assumption is that the radiator temperature can be kept approximately constant. This constant temperature radiator scheme allows the use of an LCVG-like approach to maintain adequate human thermal comfort as is achieved in a traditional gas pressure suit (Harris, 2002). Using an LCVG would effectively allow all internal heat loads to be collected and mixed in a common stream that is directed to the heat sink; in this case, a heat exchanger that interfaces to the external suit radiator surface in lieu of a water sublimator. This configuration is

depicted in Fig. 4.2, although a bypass loop might also be incorporated around the heat exchanger for additional thermal regulation.
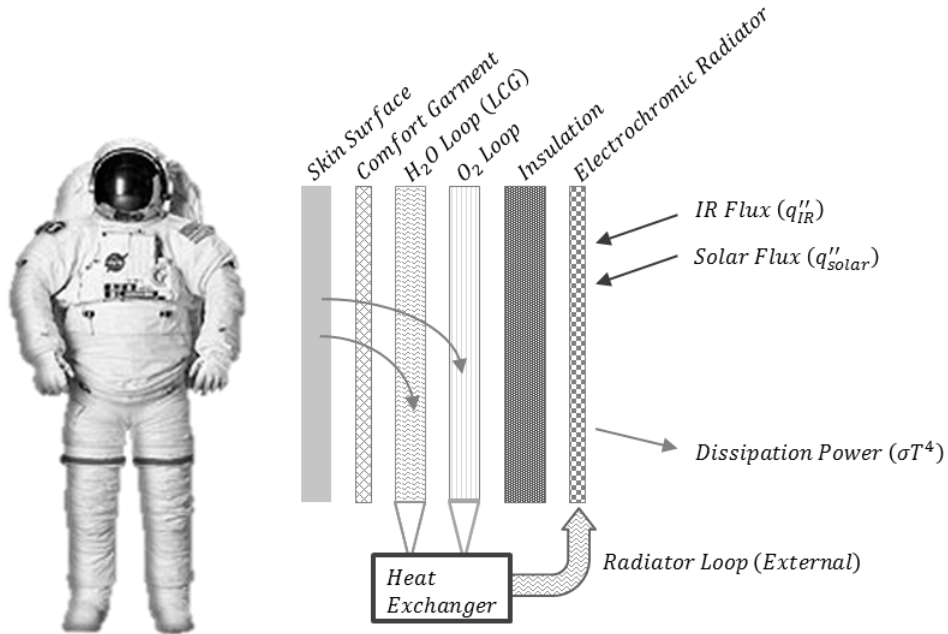
Figure 4.2. The EMU and one constant temperature radiator integration concept. Space suit image credit: NASA. Integration scheme modified from Metts & Klaus (2009).

An alternative suit radiator implementation scheme allows for heat from the astronaut's skin to transfer through the suit wall directly to the external surface material, where it can then be radiated to the space environment. In this configuration, the intent is to proportionally dissipate heat from the local area of the skin where it occurs as an extension of the complex cardiovascular interaction that helps naturally regulate body temperature. For the purposes of this initial evaluation, however, we consider the net metabolic load to be evenly distributed over the entire body surface. This constant flux integration scheme is applicable to utilization in a mechanical counter-pressure suit concept. In this case, where the

suit material conforms to the body in direct contact, locally generated heat can be transported via conductive and/or convective pathways through the material to the surface (Pitts et al., 2001). Once at the surface, it is then rejected to space at a rate that can be regulated by electrochromic modulation. The concept of transferring metabolic heat through a mechanical counter-pressure suit to the environment is depicted in Fig. 4.3. A constant temperature integration scheme can also be utilized in the mechanical counter-pressure suit concept, but is not explicitly considered in this investigation.

Once the radiator integration scheme has been defined, the pixel control mode must be determined. Two fundamental pixel control modes have been identified. The first mode allows individual electrochromic pixels to be discretely driven to intermediate emissivity states by applying a continuously variable voltage source. The second mode utilizes an averaging scheme to achieve an effective net intermediate state by selectively switching pixels to a high or low state over a defined area. To illustrate the difference in these two modes, we examine an electrochromic pixel with an absolute low emissivity state of 0.3 and high emissivity state of 0.8. In Fig. 4.4, a single pixel is driven to five discrete emissivity states by a variable potential. In Fig. 4.5, effective net intermediate emissivity values are achieved by mixing high and low states over the same area.
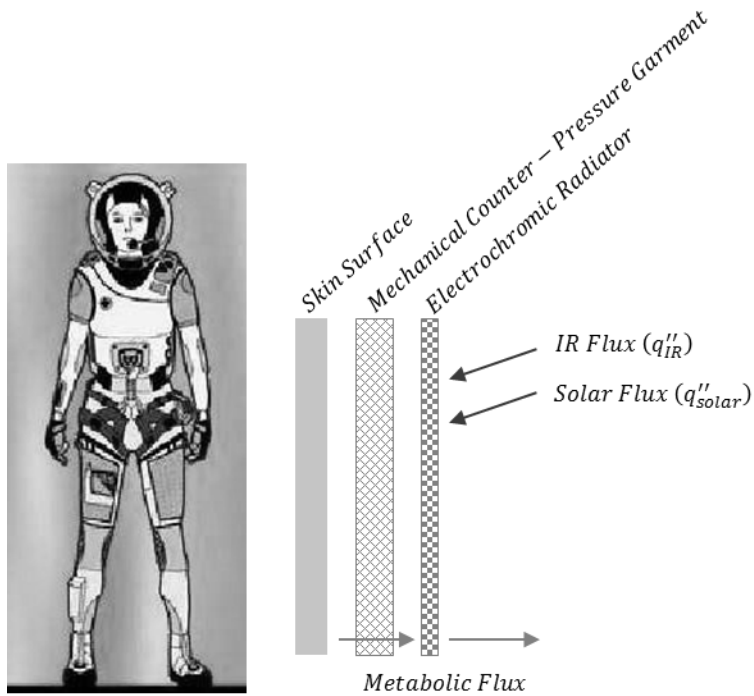
Figure 4.3. Mechanical counter pressure suit concept and constant flux concept. Space suit image credit: Professor Dava Newman, MIT (Used with permission – Illustration: Cam Brensinger). Integration scheme modified from Metts & Klaus (2009).
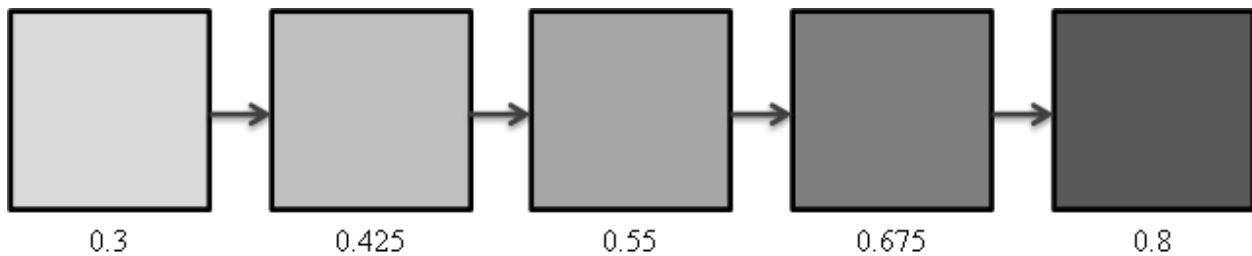
Figure 4.4. Example of intermediate emissivity settings achieved with a variable potential source
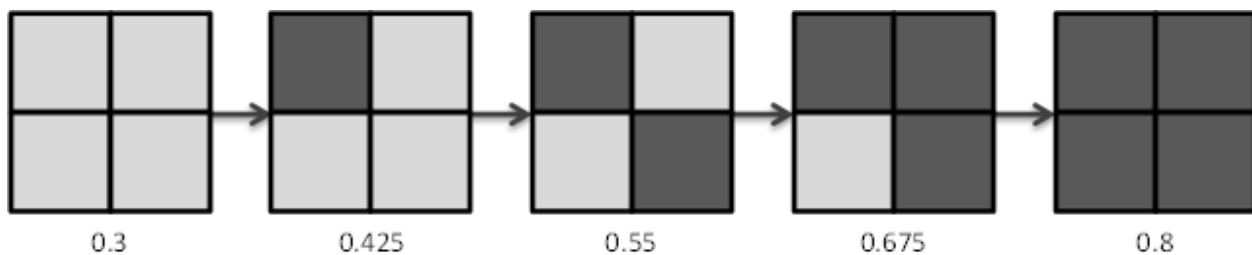
Figure 4.5. Example of effective net emissivity values achieved by high-low state mixing

In order to incorporate an intermediate voltage control mode approach as described above, the required area of each pixel is primarily driven by the properties of the suit-radiator integration scheme and is also dependent on flux variations between adjacent surfaces. In this case, each pixel requires its own variable voltage source to maintain the specified emissivity state. To the best of our knowledge, however, extensive characterization of electrochromic performance robustness in such a variable, intermediate voltage control mode has not yet been accomplished.

In the high-low mixing mode, the desired emissivity resolution will dominate how many pixels are required for a given area. That is, if the energy matching requirement dictates that all fluxes between the maximum and minimum loads be achievable across the suit, an infinite number of pixels would be required to provide a fully continuous spectrum. In reality, pixel area will be determined by some combination of electrochromic performance capacity and allowable temperature gradients. This scheme may allow a reduction in the system's electronics complexity, as independent variable voltage sources could be replaced with relays to a common source.

4.5. Environment Interaction – Methods

Here we establish the remaining parameters used throughout the analysis portion of this investigation. Without the inclusion of a deployable radiator panel, the maximum radiator area is limited to that of the space suit's outer surface. For the constant temperature integration scheme incorporated into a gas pressure suit,

the approximate area of the current EMU, $3.90\ m^2$ $(42.0\ ft^2)$, is used as the total available radiator surface area (Tepper et al., 1991). For the constant flux integration scheme indicated for the mechanical counter-pressure suit concept, the total radiator area available is approximated as the standard mean of the nude body surface area for the projected astronaut population, $1.91\ m^2$ $(20.6\ ft^2)$ (HIDH, 2010). A first-order radiating factor of 0.86 is included to scale each total area to an appropriate exposure area, as was done in Chapter 3. This radiating scale factor is included to account for areas that do not directly view the external environmental sink and are thus unavailable for radiator application (e.g. arm pits, inner thighs) (Massina et al., 2014; Tepper et al., 1991; Guibert and Tayler, 1952). The radiating scale factor is understood to be variable and dependent on suit design, and inevitably affected by specific body postures of the EVA astronaut as they move around and work on the lunar surface.

For both integration schemes described above, the available radiating surface area (multiplied by the general radiating factor of 0.86) is approximated as a single vertical cylinder for simplification as shown in Fig. 4.6. The impact of more complex geometries in future investigations can be assessed using the same principles provided here with higher resolution once a specific suit design is identified. The radii of the representative cylinders are scaled to a height of 1.8 m (~71 in.) to represent a typical astronaut. Circular planes at the top and bottom of the cylinder are not included as contributing to thermal radiation interactions for the purposes of this approximation.
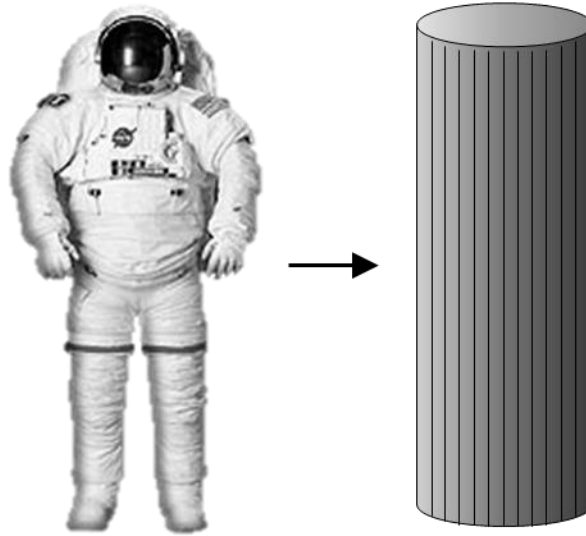
Figure 4.6. Space suit radiator surface area scaled to a cylinder approximation

The lunar pole's local surface features are simplified as an infinite plane with a uniform IR flux (IR) of $5.2 \, W/m^2$. A mean incident solar flux (S) of $1368 \, W/m^2$ is also included for solar contributions to sunlit surfaces (Gilmore, 2002). For this analysis, discretization of the radiator was achieved by dividing the 360° cylinder circumference into uniform strips extending from the top to the bottom of the cylinder with the arc width of each strip initially chosen to be 1°. The interaction of each radiator segment is then contingent on the view factor between the surface IR flux and the incident solar flux. Since no complex, compound, movements are explicitly considered (bending, walking, etc.) each area in this simplified model has a predictable view factor to the environment. Each cylinder area has a uniform view factor to the lunar surface of 0.5, corresponding to a perpendicular strip in contact with an infinite plane (Massina et al., 2014).

The remaining 0.5 of the total view factor is the interaction with deep space. For our purposes this corresponds to an interaction with the sun or the deep space environment, depending on the local orientation of the radiating body. The contribution of the incident solar flux is dependent on the position of the specific radiator area with respect to the incident radiation. A solar incidence angle (β) is introduced to quantify the relative position of the area segment with respect to the sun. Here we consider the effective suit subsolar point to be at $\beta = 90°$ which, in turn, corresponds to a sine function distribution of solar flux across the sun-facing portion of the suit. The result is that suit radiator segments from $0°$ to $180°$ have some level of exposure to solar flux and the remaining segments are effectively shaded from all incident solar radiation as illustrated in Fig. 4.7. Due to the selected lunar EVA position, albedo effects are not included. In addition, the negligible flux to deep space is assumed to be zero and therefore not included. A summary of the different thermal flux contributions for a given area segment i is provided below.

Approximate Lunar Pole Flux Environment:

For $0° > \beta > 180°$

$$q''_{IR,i} = VF * IR = 2.6 \, W/m^2 \tag{4.1}$$

$$q''_{solar,i} = VF * S * \sin(\beta) \tag{4.2}$$

For $181° > \beta > 360°$

$$q''_{IR,i} = VF * IR = 2.6 \, W/m^2 \tag{4.3}$$

$$q''_{solar,i} = 0 \tag{4.4}$$

The cylinder approximation illustrates how incident flux variations affect pixelation guidelines. Under the definition used, only half of the suit has to accommodate local variations in environmental thermal conditions at any given time. However, the most restrictive cases must be applied to the suit as a whole, since the astronaut could be completing EVA tasks at any orientation relative to the incident fluxes. That is, the suit's effective subsolar point could be located at any position on the suit depending on the astronaut's position and orientation toward the sun (e.g. back versus front facing).
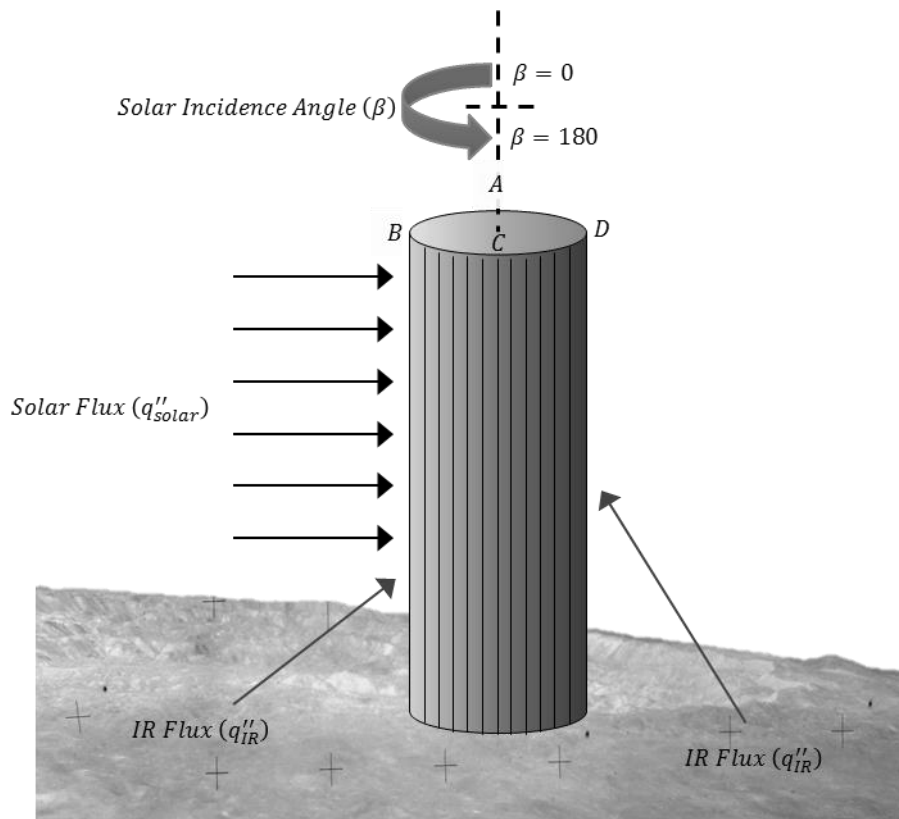
Figure 4.7. Cylinder area approximation's interactions with the lunar pole environment. A, B, C, and D correspond to β angles at 90° increments starting with A = 0°

This investigation considers radiator pixelation guidelines for three metabolic rates: a low metabolic rate of 100 W (341 BTU/hr), a nominal metabolic rate of 300

W (1024 BTU/hr), and a sustained high metabolic rate of 500 W (1706 BTU/hr). These conditions provide a reasonable range of what might be expected during a lunar EVA (HIDH, 2010). Constant radiator temperatures are approximated from the LCVG water inlet temperature automatic cooling control function described by Farrington et al. (2005). Constant flux integration is assumed to take place through a garment of zero mass and zero thermal resistance. As a result, the radiator's temperature is taken to equal the astronaut's skin temperature for the given metabolic rate. This assumption also dictates that the performance of adjacent areas will not impact one another as no heat transfer is allowed between them at the garment level. Nominal and limit mean skin temperature comfort guidelines provided by Chambers are used as first-order acceptability criteria for evaluating this integration scheme (Chambers, 1970).

4.6. Pixel Area Determination and Illustration

The fundamental governing equation for the net radiative power is given in Eq. 4.5. For the *i'th* pixel, σ is the Stefan-Boltzmann constant $\left[5.67x10^{-8}\frac{W}{m^2K^4}\right]$, A_i is the area, T_i is the temperature, ϵ_i is the emissivity, α_i is the absorptivity, $q''_{IR,i}$ is the incident infrared heat flux, and $q''_{solar,i}$ is the incident solar heat flux. Ideally the net heat rate rejected (q_{net}) equals the net heat being generated within the suit. In the event that internal loads cannot be accommodated by a purely radiator-based system, some additional thermal control mechanisms may be required to maintain the thermal balance. With this assumption, therefore, transient dynamics of energy storage by the human or system are not explicitly considered in this investigation.

$$q_{net} = \sum_{i=1}^{n} A_i q''_{net,i} = \sum_{i=1}^{n} A_i \left(\epsilon_i \left(\sigma T_i^4 - q''_{IR,i} \right) - \alpha_i q''_{solar,i} \right) \tag{4.5}$$

4.6.1. Constant Temperature Radiator Integration

The selected radiator integration approaches described earlier largely dictate the pixelation guidelines for a given EVA environment. For the constant temperature radiator integration scheme, the net flux out of a given pixel is determined by the IR power potential $\left(\sigma T_i^4 - q''_{IR,i} \right)$, scaled by the selected emissivity (ϵ_i), and further reduced by the amount of solar energy entering through that pixel $\left(\alpha_i q''_{solar,i} \right)$.

The distribution of radiative power for each pixel segment on the suit's surface while at a constant temperature is provided in Fig. 8. The trend across the 0° to 180° suit segments indicates the impact of incident solar flux absorption over those regions. Suit area indicators *A, B, C,* and *D* in Fig. 4.8 correspond to those defined in Fig. 4.7. The net dissipation over the entire suit is the sum of the contributions of each radiating segment. The radiative distribution, with variation in emissivity for each of the three operating temperatures, is calculated via Eq. 4.5 and shown in Fig. 4.9. The approximated radiator temperatures used were 296.3 K (73.71 °F), 293.7 K (69.02 °F), and 288.3 K (59.20 °F) for the 100 W, 300 W, and 500 W metabolic rate cases, respectively. These values were taken directly from Farrington's optimization of liquid cooling garment water temperature for various metabolic rates (Farrington et al., 2005).
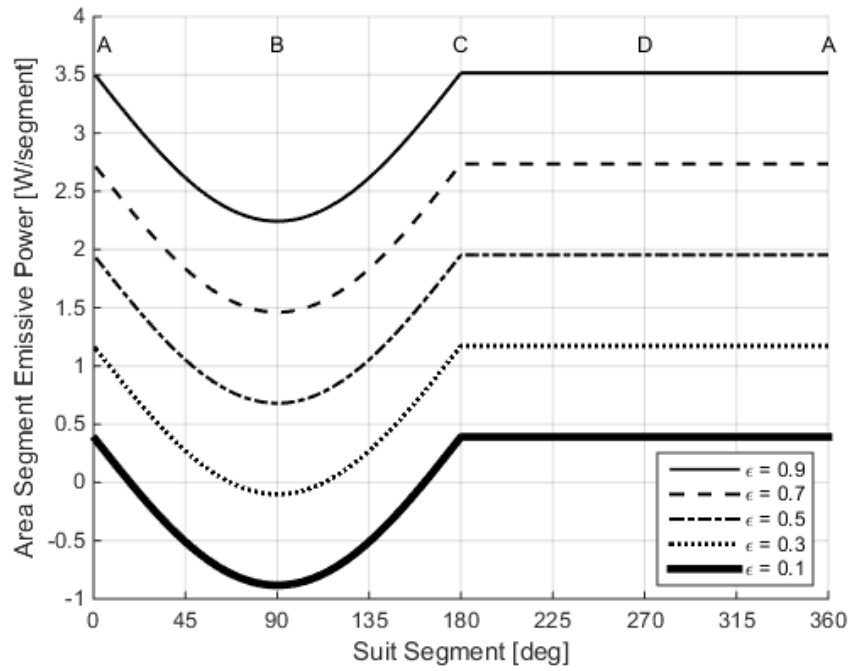
Figure 4.8. Radiative power distributions across suit segments, 293.72 K (69.02 °F)
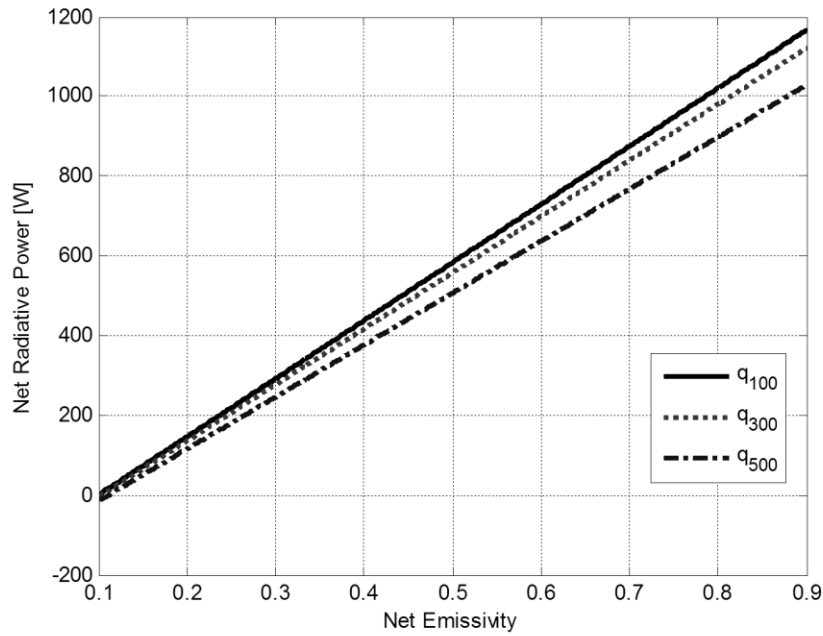
Figure 4.9. Radiative power distributions with variation in emissivity and radiator temperature

Figures 4.8 and 4.9 effectively show that there is no net benefit to discretization of electrochromic pixels in the assessed environment when the heat load is collected and allowed to supply a constant radiator temperature. That is, a single electrochromic setting is capable of dissipating the selected metabolic load range via radiation from the suit walls without additional intervention. However, the single electrochromic must be capable of supplying any intermediate emissivity state such that the required heat rejection rate between the minimum and maximum can be reliably achieved. Additional pixelation in the constant temperature integration scheme comes only from the necessity to achieve an effective intermediate emissivity state in the mixed high-low pixel control mode or to reduce the influence of external IR heat loads. If $\sigma T_i^4 < q''_{IR,i}$ for some areas and $\sigma T_i^4 > q''_{IR,i}$ for other areas, additional pixelation could be implemented to reduce the quantity of excess IR energy absorbed. This condition is not experienced in the evaluated lunar pole environment, however.

The performance of a variable emissivity, suit radiator-based thermal control system is contingent on the local heat flux environment, achievable IR emissivity modulation capabilities of the electrochromics, and how the electrochromic pixels are controlled (either continuously variable or high-low state mixing). Ideally, the electrochromics would be capable of providing the required emissivity range for the desired net power rejection requirement; however, some environmental conditions may result in saturation of emissivity settings beyond physically achievable limits of the device. Consequently, emissivity saturation would correspond to either a net

retention or expulsion of energy which results in a thermal imbalance that could lead to astronaut performance degradation and ultimate health concerns. The minimum emissivity case is defined by the full suit emissivity requirement at 100 W of heat rejection. Here, the radiator operates at its highest temperature and is rejecting heat from the lower limit metabolic rate. For our test environment this corresponds to an emissivity of ~0.169. The maximum emissivity state is defined by the full suit emissivity requirement at 500 W of heat rejection. This is where the lowest radiator temperature is required for astronaut thermal comfort but is rejecting the upper limit metabolic heat rate. For the examined environment this corresponds to an emissivity of ~0.495.

If intermediate emissivity states are not achievable using a single electrochromic pixel setting via control voltage selection, either thermal load averaging or an alternative steady-state load matching architecture must be included to provide a full range of net heat dissipation rates (see Fig. 4.1 and Fig. 4.5). While thermal load averaging is achievable in this configuration using a single pixel; additional pixelation is required for steady-state load matching to be viable. With high and low emissivity limits established, the amount of pixelation needed can be determined from the emissivity resolution (ϵ_{res}) required by the system developer. The emissivity resolution, therefore, must take into account how closely the radiative heat dissipation rate must match the intermediate metabolic load generation. That is, the definition of an acceptable effective emissivity increment,

with its resolution in terms of number of individual pixels, depends on how closely heat rejection needs to match the real-time metabolic loads.

To illustrate this consideration, we selected a 10 W dissipation interval to establish a first-order pixel quantity estimate. This assumption means that regardless of the actual metabolic load within the established high-low bounds, the dissipation rate can be set to ± 5 W of the required heat rejection. The linear relationship defined by the radiative power distribution of Fig. 9 is used to establish an allowable emissivity increment for the 10 W steps. These resolution values for the 100 W, 300 W, and 500 W cases evaluated are 0.00686, 0.00711, and 0.00767 respectively. Equation 4.6 is then solved for each metabolic case and the highest pixel quantity is used as the baseline. For the assumptions used in this evaluation, the 100 W metabolic case results in the largest quantity of pixels at a value rounded up to 48.

$$\#pixels = \frac{\epsilon_{high} - \epsilon_{low}}{\epsilon_{res}} \tag{4.6}$$

With the 48 pixel estimation based on the overall suit dissipation performance, it's important to discuss the orientation of the pixelation. If one were to consider pixelation in the vertical sense, a single pixel in this case would occupy ~7.5° of suit arc. From Fig. 4.8, however, one expects non-uniform heat dissipation with vertical suit area, as a pixel's net flux depends on its orientation with respect to the sun. The result being that the selection of a high or low pixel state becomes iterative in order to find the appropriate level of net heat rejection modulation over the entire suit area.

Instead, if each pixel is wrapped around the circumference to form a ring of electrochromic material, the integration will more closely approximate the control concept depicted in Fig. 4.5. Each vertical strip essentially sees a uniform flux from the top to bottom of the cylinder. Since the temperature of the radiator is approximately constant, the emissivity modulation is the only variable in Eq. 4.6 changing per segment. If each pixel ring is the same, a one-to-one area average of the mixed emissivity provides the required variation defined by the emissivity resolution. The 49 emissivity states then map directly to the net rejection profile shown in Fig. 4.9 for a given radiator temperature; again, with the only difference being the discrete steps between states rather than the continuous spectrum.

These results show that the constant radiator temperature architecture is feasible using either an electrochromic area that can be set to intermediate emissivity states or by mixing high-and-low emissivity states in our simulated operational environment. Definition of specific dynamic interactions between an astronaut, the suit radiator, and the external environment are warranted to further define required performance properties of the thermal control system.

4.6.2. Constant Flux Radiator Integration

In the constant flux integration scheme, the primary factor for establishing the first-order electrochromic pixel resolution is variation in the external environment on adjacent surfaces. In this case, we let the constant flux for each radiator segment dictate the operational temperature required by the particular segment. For example, if a single emissivity setting were to be used over the whole

suit in this configuration, hot and cold spots would be experienced in order to achieve the constant flux, which would directly translate to skin temperature underlying each segment. This is illustrated in Fig. 4.10 for a total area representative of integration into a mechanical counter-pressure suit. These results show that no single emissivity setting can provide a comfortable skin temperature across the entire suit surface in the evaluated environment in this configuration. Instead, pixel areas and emissivity settings must be chosen such that acceptable skin temperature comfort conditions can be maintained under all suit surfaces, described as follows.
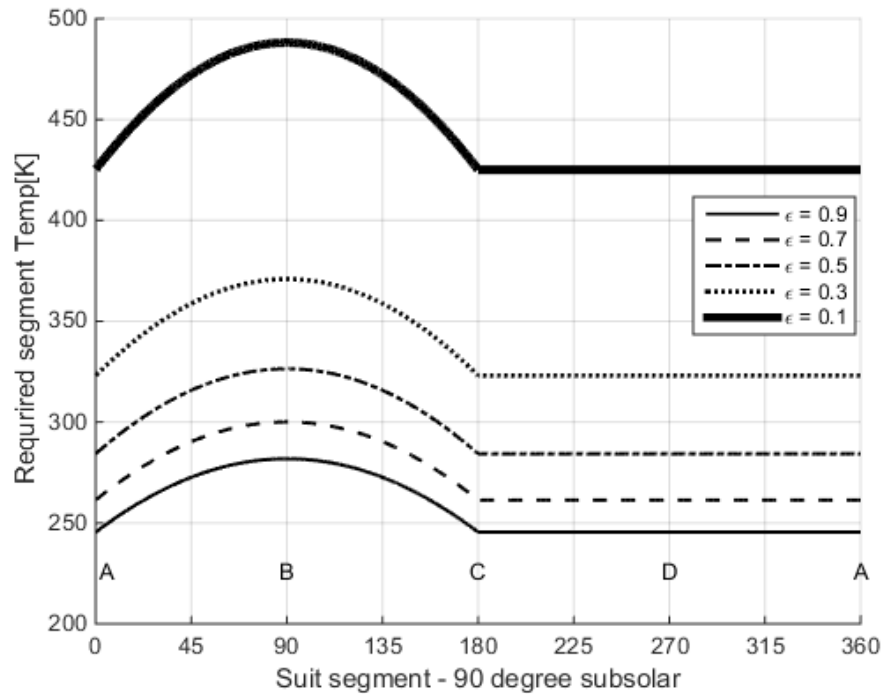
Figure 4.10. Suit temperature requirements for constant flux segment dissipation, 300 W

Here we use the mean skin temperature comfort guidelines described by Chambers (1970) in Fig. 2.3 to define a reasonable skin temperature comfort band

for a given metabolic rate. The resulting emissivity setting spectrum for a 300 W metabolic load is provided in Fig. 4.11. The necessary emissivity profiles of each metabolic case are provided in Fig. 4.12. The bulk separation of the segmented emissivity settings for each metabolic load case are the result of both variations in required flux dissipation per segment and variations in allowable surface temperatures described by the defined comfort guidelines.

The definition of these acceptable hot and cold skin temperature limits allows for first-order pixelation guidelines to be established for this conceptual integration scheme. In reality, a single selected emissivity set point may have the potential to provide an acceptable temperature condition for some adjacent number of suit segments. Using our simplified cylindrical geometry, allowable pixel size corresponds to the total degrees any one pixel can occupy before the comfort band is exceeded at a given emissivity. For example, in Fig. 11, near the suit local subsolar point ($\beta = 90°$) a single emissivity value provides an adequate temperature range for segments between 70.6° and 109.4°. However, because the suit can be located at any orientation to the sun (e.g., as the representative cylinder model is rotated, the sunlit flux profile moves to a different part of the suit) the most restrictive acceptable pixel area is defined as the maximum allowable pixel size. From Fig. 4.12, one finds this most restrictive case of pixel size to be for constant dissipation of 100 W. This restriction occurs near the edges of the sunlit side (0° and 180° in our illustration) and calls for a pixel arc length of ~0.9°. This arc length indicates ~400

pixels around the cylinder would be required for the constant flux integration scheme to be feasible.[10]
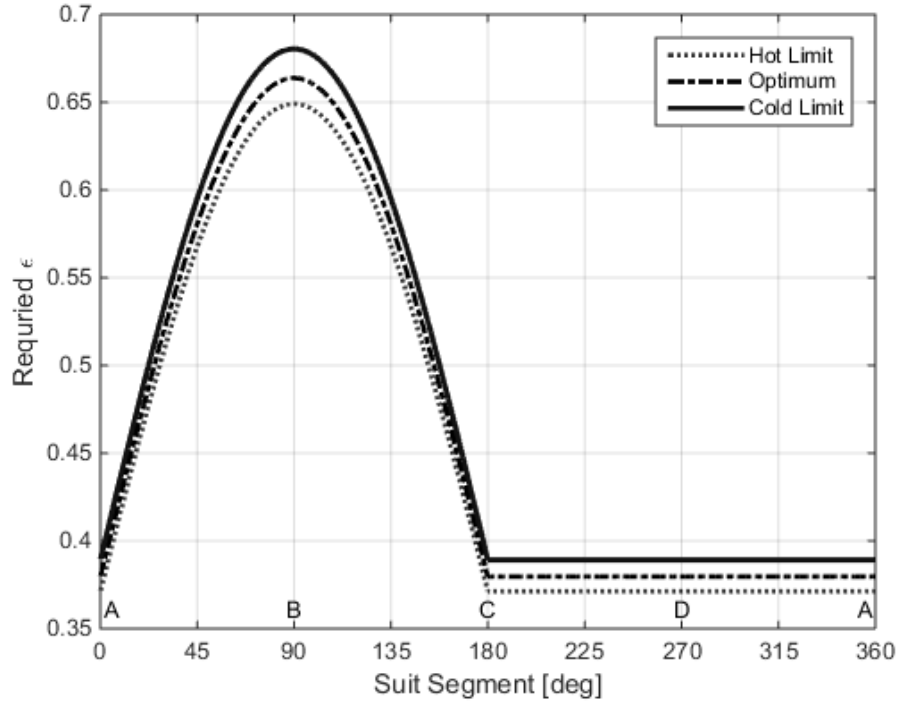
Figure 4.11. Emissivity setting requirements for constant flux at a lunar pole at 300 W of constant dissipation

---

[10] This is only pixelation required for vertical strips around the cylinder. This also applies to individual appendages in a suit with more complex geometry.
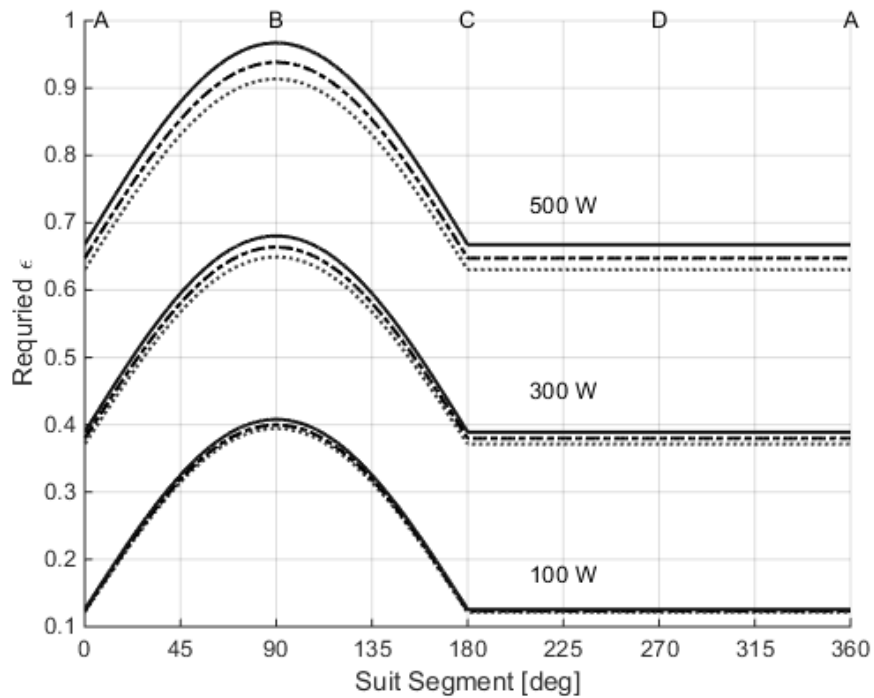
Figure 4.12. Emissivity setting requirements for constant flux in lunar pole environment

In addition to the pixelation guidelines described above, performance-driven design requirements for the electrochromic devices can also be extracted for this case. The maximum and minimum emissivities required by the investigated environment are ~0.967 and ~0.122. This emissivity variation of 0.845 provides an effective radiator energy turndown ratio of ~5:1 in the evaluated environment. That is, the system can be tuned to dissipate either 500 W or 100 W, simply by changing the radiator's emissivity set point. Although these emissivity values fall within theoretical limits of 0 and 1; to the best of our knowledge, no electrochromic device tested to date has demonstrated broadband emissivity modulation of this magnitude (Chandrasekhar et al., 2002; Kislov et al., 2003; Ashwin-Ushas Corp.; Bannon et al., 2010b; Demiryont and Moorehead, 2009; Chandrasekhar et al.,

2014). Therefore, advances in electrochromic state-of-the-art performance may need to accompany future space suit design efforts incorporating this thermal control approach.

In addition to determining the range of emissivity settings required, insight pertaining to emissivity control accuracy can also be extracted from these results. The total acceptable emissivity difference for each of the heat rejection cases is shown in Fig. 4.13. These tolerance thresholds represent another technology challenge associated with utilizing electrochromics in this manner – emissivity settings must be controllable across a range with a maximum of 0.054 and a minimum of 0.004 depending on the current metabolic condition.
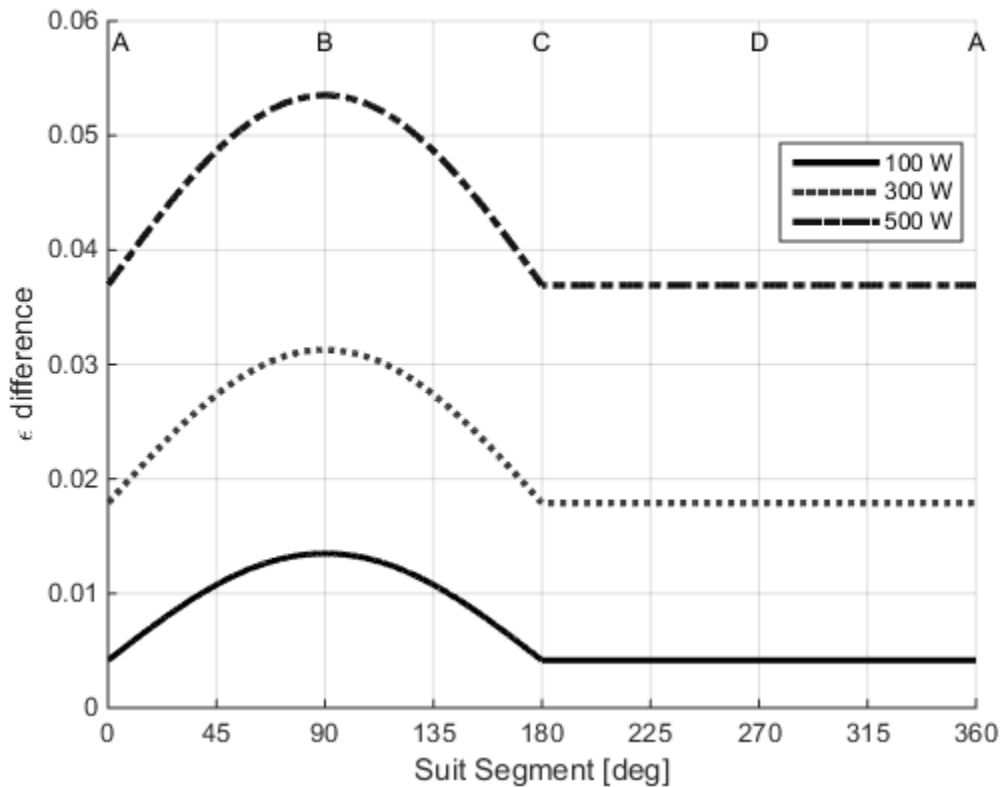
Figure 4.13. Allowable total emissivity variations for thermal comfort

Given the one-dimensional heat transfer assumptions used to evaluate the properties of the constant flux integration approach, the high-low emissivity mixing scheme was found to not be feasible. This is due to the introduction of unacceptable local hot and cold spots. However, this limitation of the high-low emissivity application may be overcome if the counter-pressure garment can sufficiently distribute these temperature gradients via lateral conduction in the material. As further design considerations such as this are included, the specific properties of a counter-pressure material will inevitably affect the performance requirements of the full suit radiator concept and will need to be modeled in more detail to assess ultimate feasibility.

4.6.3. Discussion

The selected EVA operational environment dictates the feasibility for incorporating each of the integration architectures in this first-order approximation. With a constant radiator temperature, allowable operational environments are restricted by the temperature potential provided by the radiator (Massina et al., 2014). For constant flux integration, operational environments are restricted to those that balance metabolic loads with heat rejection requirements to provide the required skin comfort condition over the entire suit surface. The already large range in required emissivity settings needed for constant flux integration suggests that this integration scheme will no longer meet the established dissipation requirements in higher flux (e.g., hotter) regions of the moon. Additionally, evaluation of realistic suit geometries will introduce additional complexity to the

environmental interactions and inevitably require greater pixilation for the constant flux case. The introduction of more complex geometries also applies to the lunar surface topography beyond the simplified flat plane used here. Future investigations should include a dynamic environment simulation tool to provide a higher fidelity assessment of the architecture's feasibility (Hager, 2013; Hager et al., 2014; Hager et al., 2015).

4.7. Summary

The use of variable infrared electrochromic devices to actively control heat rejection from a full space suit radiator system appears to remain feasible after introducing more complex environmental interactions beyond those used in previous investigations. A simplified space suit geometry and lunar pole environment was used to illustrate the impacts of incorporating different heat transfer pathways and electrochromic material integration techniques. The constant radiator temperature integration architecture was shown to be capable of utilizing one, full suit electrochromic pixel if the full range of required emissivity values is achievable, or ~48 pixels if high-low emissivity mixing is implemented. Under the evaluated conditions, electrochromic devices in the constant temperature architecture must provide an emissivity range of 0.169 to 0.495.

The constant flux radiator integration architecture was found to be more sensitive to incident heat flux distribution and required ~400 pixels if a controlled, variable emissivity electrochromic device could be utilized. Electrochromic devices in the constant flux architecture must provide an emissivity range of 0.122 to 0.967.

Constant flux, high-low emissivity mixing was not considered here because of the local hot and cold sections that are introduced without including lateral suit wall conduction.

Related Output Publication:

Massina, C.J. and Klaus, D.M. (2015). Defining a Discretized Space Suit Surface Radiator with Variable Emissivity Properties, *J. Thermal Science and Engineering Applications*, 7(4), 041014-041014-9, doi: 10.115/1.4041132.

CHAPTER 5

Evaluation of Radiators with Discretized Emissivity Properties

5.1. Abstract

In this chapter, the performance characteristics of radiators with two distinct emissivity states selected over four discretized area sections are evaluated. The low emissivity state was supplied by the surface finish of the test articles ($\epsilon = 0.34$ or 0.38), while the high emissivity state was provided by coating selected areas with a high emissivity paint ($\epsilon = 0.98$). The two test articles were constructed from different materials, aluminum 6061 and stainless steel 304, in order to illustrate performance variations resulting from differences in thermal conductivity. The adopted approach allowed the experimental evaluation to reproduce variations in emissivity that could be supplied by a variable infrared emissivity electrochromic device, while reducing the uncertainty associated with testing of currently available devices. The results showed that mixing emissivity states of a radiator provides an area-averaged intermediate emissivity state regardless of the thermal conductivity or heat input scheme to the substrate material. However, as shown in the previous chapter, mixing the emissivity states of a radiator operating under a constant heat flux can result in potentially unfavorable temperature variations across the surface of a substrate material that has low thermal conductivity.

5.2. Introduction

Radiators with selectable surface properties will provide spacecraft and space suit designers with the ability to increase the range of environments that their vehicles can operate within. Ideally, spacecraft thermal control can be achieved through purely passive techniques, such as radiators with static property surface coatings (Gilmore, 2002). However, secondary mechanisms such as heaters, thermal switches, louvers, and phase change materials are often required due to variations in spacecraft heat-generation and/or external environments. In the contemporary EMU space suit, key thermal control mechanisms include insulation, heaters, and a water ice sublimator to keep the EVA astronaut comfortable (Larson and Pranke, 1999; Harris, 2001). In both spacecraft and EVA applications, including robust variable heat rejection mechanisms into the vehicle's thermal control system can decrease consumable losses, reduce overall system complexity, and increase the operational envelope of the vehicle (Metts et al., 2011; Hill et al., 2012).

Variable IR emissivity electrochromic materials are one technology capable of providing variable heat rejection for spacecraft and EVA systems. Several studies have demonstrated the broadband IR emissivity (emittance) modulation potential of these materials (Chandrasekhar et al., 2002; Kislov et al., 2003; Hale and Woollam, 1999; Demiryont and Morehead, 2009; Bannon et al., 2010b; Chandrasekhar et al., 2014), and have considered their use in a variety of space applications ranging from CubeSats to the Altair lunar lander. In addition to rigid vehicle mounted concepts, integration of electrochromics onto the exterior of a space suit has been shown to

theoretically provide a reduction in consumable losses during EVA (Metts et al., 2011; Metts & Klaus, 2012).

Fundamentally, electrochromic based suit radiator architectures will operate in either a constant temperature or constant heat flux scheme (Massina and Klaus, 2015). The complex dynamic interaction of a space suit with the local environment requires that an electrochromic system be capable of achieving a wide range of emissivity set points in order to actively maintain the astronaut's thermal balance. Intermediate emissivity states, those between maximum and minimum achievable values, could be provided through appropriate voltage selection or by mixing the emissivity states of adjacent pixels.

Several previous tests of electrochromic materials have focused on demonstrating the performance potential of the devices in thermal vacuum environments (Demiryont and Moorehead, 2009; Bannon et al., 2010b; Chandrasekhar et al., 2014). These tests primarily emphasized the identification and demonstration of the maximum emissivity transition achievable by the evaluated electrochromic device. The variability of the achieved high and low emissivity states within those evaluations illustrates the current inconsistency of performance in current state-of-the-art electrochromic devices.

In electrochromic devices, the change in IR properties is a function of the device's composition and the applied voltage potential across the electrochromic film (Granqvist, 1995). For a given device, a discrete voltage potential will generally

yield a consistent output emissivity state regardless of the previous setting.[11] However, to our knowledge, electrochromic performance using intermediate voltages over many cycles has yet to be characterized.

This evaluation provided proof-of-concept for the operational potential to mix emissivity states of adjacent areas to achieve an intermediate emissivity state between the limits of the surface coatings or electrochromic potential as described in chapter 4. Thermal surface finishes with fixed emissivity properties were used to approximate emissivity states that could be supplied by an electrochromic device. This approach reduced the uncertainty associated to testing with currently available devices and allowed the modeled performance to be more readily compared to the measured performance of a given configuration. Test articles were constructed from aluminum 6061 and stainless steel 304 to determine differences in performance associated with the thermal conductivity of the substrate material. Calorimetry was used to determine the radiative surface properties of each test article configuration. The resulting operational potential is discussed in relation to its impact on space suit thermal control system performance.

5.3. Background and Method

Calorimetry in a thermal vacuum environment is a widely accepted method for determining radiative surface properties (Mychkovsky and Ponnappan, 2005; ASTM, 2010; Bannon et al., 2010b; Gaier et al., 2010; Chandrasekhar et al., 2014). Heat dissipation from the test coupon is constrained to radiation in thermal vacuum

---

[11] Personal communication, Prasanna Chandrasekhar, Ashwin-Ushas Corporation, 23 March 2014.

testing by removing the convection potential and limiting conductive heat paths away from the test article. Under steady-state conditions, the pertinent variables can be measured and used to characterize the radiative properties of the test article. Equation 5.1 describes the emissivity of a surface in relation to the heat load and environment (Bannon et al., 2010b), where ϵ is the empirically derived broadband IR emissivity, Q_{in} is the total test article heat input, Q_{loss} is the amount of heat lost from sources other than radiation from the test article's front surface (contributions from view factors, edges, and conductive pathways), V is the voltage applied to the heater(s), R is the resistance of the heater(s), A is the test article area, σ is the Stefan-Boltzmann constant, T_{surf} is the test article surface temperature, and T_{sink} is the environmental sink temperature.

$$\varepsilon = \frac{Q_{in} - Q_{loss}}{\sigma A\left(T_{surf}^4 - T_{\sin k}^4\right)} = \frac{V^2\big/R - Q_{loss}}{\sigma A\left(T_{surf}^4 - T_{\sin k}^4\right)} \tag{5.1}$$

In this evaluation, Eq. 5.1 was modified to reflect the potential for different heat inputs and temperatures across the test article. The result is Eq. 5.2, used across all tests to calculate the effective net emissivity of the given configuration. The net heat loss term was neglected due to the test article's construction and mounting scheme. Test results also showed that empirically derived emissivity values were consistent with those expected, which increased the confidence in the assumption that heat losses were negligible. The resistance of each heater element was taken at the start of every run with a Fluke 87V multimeter. Heater voltages were taken with the same device each time the power supply settings were changed.

$$\varepsilon_{net} = \frac{\sum \left(V_i^2 / R_i \right)}{\sigma A \left(\overline{T}_{rad}^4 - T_{\sin k}^4 \right)}$$

<div align="right">(5.2)</div>

The standard assembly of a test article is shown in Fig. 5.1, and is based on the test article construction of Bannon et al. (2010b). The configuration features a guard plate which acts to reduce radiative heat transfer, and thereby uncertainty, from the uncoated (non-test, back) side of the plate. The guard plate was controlled to have a temperature approximately equal to the primary test article. By controlling the temperature difference between the two plates to ±2 °C, radiation and conduction heat transfer between the primary test article and guard plate was minimized or eliminated.

Each test article has a 4"x4" (10.16 x 10.16 cm) surface area divided into four discrete 1"x4" (2.54 x 10.16 cm) sections which are either coated to provide a high emissivity or left uncoated to have a low emissivity. Each discrete section also has an independent heater. This allowed the test articles to be evaluated under either a constant heat flux input or nearly constant surface temperature condition. Again, this depended on the suit integration concept, introduced in Chapter 4, and the material under evaluation. The high emissivity state provided by coating selected areas of the radiator's surface with Krylon flat white spray paint having an IR emissivity of ~0.98 (Infrared Thermography, ret. 2015). The low emissivity state was provided by the uncoated aluminum or stainless steel test articles' surface properties. Each material's baseline low emissivity value was obtained via the same thermal vacuum test protocol as when coated.

Figure 5.1. Test article, front and back. Primary test surface has 4 independently controlled 1"x4" (2.54 x 10.16 cm) heaters (right), aluminum tape is included to reduce potential for heater-damaging hot spots.

5.3.1. Test Article Preparation

Both the aluminum and the stainless steel test article plates were constructed and finished using the same process, which is outlined below.

1. Outer dimensions and thru features machined with precision waterjet

2. Thermocouple mounting channel machined into the rear surface

3. Scotch-Brite ('ultra fine' 7448 followed by 'light duty' 7445) to remove major imperfections on the radiator's surface

4. Ultrasonic cleaned to remove remnant material

5. Measured outer dimensions to ±0.001" (0.025 mm) and mass (not used in calculations)

6. Measured surface roughness with a Mahr Pocket Surf IV (SS 304 = 14 µm/µinch and Al 6061 = 22 µm/µinch)

7. Aluminum tape used to secure thermocouples in appropriate locations to within ±1/16"

8. Heaters placed on back side of test article (over the thermocouple channel)

9. Aluminum tape placed over single heater strips ensure uniform heat deposition

10. Test article attached to the guard plate with nylon fasteners

In step 4 of the preparation sequence, the test articles were cleaned together in a Liquinox/deionized water bath. The use of deionized water contributed to the oxidation and resulting degradation of the surface properties (increase in emissivity) of the aluminum test plate. The degradation resulted in a baseline aluminum emissivity of ~0.38. This value was then consistent with the obtained baseline stainless steel emissivity of ~0.34.

5.3.2. Test Flow

Each test article was evaluated in the same manner, and the basic progression is provided below. For constant heat flux test conditions, a total heat flux of ~1.55 W was used. This value roughly scales to a nominal EVA metabolic rate of 300 W for a crew member with a total radiating surface area of 2 m^2. The high thermal conductivity of aluminum resulted in nearly uniform plate temperatures regardless of the surface coating configuration. The thermal properties of the stainless steel test article resulted in significant thermal gradients in partially coated configurations. As such, a constant temperature test case was run independently for the stainless test article. The target temperature for each of those test conditions was 10 °C. Figure 5.2 shows the 4 different configurations as

tested in the thermal vacuum chamber. A diagram and photo of the test apparatus integrated into the vacuum chamber is provided in Fig. 5.3.
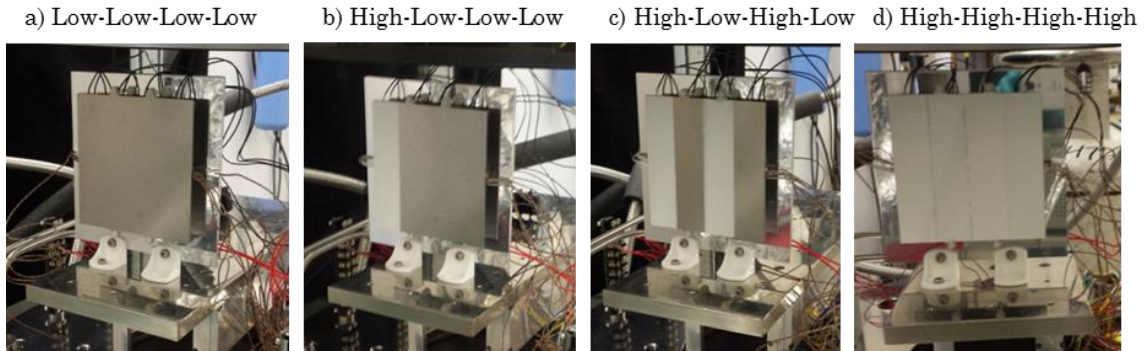
Figure 5.2. Test article configurations
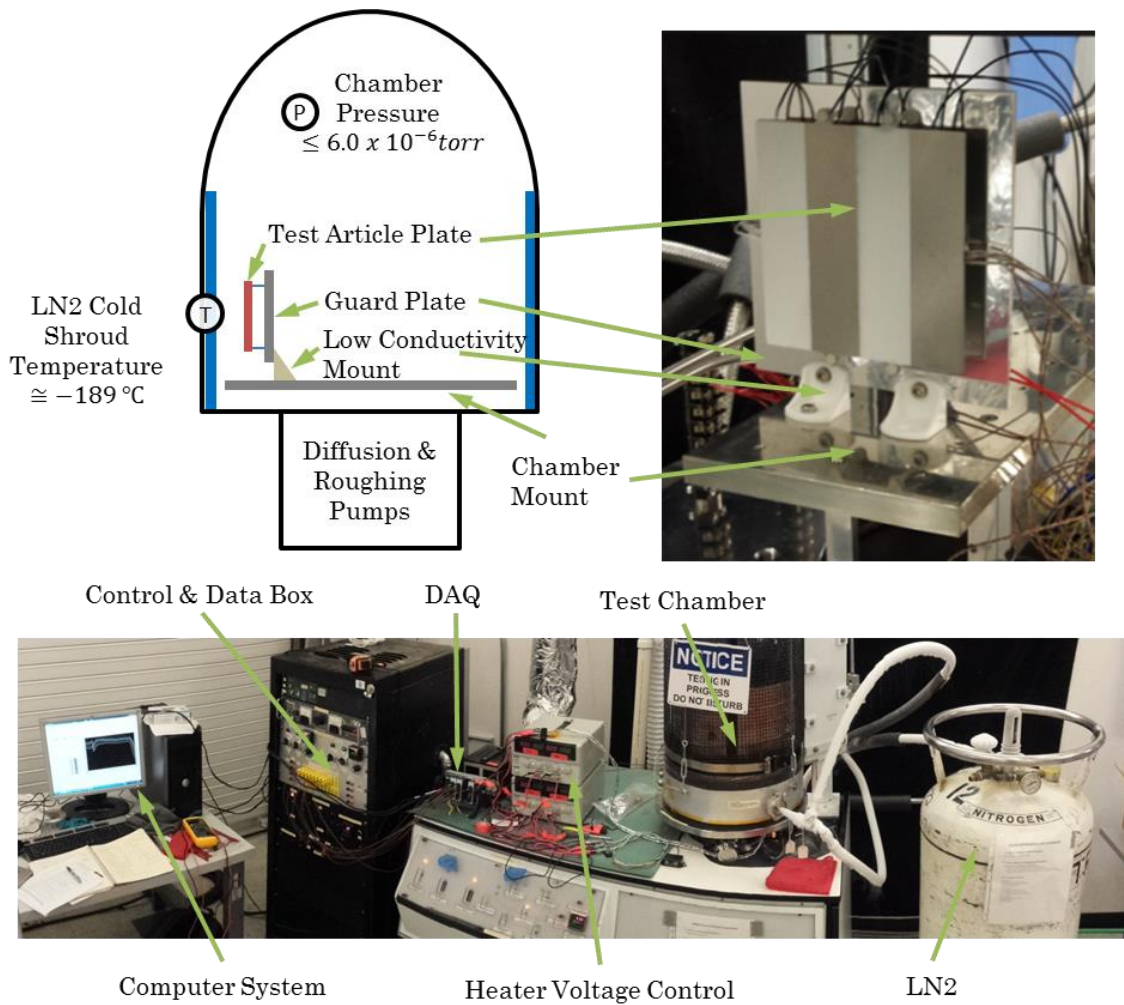
Figure 5.3. Test article configuration and general laboratory layout

Test Progression:

1. Baseline low emissivity state (uncoated) obtained in thermal vacuum

2. First 1"x4" (2.54 x 10.16 cm) section coated with Krylon Flat White Paint (4 passes)

3. Evaluation of single section with high emissivity coating in thermal vacuum

    a. Heaters used to supply constant total heat flux of ~1.55 W

    b. Heaters used to supply constant temperature (stainless steel)

4. Second 1"x4" (2.54 x 10.16 cm) section with Krylon Flat White Paint (4 passes)

5. Evaluation of dual section with high emissivity coating in thermal vacuum

    a. Heaters used to supply constant total heat flux of ~1.55W

    b. Heaters used to supply constant temperature (stainless steel)

6. Remaining low emissivity sections coated with Krylon Flat White paint (4 passes)

7. Fully coated test article tested in thermal vacuum to obtain verification of high emissivity state at uniform operating temperature

8. Each test article underwent an ice bath immersion to provide a 0 °C thermocouple calibration test point

5.3.3. Experimental Uncertainty

The effective emissivity value for each test case was calculated via Eq. 5.2. Presented with that value is the associated experimental error that was calculated through the standard multivariable method for random errors found in Eq. 5.3

(Taylor, 1997). The primary sources of uncertainty were introduced by the power input calculation and the thermocouple measurement accuracy. These uncertainties were largely a consequence of the limitations of the facility. Namely, the vacuum chamber was limited to temperature collection with Type K thermocouples. No provision for higher accuracy data collection devices was available.

$$\delta\varepsilon = \sqrt{\left(\frac{\delta\varepsilon}{\delta V}\delta V\right)^2 + \left(\frac{\delta\varepsilon}{\delta R}\delta R\right)^2 + \left(\frac{\delta\varepsilon}{\delta A}\delta A\right)^2 + \left(\frac{\delta\varepsilon}{\delta\bar{T}_{rad}}\delta\bar{T}_{rad}\right)^2 + \left(\frac{\delta\varepsilon}{\delta T_{\sin k}}\delta T_{\sin k}\right)^2}$$

(5.3)

Before each test run, a steady-state room temperature deviation in thermocouple temperature data was obtained as a proxy for relative precision of the test fixture and data acquisition system. During these measurements, the thermocouples were observed to have a maximum precision deviation of $\leq 0.5\,°C$. This value is presented with all temperature data as an approximate measurement of the precision. This helped increase the overall confidence in the observed trends across the test article. Temperature data also includes the manufacturer provided measurement accuracy of $\pm 2.2\,°C$. The high quality of the relative precision observed was attributed to the consistency of the lead materials used in the thermocouple's construction within the purchased lot.

A $0\,°C$ ice bath test was completed on each test article to provide a single calibration point. The aluminum test article's thermocouples had a mean of $0.05 \pm 0.07\,°C$, and the stainless steel test article's thermocouples had a mean of $0.15 \pm 0.08\,°C$. In either case, these results were well within the presented limits for precision of the test data.

86

5.3.4. Data Interpretation and Test Article Mapping

Test data is presented to directly correspond to their location relative to the test article. Four 1" (2.54 cm) wide heaters were used to control the heat input to a given discretized area. Thermocouples were mounted at 0.5" (1.27 cm) intervals across the center of the plate. These features are represented in Fig. 5.4 below.
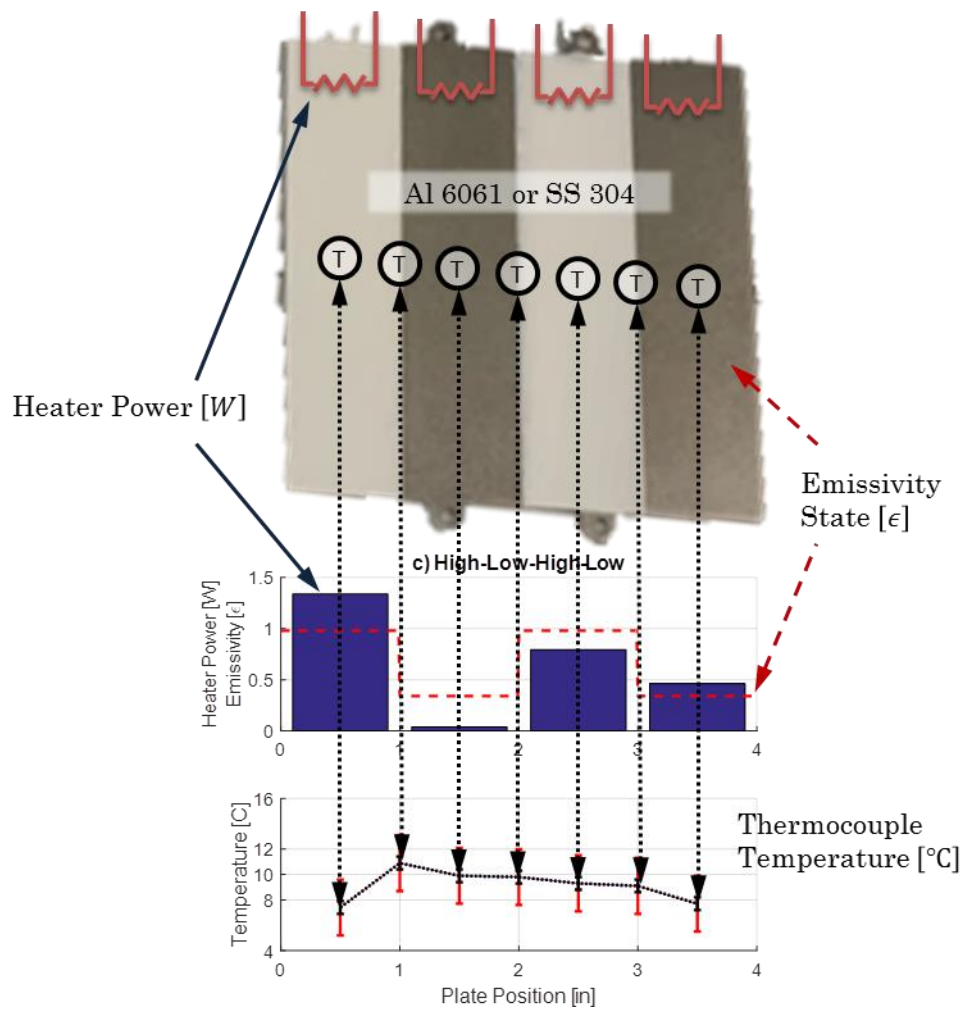
Figure 5.4. Test article features mapped to output data

5.3.5. Analytic Model

A model of the test article was created to predict the variation in temperature across the radiator plate with a specified heat input. Under steady-state conditions, the model was implemented as a multi-equation solver as defined in Eq. 5.4. The modeled radiator's surface was divided into 16 equal segments that provided a discretization (i.e. mesh) independent solution. Elements corresponding to a low emissivity were given the experimentally determined values of 0.38 for aluminum and 0.34 for stainless steel. Elements with a high emissivity had an assumed value of 0.98 corresponding to approximate broadband emissivity provided by the Krylon Flat White paint (Infrared Thermography, ret. 2015).[12] The modeled thermal conductivity (k) of aluminum was 167 $\frac{W}{m^2 K}$ and stainless steel was 14.9 $\frac{W}{m^2 K}$ (Incropera et al., 2007).

$$\bar{T_i} = \begin{bmatrix} q_1 - \sigma \varepsilon_1 A_1 \left(T_1^4 - T_{shroud}^4\right) - kA_{thk}/x\left(T_1 - T_2\right) \\ q_2 - \sigma \varepsilon_2 A_2 \left(T_2^4 - T_{shroud}^4\right) + kA_{thk}/x\left(T_1 - T_2\right) - kA_{thk}/x\left(T_2 - T_3\right) \\ \vdots \\ q_i - \sigma \varepsilon_i A_i \left(T_i^4 - T_{shroud}^4\right) + kA_{thk}/x\left(T_{i-1} - T_i\right) \end{bmatrix} \tag{5.4}$$

This approach assumes 1-D conduction along the axis perpendicular to the orientation of the 4 individualized quadrants. The radiation contribution is assumed to be isolated to the side facing the cold shroud. No sources of heat leak are explicitly considered in this equation, nor is the slight temperature drop associated to the resistance across the thickness of the plate.

---

[12] The emissivity values provide by this source are presented for 3 μm and 10 μm wavelengths. A true broadband emissivity (emittance) was not identified through references.

5.4. Results

5.4.1. Empirical Emissivity Determination

For each test case, the effective emissivity was determined by Eq. 5.2. Radiator temperatures were taken as a pseudo time average, 3-4 steady-state data points were collected over an interval ≥ 30 minutes. Differences in temperature over this duration were attributed to sensor noise rather than actual variations in temperature. The error associated with the predicted emissivity was calculated according to Eq. 5.3. Table 5.1 provides the experimentally derived net emissivity values, and their corresponding uncertainties for each condition tested. Again, because all aluminum test points resulted in nearly constant temperature outputs, no explicit 10 °C constant temperature data was collected. These values are consistent with an area average net emissivity calculation regardless of heat input configuration (Wertz et al., 2011).

Table 5.1 Empirically derived net emittance values in mixed state conditions
(L – low emissivity & H – high emissivity)

		Constant Flux	Constant Temperature
LLLL	Al	0.38 ± 0.039	
	SS	0.34 ± 0.035	0.33 ± 0.033
HLLL	Al	0.53 ± 0.056	
	SS	0.50 ± 0.053	0.52 ± 0.044
HLHL	Al	0.68 ± 0.070	
	SS	0.66 ± 0.068	0.71 ± 0.059
HHHH	Al	0.95 ± 0.099	
	SS	0.96 ± 0.13	1.08 ± 0.11

5.4.2. Constant Heat Flux

Steady-state constant heat flux input temperature profiles for each test case are found in Fig. 5.5. The heat input for each condition was controlled to an approximately constant 1.55 W, equally divided between the 4 primary test article heaters. The result of the holding the heat input constant across all coating conditions is a net drop in steady-state operating temperature across all sections of the test article. The analytical model was applied to each of the mixed emissivity conditions (high-low-low-low and high-low-high-low). In each case the predicted results showed good agreement with empirical data. In the stainless steel test cases, edge effects, un-modeled heat leak, resulted in significant temperature drops near plate edges. This was observed under all coating conditions and largely explains the differences from the theoretical prediction. The primary difference in the two substrate materials is their thermal conductivity. The aluminum has an order of magnitude higher thermal conductivity, which results in a nearly constant temperature across the plate regardless of differences in the surface emittance or edge effects.
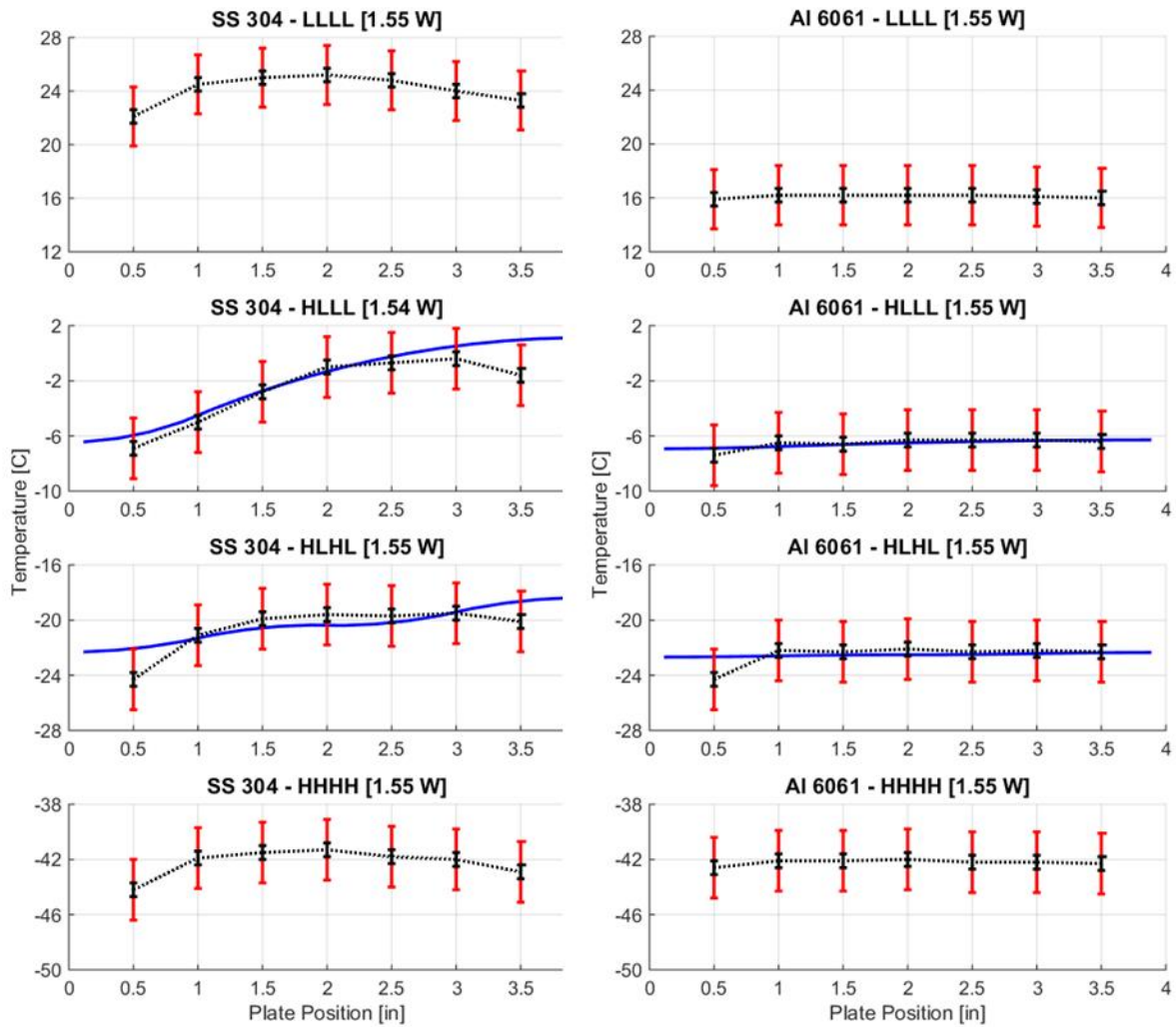
Figure 5.5. Stainless steel (SS 304) and aluminum (Al 6061) constant flux temperature profiles, solid lines are from the analytic model and dashed lines are experimental results. Inner error bar represents relative thermocouple precision and outer error bar represents absolute thermocouple accuracy. Low emissivities (L) result in higher temperatures and high emissivities (H) result in lower temperatures.

5.4.3. Constant Temperature

The stainless steel test article experienced a maximum temperature difference of 6.5℃ across all test cases under the constant heat input conditions. This variation is considered significant because it is well outside of the observed measurement precision and also outside the manufacturer's accuracy limits. As such, it was desirable to attempt to control the test article to a uniform temperature to determine if there were any significant differences in the net emissivity calculation.

In each test case, the 4 individual heaters were manually controlled in an attempt to force the test article to have a constant surface temperature. The target temperature across the test article's surface was 10 °C. The individual heat inputs, section emissivity properties, and temperature profiles for each test condition are provided in Fig. 5.6. Similar to the constant heat flux input case, the combination of edge effects and the relatively minimal control over area specific heat inputs made it difficult to consistently achieve a uniform test article temperature. This was also thought to slightly degrade the overall prediction of the surface's effective emittance, due in large part to uncaptured thermal gradients across the test article's surface.
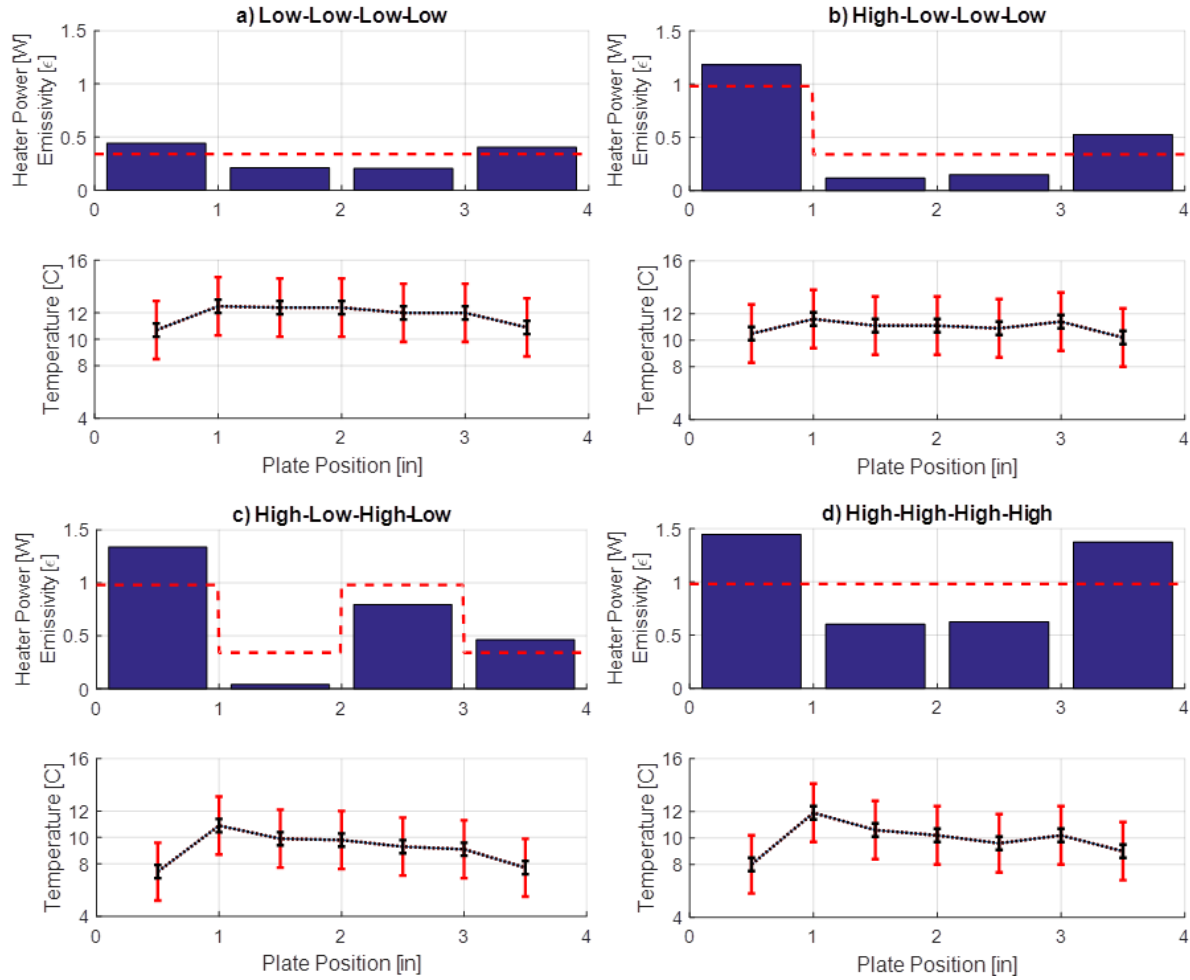
Figure 5.6. Stainless steel 304 constant temperature profile; heat input, emissivity, and temperature profiles

5.5. Discussion

These data showed that the net emissivities determined in both heat input scenarios agreed within the limits of uncertainty associated to the calculation. However, the inability to accurately produce a constant temperature across the stainless steel test article suggests that there are likely uncaptured thermal gradients that result in an apparent skew of the calculated emissivity. Under constant heat flux conditions, while thermal gradients also exist, they are likely accounted for in the unweighted averaging of the thermocouple temperature data.

93

This test series also provided proof-of-concept verification for intentionally mixing the emissivity values of discretized areas to achieve a predictable net intermediate emissivity state (Wertz et al., 2011). Additional permutations of area coating could be examined for their effect on overall surface temperature and emissivity properties. For example, additional area discretization could be done while still achieving the desired net emissivity properties. Instead of coating a single 1"x4" (2.54 x 10.16 cm) area to achieve an emissivity state of 0.5 and accounting for the induced thermal gradient, the 1" (2.54 cm) strip could be additionally divided into smaller widths and spread out over the test article's surface. This would provide the same overall emissivity, while changing the temperature profile across the test article.

These results also provide practical inputs for space suit designers should a similar intentionally discretized emissivity radiator architecture ever be considered in the future. With integration into a mechanical counter-pressure suit operating in a uniform flux heat dissipation scheme, the thermal conductivity of the pressure garment has a significant impact on thermal gradients experienced by the astronaut. A garment with a thermal conductivity and thickness consistent with the stainless test article evaluated in this investigation could lead to unfavorable temperature gradients of an astronaut's skin temperature. Unfavorable EVA thermal conditions could result in notable discomfort for the astronaut and ultimately lead to degraded performance. The 6-7℃ temperature range observed in the stainless steel test article is near the upper limit of acceptable skin

temperatures for human thermal comfort provided in Fig. 2.3 (Chambers, 1970). This result suggests that a garment's thermal performance should be no worse than the evaluated stainless steel test article, and that thermal properties the same order of magnitude as the evaluated aluminum test article are needed to avoid significant variations in skin temperature and potential performance degradation.

These data also have broader impacts for the design of spacecraft thermal control systems. In general, spacecraft radiators are designed and sized for a specific mission environment. Their thermal control coatings are generally uniform and have static radiative properties. Using available surface finishes, a desired net emissivity state could be achieved by partially coating appropriately selected surface areas. This may be of particular importance for CubeSat designers, where a given mission depends on relatively fine control of thermal radiation. Additionally, if variable emissivity electrochromics were integrated onto the spacecraft's surfaces, a simple bi-modal (two set point) voltage controller could be implemented across a matrix of devices to achieve some range of effective emittance values.

5.6. Conclusions

This investigation compared empirical test results to an analytic model that provided proof-of-concept for discretizing emissivity states across a radiator's surface area in order to obtain an area averaged net emittance. The results showed that the mixing of high and low emissivity states consistently provided a predictable net emittance state that is valuable in several spacecraft thermal control applications. As thermal conductivity of the radiator material decreases, the ability

to maintain a nearly constant temperature is greatly reduced. This phenomenon is especially important in space suit integration applications where garment materials are generally designed to minimize heat transfer in all directions. Successful implementation of a discretized emissivity space suit radiator operating in a uniform heat flux scheme requires garment materials with relatively high thermal conductivities to avoid unfavorable skin temperature gradients.

Expected Output Publication:

Massina, C.J., Nabity, J.A., and Klaus, D.M. (20YY). *Evaluation of Radiators with Discretized Emittance Properties.* [Working Title – In Prep]

CHAPTER 6

Considerations of Human Thermal Response

6.1. Abstract

Space suit thermoregulation has traditionally been achieved by sublimating water to space. Incorporation of a full suit radiator using variable emissivity electrochromic devices is one proposed alternative for reducing or eliminating the water mass loss incurred for cooling by sublimation. This concept allows the majority of a space suit's outer surface area to operate as a radiator, while the electrochromic's controllable surface properties enable variable heat rejection rates. Internal heat loads are balanced to the total radiated energy by selecting the emissivity of the electrochromic surfaces. Steady-state evaluations of this concept indicate that high metabolic loads and/or hot lunar surface locations can exceed the radiative heat dissipation capacity, however, the net impacts of dynamic internal and external environments on an astronaut's thermal condition have not yet been fully considered for this application. Here we present an evaluation method for determining transient environmental thermal impacts on a simulated human in a space suit using variable radiative cooling. Four test scenarios are used to illustrate the utility of the method for an astronaut in a simplified lunar pole environment. The scenarios considered were chosen such that comfort requirements could be maintained throughout the duration of each of the simulations. Overall, the approach described here can be used in future investigations to advance the

characterization of the electrochromic suit radiator architecture's working environment envelope.

6.2. Introduction

While these fundamental radiator integration architectures have been identified in the past, to our knowledge transient impacts of the suit's thermal control architecture on the human thermal condition (i.e., stored heat balance) have not been specifically addressed. Past investigations have generally been conducted using steady-state internal and external load conditions (Metts and Klaus, 2009; Metts et al., 2011; Massina and Klaus, 2015).

Ultimately, the full surface, variable emissivity radiator system must be capable of maintaining the suited astronaut's thermal balance such that physical and mental performance degradation is avoided (Buckey, 2006). As such, unfavorable variations in the amount of energy retained or expelled by the body should be mitigated by the thermal control system (HIDH, 2010; Ochoa et al., 2006). Inability of the system to maintain the human thermal balance can result in an increase or decrease in core temperature, which will eventually lead to hyperthermia or hypothermia. While variations in stored energy result in temperature variations, these energy changes are commonly tracked as variations in body heat storage (BHS), a parameter commonly used to establish thermal comfort guidelines (HIDH, 2010).

The purpose of this investigation is to demonstrate the impacts of a thermal control system based on a full suit electrochromic radiator architecture as a function

of the astronaut's thermal state. In short, if the architecture is not capable of maintaining acceptable upper and lower BHS values, additional thermal control mechanisms must be implemented into the system. In order to complete this first-order investigation, a simplified model of a human within a suit that is interacting with a lunar pole environment was constructed. The model was created around a flat plate with equal area approximation of a two sided radiator. Each radiating area was allowed to view a different external heat flux environment and each area was considered to have independently controllable surface properties (Massina et al., 2014). That is, the emissivity of either radiating surface could be selected through a simulated IR electrochromic device. Net thermal resistance and capacitance heat transfer properties from each of the radiator surfaces to the human's skin are selectable within the code. The human was modeled as a simplified 'two compartment' human where each compartment shares a common blood pool (Crawford et al., 2000). Each compartment consisted of thermal nodes with properties representative of a human's core, muscle and fat, and skin.

This investigation considers permutations of a single suit configuration in a lunar pole environment. The layer which couples the radiator to the skin surface is considered massless and without thermal resistance. That is, the layer has no impact on transient heat transfer dynamics. The result is essentially an ideal test case where the electrochromic devices provide their emissivity modulation potential directly to the skin surface which in turn drives the radiator's temperature. Within

this configuration, we examine the impact of variations in metabolic rate and external environment fluxes on human thermal comfort.

6.3. Background

NASA's Human Integration Design Handbook (HIDH) states that the accepted means of calculating BHS is to use either the 41-Node Metabolic Man or Wissler model in space suit thermal control applications. These models have been used by NASA for several decades and are considered to provide adequate accuracy for initial modeling efforts (HIDH, 2010). For this investigation, we used a structural derivative of the 41-Node Metabolic Man architecture to approximate a two compartment man, as has been done in previous EVA investigations (Crawford et al., 2000). The inclusion of the human thermal approximation, in this capacity, allows thermal balance recovery dynamics to be observed under conditions where emissivity saturation results in excess expulsion or retention of energy. These dynamics would largely be lost if the model were to exclude human thermal properties and instead use a direct heat flux from the core approximation. Additionally, the overall approach reduces computation complexity and allows each compartment to directly couple to an approximated radiator surface and asymmetric environmental loading.

A block diagram of the interactions of a single compartment is shown in Fig. 6.1. Each of the simulated human compartments consists of a core node, a muscle and fat node, and a skin node which are connected passively through conduction and actively through blood flow (convection). The two compartments are connected

thermally through interactions with the common blood pool. Outside of the skin layer, a heat removal layer (HRL) can be included and given properties representative of a given cooling garment or alternative cooling mechanism(s). The HRL is directly coupled to the electrochromic radiator where the interaction with the external environment takes place. Finally, the electrochromic devices serve as the control actuator at the radiator's external surface and provide the final modulation of radiated energy to the environment. The performance of the variable IR emissivity electrochromics can be restricted to quasi-realistic boundaries in terms of both total IR emissivity modulation potential (maximum achievable high and low states) and IR state transition dynamics (response time). The emissivity of either radiating area can be independently controlled similar to an integration that consists of two electrochromic pixels.
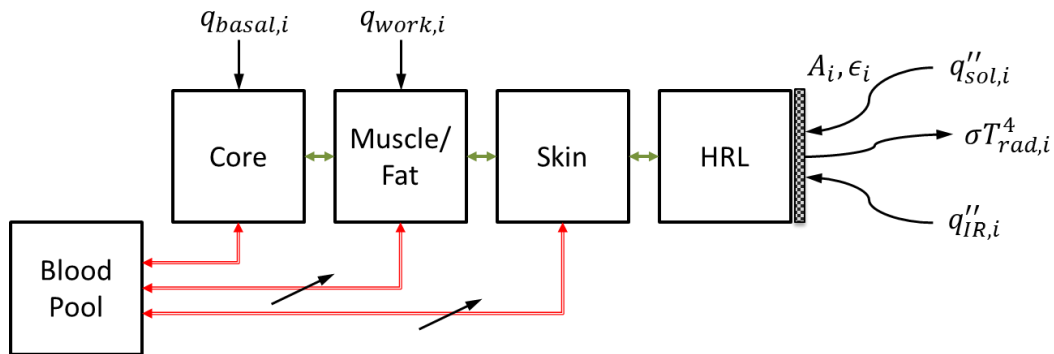
Figure 6.1. Heat transfer block diagram, direct radiative coupling

The fundamental thermal rate balance for our system is given in Eq. 6.1; the subscript i is used to denote the compartmentalization of the model used. That is, each compartment can have its own unique thermal inputs, thermal outputs, and control variable (independent emissivity setting ϵ_i). Here the difference between

heat inputs to either compartment (metabolic rate $\left(q_{MR,i}\right)$, incident IR flux $\left(q''_{IR,i}\right)$, and incident solar flux $\left(q''_{sol,i}\right)$) and heat outputs (radiated energy $\left(\sigma \epsilon_i A_i T^4_{rad,i}\right)$ where σ is the Stefan-Boltzmann constant, A_i is the compartment's radiating area, and T_{rad} is the radiator temperature) results in some amount of energy stored. The net metabolic rate per compartment is comprised of a basal rate $\left(q_{basal,i}\right)$ and a work rate $\left(q_{work,i}\right)$, Eq. 6.2. Basal energy is generated within the core node, while work energy is generated within the muscle/fat layer as depicted in Fig.6.1.

The model is simplified in terms of heat generation and heat exchange mechanisms of the human. For instance, metabolic rates associated to work in different compartments could be distributed throughout the simulated human layers rather than purely concentrated in the muscle/fat layer. Also, heat rejection in humans is not limited to conduction to the skin surface, additional mechanisms such as respiration and sweating could also be included. Note the differentiation of heat input from solar and IR spectrum radiation sources. Here solar absorptivity is understood to be synonymous with *absorptivity* (α). Values for a segment's emissivity (ϵ) are understood to represent the ratio of IR spectrum energy emitted or absorbed, per Kirchhoff's law of radiation (Incropera et al., 2007; Gilmore, 2002).

$$q_{stored} = \sum\left[q_{MR,i} + \epsilon_i A_i q''_{IR,i} + \alpha_i A_i q''_{sol,i} - \sigma \epsilon_i A_i T^4_{rad,i}\right] \quad (6.1)$$

$$q_{MR,i} = q_{basal,i} + q_{work,i} \quad (6.2)$$

In the event that radiative heat rejection does not balance with metabolic and environmental loads, any excess energy may be stored or released by the system. Such a result will correspond to a net change in energy contained within the space suit and human system. While energy changes can be experienced by any element of the model, stored energy fluctuations within the core will directly translate to a change in core temperature. Small changes in core temperature can have significant impact on an astronaut's physical and mental performance (Buckey, 2006; HIDH, 2010). In the event that a net balance cannot be achieved by this system, additional mechanisms could be included in the thermal control architecture, such as a sublimator or heaters. For this initial investigation, however, no such added mechanisms are included.

Several potential configurations of the HRL could be implemented; here we highlight the form of what we consider to be the two fundamental integration schemes (Metts and Klaus, 2009; Massina and Klaus, 2015). The primary difference between the integration schemes is the degree of coupling between the internal and external environments. Fig. 6.1 depicts the direct radiative coupling of the crew member to the radiation environment. Heat generated within the suit moves directly through the human and suit layers to the radiator, where the variable IR properties of the electrochromic regulates the net heat rejection of the system. This is the only scheme considered in this evaluation.

The second integration scheme indirectly couples the internal and external environments. In this indirect scheme, the energy transferred to the HRLs from

either human compartment would be collected in a common location before being directed to radiator segments for dissipation. This notion can be thought of as a dual-loop architecture where a cooling garment water loop interfaces with a radiator cooling loop that subsequently rejects the heat loads to the environment. In either integration scheme, the heat transfer efficiency is largely a function of the properties of the heat removal layer and any additional system interactions that occur between the skin surface and the radiator. The inclusion of a generic HRL allows variations in resistance and capacitance properties to be easily input and examined for their impact on the human thermal condition in future investigations.

6.4. Methods

6.4.1. Thermal Model

The human model used in this investigation parallels the work of both Crawford et al. (2000) and Campbell et al. (2000). Both of these models find their roots in the earlier work of Montgomery (1974) and Stolwijk and Hardy (1966). Our model follows an approximately "average" crewmember with a height of 1.8 m, nude body surface area of 1.8 m², and a total mass of 78.5 kg. Note that the total body mass used by Crawford was 73 kg, to which we added 5.5 kg to directly account for the blood volume's thermal mass. A block diagram of one compartment of the considered thermal model is provided in Fig. 6.1 above. The model is symmetric around the common blood pool which is representative of the circulatory system. Each block represents a node in the thermal model and has the associated

properties provided in Table 6.1. The heat balances for each node of a single compartment in the thermal model are found in Eqs. 6.3-6.7 below.

Subscripts are used throughout to denote the nodal position of the given property. Subscript notations for each layer are presented in the title of the corresponding equation titles below. Additionally, i is used to denote participation of one of the two bulk compartments, and j represents the human nodes which comprise a single compartment (core, muscle/fat, and skin). Each node has a corresponding temperature (T), representative mass (m), specific heat (c_p), and thermal resistance to heat transfer between adjacent nodes (R). Additionally, blood mass flow rate through a given body thermal node is denoted by $\dot{m}$.

Core Layer (c):

$$m_c \, c_{p,c} \frac{dT_{c,i}}{dt} = \dot{m}_{b \to c} c_{p,b} \left(T_b - T_{c,i} \right) - \frac{1}{R_{m,f \to c}} \left(T_{c,i} - T_{m,f,i} \right) + q_{basal,i} \tag{6.3}$$

Muscle/Fat Layer (m.f):

$$m_{m,f} \, c_{p,m,f} \frac{dT_{m,f,i}}{dt} = \dot{m}_{b \to m,f} c_{p,b} \left(T_b - T_{m,f,i} \right) + \frac{1}{R_{c \to m,f}} \left(T_{c,i} - T_{m,f,i} \right) - \frac{1}{R_{m,f \to skin}} \left(T_{m,f,i} - \right.$$

$$\left. T_{skin,i} \right) + q_{work,i} \tag{6.4}$$

Skin Layer (skin):

$$m_{skin} \, c_{p,skin} \frac{dT_{skin,i}}{dt} = \dot{m}_{b \to skin} c_{p,b} \left(T_b - T_{skin,i} \right) + \frac{1}{R_{m,f \to skin}} \left(T_{m.f,i} - T_{skin,i} \right) -$$

$$\frac{1}{R_{skin \to HRL}} \left(T_{skin,i} - T_{HRL,i} \right) \tag{6.5}$$

Blood Pool (b):

$$m_b \, c_{p,b} \frac{dT_b}{dt} = c_{p,b} \sum_{i=1}^{2} \sum_{j=1}^{3} \dot{m}_{b \to i,j} \left(T_{j,i} - T_b \right) \tag{6.6}$$

Heat Rejection Layer (HRL):

$$m_{HRL}\, c_{p,HRL} \frac{dT_{HRL,i}}{dt} = \frac{1}{R_{HRL \rightarrow skin}}\left(T_{skin,i} - T_{HRL}, i\right) + A_i \alpha q''_{sol} + A_i \epsilon_i q''_{IR,i} - \sigma \epsilon_i A_i T^4_{HRL,i} \quad (6.7)$$

For this investigation we did not consider any influences of the heat removal layer. As such, the skin layer directly interacts with the external environment as seen in Eq. 6.8 below.

Skin Layer – Direct Interaction with Environment:

$$m_{skin}\, c_{p,skin} \frac{dT_{skin,i}}{dt} = \dot{m}_{b \rightarrow skin} c_{p,b}\left(T_b - T_{skin,i}\right) + \frac{1}{R_{m,f \rightarrow skin}}\left(T_{m.f,i} - T_{skin,i}\right) + A_i \alpha q''_{sol} +$$

$$A_i \epsilon_i q''_{IR,i} - \sigma \epsilon_i A_i T^4_{skin,i} \quad (6.8)$$

Table 6.1. Single compartment model parameters, adapted from Crawford et al. (2000) and Montgomery (1974)

Compartment (node)	Specific Heat [kJ/kg·K]	Thickness [m]	Mass [kg]	Capacitance C [kJ/K]	Resistance (with next layer toward core) [K/W]
Core[13]	3.095	0.070	13.95	43.18	N/A
Muscle, Fat[14]	3.499	0.042	20.65	72.26	0.1111
Skin	3.766	0.002	1.90	7.155	0.0053
Blood Pool[15]	3.766	N/A	5.5	20.71	variable
HRL[16]	0	0	0	0	0

The active heat transfer between the blood pool and other body segments is a function of the flow rate of the blood through those segments. For this investigation, we assumed a uniform and constant blood flow to each of the body compartments.

---

[13] Core is comprised of skeleton, connective tissue, viscera, etc. all lumped together in this approximation.

[14] Assume 12% total body fat all contained within this layer. Capacity is split by mass between the muscle and fat contained within this layer.

[15] Blood pool values are not scaled to one compartment as that node interacts with all modeled body compartments.

[16] Assumed to make no contribution in this investigation.

In reality, several additional control mechanisms exist for the regulation of blood flow rates to the various parts of the body. For instance, in the case of high metabolic work rates, blood flow to muscle tissue will tend to rise to accommodate the new work rate. Blood flow to the skin is additionally influenced by the temperature of the skin. In cold environments blood vessels will tend to constrict, reducing blood flow. In hot environments blood vessels will tend to dilate, allowing for an increase in blood flow rate (Crawford et al., 2000; Stolwijk and Hardy, 1966).

Similarly, the human model assumes a uniform tissue thermal conductivity of 0.42 W/(m·K) (Crawford et al., 2000). In reality, the conductivity of tissues will vary with its composition (viscera, muscle, fat, etc.) but all are of the same order (Incropera et al., 2007).[17] For this level of analysis, we consider these differences to minimally contribute to the overall system performance; however, additional fidelity would be appropriate for future investigations.

Body heat storage values can be used as a metric to determine if a given overall thermal condition is acceptable for an astronaut's performance. The HIDH defines the acceptable comfort interval for a given metabolic rate (*MR*) in Eq. 6.9 (HIDH, 2010). That is, for a given metabolic rate and amount of stored energy during the simulated EVA, the accumulation of stored energy (*Q_{stored}*) should not exceed this range at any given time. Thus, our heat rejection system must provide controlled energy regulation such that BHS values never violate the absolute highs or lows prescribed here. The inability of the electrochromic system to meet the

---

[17] For additional information on modeled thermal conductivity see Stolwijk & Hardy (1966)

energy storage criterion dictates that an additional thermal control mechanism is required to maintain thermal comfort.

$$\Delta Q_{stored} = \frac{MR - 81}{3.87} \pm 19 \, W \cdot hr \qquad (6.9)$$

In addition to the comfort band for energy storage, ultimate limits for heat rejected or retained exist for the onset of cognitive and physical performance degradation. The limit per body mass for the onset of cognitive performance degradation is provided in Eq. 6.10. The limit per body mass for the onset of physical performance degradation is provided in Eq. 6.11 (HIDH, 2010).[18] The region between the comfort band described by Eq. 6.9 and the cognitive degradation limits of Eq. 6.10 constitute relatively acceptable hot and cold sensation regions. While operation in these regions may be generally undesirable, ultimately the astronaut will still be capable of performing their tasks with little impact to their wellbeing.

Cognitive Performance Degradation Onset:

$$4.7 \frac{kJ}{kg} > \Delta Q_{stored} > -4.1 \frac{kJ}{kg} \qquad (6.10)$$

Physical Performance Degradation Onset:

$$6.0 \frac{kJ}{kg} > \Delta Q_{stored} > -6.0 \frac{kJ}{kg} \qquad (6.11)$$

---

[18] Alternative stored body heat guidelines are available in the NASA Space Flight Human System Standard (STD-3001).

6.4.2. Environment Model and Suit Interaction

A lunar pole environment was approximated to define the incident flux contributions to the suit's radiator surfaces. The nominal potential IR flux is defined as $5.2\,W/m^2$ and the maximum nominal incident solar flux is defined as $1375\,W/m^2$ (Gilmore, 2002). The contribution of either of these total fluxes is scaled by the view factor to the radiator's surface. Here we use a constant first-order view factor approximation of 0.5 to either flux source (IR and Solar), which corresponds to our model geometry, a vertical flat plate on an infinite lunar plane (Massina et al., 2014). The nature of our location on the moon and the examined geometry is that one radiator surface will always be shaded by the other; the result is that one of the two radiator surfaces will always have a zero solar flux contribution. Various higher fidelity simulation techniques could be utilized to refine these estimates for more complex suit and/or lunar surface geometries in future investigations (Hager et al., 2015).

The electrochromic coatings are assumed to have a constant solar absorptivity (α) of 0.2, which is consistent with nominal values of the current space suit's Ortho-fabric outer layer of 0.18 (Larson and Pranke, 1999). The solar absorptivity of the surface will ultimately be dictated by surface coating used in the final design. Also note that the lower this assumed value is, the less influence solar spectrum energy will have on the radiator's capacity to reject heat. In this investigation a purely theoretical electrochromic IR emissivity (ϵ) range of 0.1 to 0.9 is considered. To our knowledge, broadband emissivity variation of this magnitude

has not yet been demonstrated in such devices.[19] This range could be expanded or additionally restricted in future investigations.

The configuration of our model is representative of a simple two electrochromic pixel system. Each radiator area has an independently controllable pixel, where the emissivity value can be set to any value within the controllable range (0.1 to 0.9). When the controller output is set to be limited to this range, any excess in the control output results in emissivity "saturation" to the corresponding high or low value. For this investigation, we assume instantaneous emissivity transitions of the electrochromic devices. In a physical system, some lag may be introduced between the sensing of a need to vary emissivity, the application of a new control voltage, and the manifestation of the physical change in surface properties. Additional work is required to define actual transition dynamics in terms of both lag and required voltage application.

6.4.3. State-Space Implementation

A state-space representation of the system was constructed using the equation set above (Eqs. 6.3, 6.4, 6.6, and 6.8), where each equation represents an individual row in the matrix (f), and implemented in MATLAB and Simulink software packages. The thermal system's variables were modeled as either a state, an input, or a disturbance. The state variable matrix (x) consists of the

---

[19] Advertised broadband emissivity variations are currently in the 0.5 range. The high or low emissivity value may be selected which defines the converse state. That is if you want a low emissivity value of 0.2, the high state is limited to 0.7. www.ashwin-ushas.com. Retrieved Jan. 2014.

temperatures of each node. The input matrix ($\boldsymbol{u}$) is comprised of the emissivity setting of either radiator surface. Finally, the disturbances matrix ($\boldsymbol{d}$) is comprised of the heat associated to metabolic work input along with variations in the external solar and IR flux environments to either radiator surface. Due to the nonlinearities in Eq. 6.8, the system is linearized about a reasonable set of initial conditions ($\boldsymbol{IC}$). The general form of the linearized system is found in Eq. 6.12, and the desired output is found in Eq. 6.13 where $\boldsymbol{C}$ and $\boldsymbol{D}$ matrices are used to extract the variables of interest.

$$\delta \dot{x} = \left[\frac{\delta f}{\delta x}\right]_{IC} \delta x + \left[\frac{\delta f}{\delta u}\right]_{IC} \delta u + \left[\frac{\delta f}{\delta d}\right]_{IC} \delta d \tag{6.12}$$

$$\delta y = C \delta x + D \delta u \tag{6.13}$$

In order to fully define the system, the following set of initial conditions was used to solve for the otherwise unknown variables. The variables defined by the initial conditions include the core temperatures, the blood temperature, the metabolic work rate, and the environmental fluxes to either radiator surface. Core temperatures and the initial blood temperature were initially assumed to be a nominal 37 °C. The initial metabolic rate is considered to be a nominal EVA metabolic rate of 300 W. The sunlit side flux contributions were set to $q''_{IR} = 2.6\ W/m^2$ and $q''_{sol} = 687.5\ W/m^2$. The shaded side environmental flux contributions were set to $q''_{IR} = 2.6\ W/m^2$ and $q''_{sol} = 0\ W/m^2$. The reduction from the total potential incident flux is due to the inclusion of the view factor to the given flux source.

While controller development was not the focus of this investigation, including one was required nonetheless. The control logic utilized for this investigation was generated using MATLAB's Linear-Quadratic Regulator (lqr) design function and considered each of the core temperatures as the primary variable being controlled. That is, the control logic implemented was designed to minimize variations in core temperature unless there was a change in the desired set temperature (which we did not consider). The calculated optimal gain matrix was then implemented into the dynamic model (MATLAB, 2014; Brogan, 1991). While this control development approach was taken in this investigation, other methods could be implemented in the future.

6.4.4. Modeled Input Variations (Disturbances)

In order to demonstrate the utility of the model, four independent test scenarios were evaluated for their impact on the system's overall performance. The scenarios were split into two categories: system disturbances resulting from variations in metabolic rate and system disturbances resulting from variations in external environment fluxes. The scale of the disturbances for this first-order investigation were largely arbitrarily chosen but based on reasonable expectations for what would be experienced on the lunar surface; more appropriate numeric inputs could be used in future investigations. The duration of a given simulation can be chosen as any amount of time the user wishes. Here we use a simulation duration of 3,600 seconds (1 hour). This length tends to be sufficient in terms of

identifying if any divergence of the output will occur for the given test scenario. Graphical representations of each disturbance variation scenario are provided in the results section.

6.4.4.1. *Metabolic Profiles*

The first metabolic profile assumes a cyclic 200 W variation around the nominal 300 W initial condition. The result is a metabolic profile that varies between 100 W and 500 W, which is considered consistent with variations that might be expected during an EVA. Metabolic changes of this order are expected to occur routinely over several EVAs. The metabolic variation occurs at a frequency of 0.004 Hz (~26 minute period); this frequency was arbitrarily selected but represents relatively gradual changes in the metabolic rate.

The second metabolic profile assumes that a transition from the nominal 300 W to a sustained 450 W occurs in approximately seven minutes. The 450 W metabolic rate was held constant for ~18 minutes before ramping down over approximately 9 minutes, to a minimum metabolic rate of 150 W. While this test case occurs over an hour, the profile is more consistent with those used in other evaluations.

6.4.4.2. *External Environment Profiles*

In both of these environmental variation test cases, a constant nominal 300 W metabolic rate was considered. The first environmental variation profile

examined approximates the thermal impact on a suited astronaut that is 'spinning' in place. Initially the sunlit suit surface has the maximum solar radiation exposure while the other has zero. As the approximated astronaut rotates, the angle of the incidence of the solar radiation relative to that surface varies, changing the value of the incident flux. As the initially sunlit surface moves into a shaded regime, the initially shaded surface becomes sunlit. Throughout the rotation, a shaded pass results in a zero solar flux contribution to the heat balance. These variations are approximated as a continuous frequency sine wave of 0.005 Hz.

The second environment change profile examines how the system responds to a bulk change in incident infrared flux. Here either radiator is exposed to the same variation in infrared radiation, with the only difference that the initially sunlit side retains its solar flux contribution. Incident radiation begins at the nominal level of 2.6 W/m^2, a step increase of 100 W/m^2 occurs at 10 minutes, and an additional 125 W/m^2 is encountered after 25 minutes before the incident IR flux returns to the nominal at 31.5 minutes.

6.5. Results & Discussion

Each of the four test scenarios begin with the same set of initial conditions. As stated above, the blood pool temperature and the core temperatures of each compartment were set to a nominal 37 °C. Temperature drops are experienced through each tissue layer due to the thermal resistance between them. The muscle and fat layer of either compartment has an initial temperature of 32.5 °C, and the skin surface temperature of either compartment is initially 31.7 °C. The initial skin

temperature is consistent with the comfort band described by Chambers for the initial 300 W metabolic rate (Chambers, 1970). The difference in incident flux composition to either radiator surface results in variations in initial emissivity settings of the two surfaces. The initial emissivity setting for the sunlit side was 0.6334 while the shaded side was 0.3503. Note that these initial emissivity values are well within the saturation boundaries imposed by the physical system, making an EVA at these steady-state conditions feasible.

The results of each test scenario are presented using three separate graphs. For each case, the scenario's disturbance variation is provided in the top chart. The second chart is the control response to the disturbance; the response is provided in terms of an absolute emissivity setting for either the initially sunlit (1) or initially shaded (2) radiator surface. The final chart displays the impact to the human thermal system in terms of a temperature variation around the initial state temperature of the tissue.

The result of the first metabolic variation test scenario is found in Fig. 6.2. The cyclic metabolic variation of this magnitude results in emissivity clipping (saturation) on both the high limit for the sunlit side (1) and low limit for the shaded side (2). The result of the emissivity clipping is that excess energy is either being retained or expelled from the human. If this phenomenon were to continue in a given direction, the human would eventually experience a state of hyperthermia or hypothermia depending on if excess energy was stored or emitted. In this particular test case, the cyclic exposures to these limits are short enough that the

system can compensate for the excess energy within the following high or low metabolic swing. The energy storage compensation is also evident from the phase shift between the metabolic variation and emissivity control response after the initial increase. This response is attributed to the system's apparent leveraging of the lower metabolic rate to provide an overall cooling effect on the human. A similar phenomenon occurs during the transition from low to high metabolic rates. The nature of this particular cyclic variation and the controller's response results in an absence of emissivity clipping on the sunlit side after the first event. It's also worth noting that the emissivity settings do not return to specific limit values with each cycle. This is again the result of the energy storage compensation that continues as the metabolic load varies.

The primary impact to the human's thermal condition is the variation in skin temperature that is experienced as the metabolic rate changes. The trend exhibited by the response is again consistent with the comfort skin temperatures described by Chambers; as the metabolic rate rises the skin temperature tends to decrease, as the metabolic rate decreases the skin temperature tends to rise (Chambers, 1970). This temperature response is a consequence of the change in heat flow through an otherwise constant thermal resistance. Due to the nature of the model scenario and control implemented, very little excess heat is retained or emitted by the system. The result is a stable core temperature and only minimal changes in body heat storage.
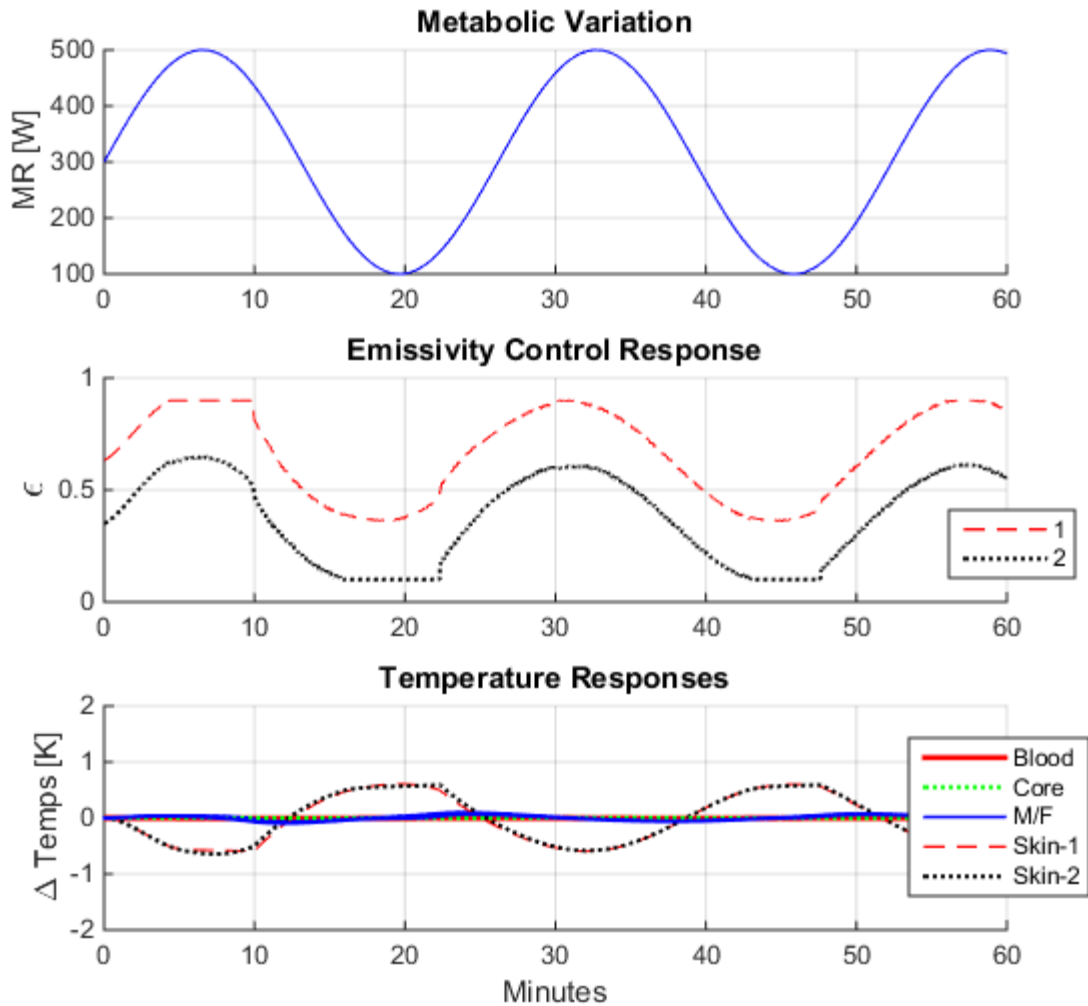
Figure 6.2. Response to 200 W metabolic load variations at 0.004 Hz, constant IR and Solar flux conditions

The result of the second metabolic variation test scenario is found in Fig. 6.3. Here, the emissivity of either radiator surface mirrors the change in metabolic rate until the new steady-state condition is achieved. No emissivity clipping is observed at either the high or low emissivity limits. Small overshoots in the transition to the new steady-state are observed for both the increasing and decreasing metabolic rate conditions. These are attributed to oscillations of the control algorithm until the

new condition is achieved. In this case, the skin temperatures again mirror the change in metabolic rate in an inverse fashion and only minimal changes in body heat storage are experienced.
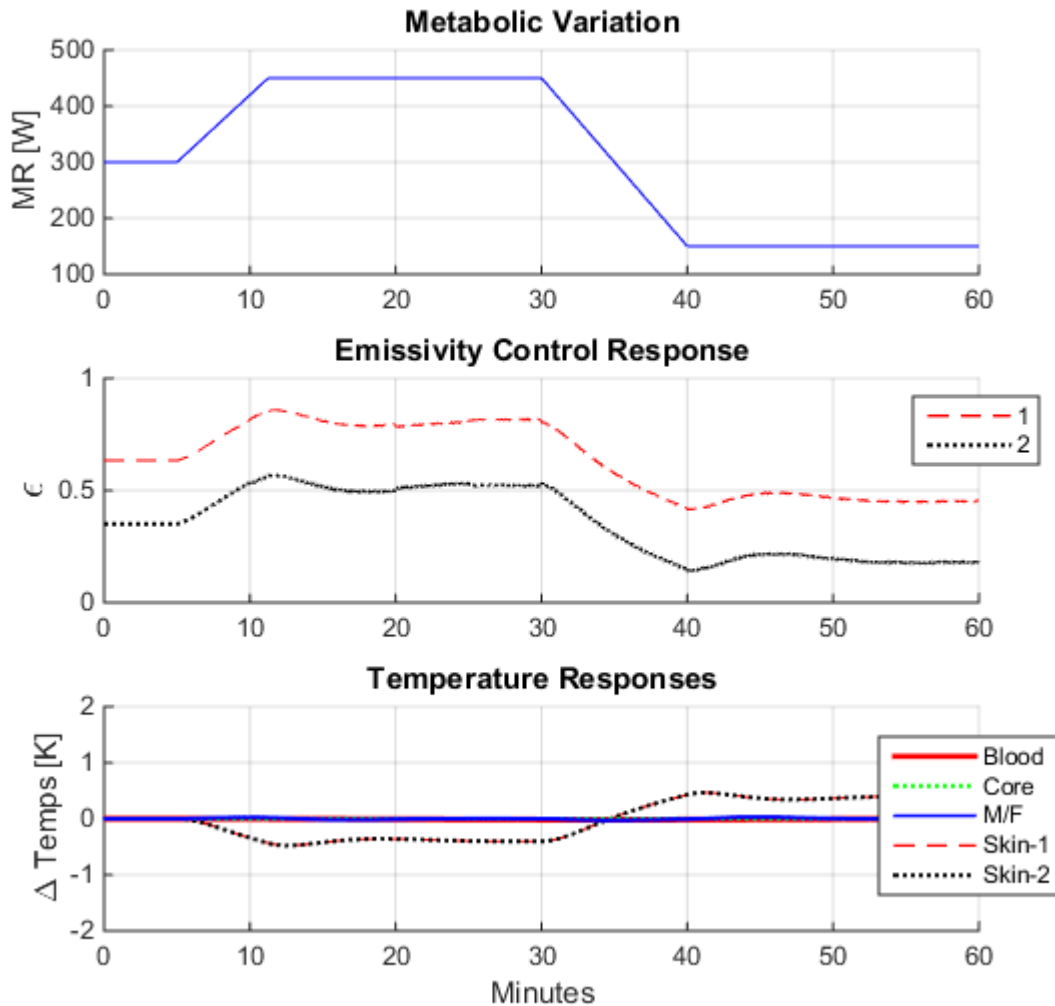
Figure 6.3. Response to ramped metabolic rates

The result of the first environmental variation test scenario is found in Fig. 6.4. The uniform variations in solar spectrum energy between the two radiator surfaces lead to repeatable variations in the emissivity settings of either radiator. As may be expected, variations in solar spectrum energy of this magnitude, between

initial maximum and minimum values, do not lead to any significant deviation outside of the initial emissivity states. Additionally, note that without a change in metabolic rate, or any significant retention of external radiation, very little change in temperature is experienced by the simulated human. Essentially the system was fully capable of mitigating the contributions of the external environment and keeping the human subject comfortable.

The result of the second environmental variation test scenario is found in Fig. 6.5. As the astronaut is exposed to bulk variations in IR flux conditions, the radiator is able to compensate for the initial 100 W/m^2 increase in flux through purely a change in emissivity. Through this initial transition, no significant change in body temperatures is experienced. However, the second increase in IR radiation of 125 W/m^2 results in a state where the sunlit side of the suit is not able to adequately balance with the environment. The result is clipping of the emissivity state on that surface, and the system begins to retain some amount of energy at that surface. As such the entirety of the human system begins to experience temperature fluctuations and the shaded side of the suit continues to increase its emissivity in order to compensate for the imbalance of the sunlit side. After the IR environment returns to the baseline value, the control system continues to compensate for the previous over exposure and resulting changes to body temperatures until eventually the system stabilizes to the initial state values. It's important to note that if the exposure time is sufficiently long, the system may not be able to compensate and a

more significant temperature disturbance will be experienced that may distress the

human.
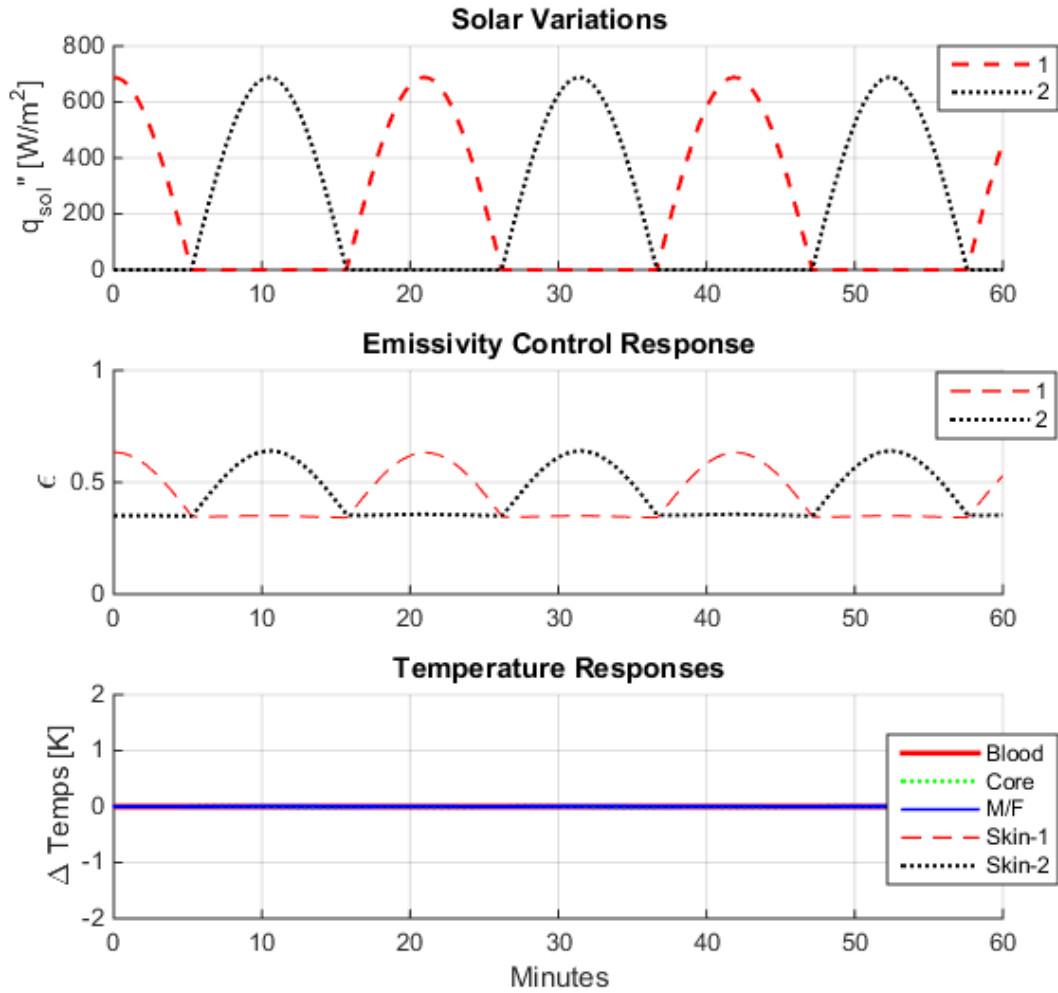
Figure 6.4. Response to rotational variation in incident solar flux, 300 W metabolic rate
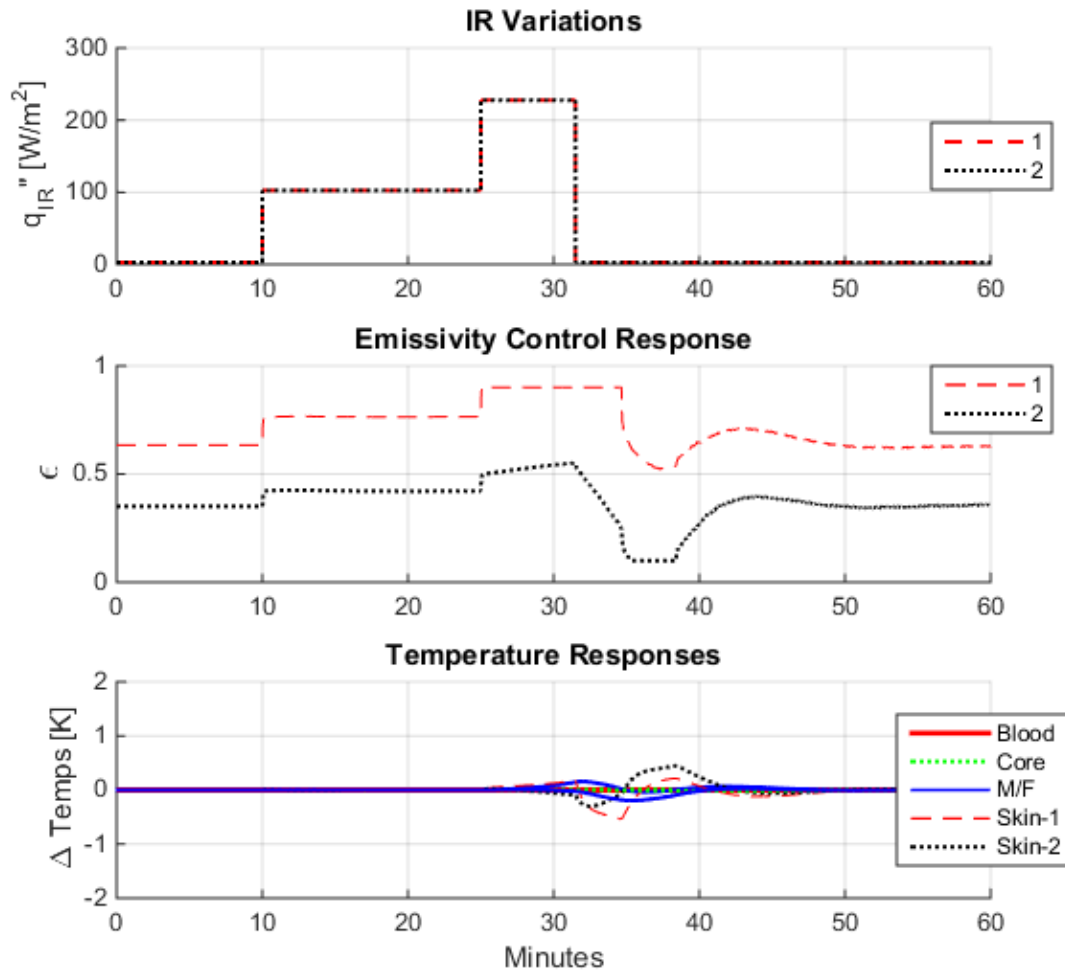
Figure 6.5. Response to bulk IR flux variations, 300 W metabolic rate

As alluded to in the previous discussion, the nature of the modeled system and the control imposed dictates that essentially no change in stored energy would be experienced. The result is a constant value very near zero for total body heat storage variations. While the simulated system will not map one-to-one with the energy storage comfort guidelines of Eq. 6.9 because of this modeling artifact, the response suggests that cognitive and physical impairment limits will not be encountered under disturbance conditions that the system is able to compensate for.

If an environmental condition is experienced that results in prolonged saturation of the emissivity in either the high or low sense, however, the thermal balance may diverge resulting in impairment of the astronaut. While the control algorithm selected for this simulation proved to be adequate for all test scenarios presented, there were other cases where instability (astronaut impairment) was encountered after prolonged emissivity clipping. This was true even after conditions were returned to the initial stable state of the simulation.

6.6.   Conclusions and Future Work

Overall the simulation approach described here can be used to advance the characterization of the electrochromic suit radiator architecture's working envelope. In addition to beginning to identify saturation limits in either internal or external environments, similar analysis could be used to help define allowable HRL properties for a set of relevant EVA environments. The fidelity of the human model can also be improved upon, as several human thermoregulatory responses were not included in this study for the sake of simplicity. The primary improvement for future investigations will be to include variations in modeling the blood flow response to both metabolic work rate and skin temperature changes. Additional improvements could also include adding sweating and shivering responses to exposure to high and low stored energy cases, and additional compartmentalization of the human (e.g. adding arms, legs, etc.). It's worth noting, however, that prolonged sweating or shivering may be undesirable during EVA due to an increased risk of dehydration or pre-hypothermic conditions.

6.7. Summary

This investigation considered how the human thermal condition was affected by variations in internal metabolic loads and external heat flux conditions during EVA on the lunar surface. The proposed full suit electrochromic radiator architecture, with direct radiative coupling, was examined for its potential to maintain human thermal comfort throughout these variations. We assumed that the electrochromic devices were directly coupled to the skin via a mechanical counter pressure suit, the result of which allowed the skin temperature to directly dictate the radiator temperature. A nominal metabolic rate of 300 W and a generic lunar pole environment was used to define initial conditions used in four test cases. The test cases presented here included two metabolic variation profiles and two external environmental change profiles. In each of these cases, the electrochromic architecture was able to adequately maintain the human's thermal condition at the level of the simulation. Exposure to conditions which saturated the theoretical emissivity limits of 0.1 and 0.9 resulted in a change in the amount of energy stored by the human. If these conditions were experienced for a prolonged period of time, cognitive and physical degradation would be experienced unless additional thermal control mechanisms are included. The use of a human thermal model in this way demonstrates that additional information can be collected to refine the effective environmental working envelope for a full surface, electrochromic radiator space suit architecture.

Related Output Publication:

Massina, C.J., Nabity, J.A., and Klaus, D.M. (2015). Defining Allowable Heat Transfer Transients to Incorporate a Full Suit Radiator with Variable Emissivity Surfaces into a Space Suit Thermal Control System, ICES-2015-26, *45th International Conference on Environmental Systems*, Belleview, WA.

CHAPTER 7

Prospects for Extension to Martian EVA

7.1. Abstract

Extravehicular activity (EVA) will play an important role as humans begin exploring Mars, which, in turn, will drive the need for new enabling technologies. For example, space suit heat rejection is currently achieved through the sublimation of ice water to the vacuum of space; a mechanism widely regarded as not feasible for use in Martian environment pressure ranges. As such, new, more robust thermal control mechanisms are needed for use under these conditions. Here we evaluate the potential of utilizing a full suit, variable emissivity radiator as the primary heat rejection mechanism during Martian surface EVAs. Diurnal and seasonal environment variations are considered for a latitude 27.5 °S Martian surface exploration site. Surface environmental parameters were generated using the same methods used in the initial selection of the Mars Science Laboratory's initial landing site. This evaluation provides theoretical emissivity setting requirements to evaluate the potential of the system's performance in a Mars environment. The thermal control architecture is capable of dissipating a standard nominal EVA metabolic load of 300 W in all conditions with the exception of summer noon hours, where a supplemental heat rejection mechanism with a 250 W capacity must be included. These results can also be used to identify when conditions are the most favorable for conducting EVAs. Preliminary analysis

indicates that the full suit, variable emissivity radiator architecture provides a viable means of EVA thermal control on the Martian surface.

7.2. Introduction

When humans take their first steps on the Martian surface, a space suit will be required to support human life and enable functionality of the explorers (Waligora and Sedej, 1987; Klaus et al., 2006). Over the history of human spaceflight, EVA has played a key role in the success of many missions. The cumulative loss of water associated with sublimator-type systems, over several EVAs, is largely considered too costly for Mars exploration (Jones, 2009; Bue et al., 2013). Additionally, Martian surface pressures are generally between 4.8 and 10 torr, which is just above the general operational limit of 3.5 torr for a sublimator system, making their use unrealistic (Kuznetz, 1990; Harris, 2001; Pater and Lissauer; 2010).

In recent years, a derivative of the Chameleon Suit concept for thermal control has been under investigation in our lab (Metts et al., 2011). The concept utilizes variable IR emissivity electrochromics on the outside of the full suit radiator to actively modulate heat exchange with the environment. Initial feasibility studies showed that the architecture provided a viable means of reducing the water mass losses in a lunar environment (Metts and Klaus, 2012). Additional investigations elaborated upon this work to include more complex environmental interactions, defined initial pixel sizing considerations, and evaluated the impact on the human's thermal condition (Massina et al., 2014; Massina et al., 2015; Massina and Klaus,

126

2015). To date, however, these feasibility assessments have focused on lunar surface applications.

Here we provide a first-order feasibility assessment of using an electrochromic radiator based control architecture for EVA thermal control on the Martian surface. Theoretically required steady-state emissivity settings are calculated over the Martian day for several metabolic rates. The thermal environment of Mars at latitude 27.5° S was used as the basis for this investigation. Seasonal variations in the external environment, based off the work of Vasavada et al. (2012), are included for completeness.

7.3. Background

7.3.1. Full Suit, Variable Emissivity Radiator Extension

Integration of the proposed full suit radiator architecture is envisioned to occur via one of two fundamental schemes. The human would be coupled to the radiator either directly via conductive heat transfer from the skin through the suit wall, or indirectly, via some dual-loop convective architecture that collects and distributes the heat for dissipation (Metts and Klaus, 2009; Massina and Klaus, 2015). While some suit integration architectures could accommodate either coupling method, direct coupling is generally associated with use in a mechanical counter pressure suit (Pitts et al., 2001), while indirect coupling is generally associated with use in a traditional gas pressure suit.

There are two key differences between the architectures, the radiator's surface area and the nature of the heat path between the astronaut and the

radiator. The total surface area of a tight fitting mechanical counter pressure suit is approximately that of a nude astronaut and using the standard average of the expected crew population gives an expected total area of 1.91 m² (HIDH, 2010). The total surface area of a traditional gas pressure suit is roughly double that of a nude astronaut at approximately 3.90 m² (Tepper et al., 1991). An additional radiating area factor can be included to restrict the total available area to that which is actively participating in radiation exchange with the external environment (e.g. omitting arm pits, inner thighs, etc.). The actual radiating factor is dynamic, however, and will generally vary with body posture (Guibert and Taylor, 1968).

By including variable IR electrochromic devices on the exterior of the space suit, the system can actively modulate its surface properties and thereby alter the radiation interaction between the suit and the local environment. The feasibility of utilizing electrochromics in this type of application was made possible by advancements in the robustness of the devices over multiple flexion cycles (Kislov et al., 2003). Broadband emissive property variations of as much as 0.50 have been demonstrated in some devices, and can currently be tailored to a minimum low state of 0.19 or a high state of 0.90 (Chandrasekhar et al., 2014). If a purely radiative system cannot sustain the thermal balance, some additional mechanism may be warranted. Depending on the nature of the control deficiency, mechanisms could include heaters, a phase change material [venting or non-venting], additional insulation, etc. Ideally, these alternative mechanisms would be relatively simple and not introduce unnecessary system complexity or mass. Note that we consider

the term emissivity (ϵ) to be synonymous with IR emissivity and IR absorptivity. This is done with the understanding that the fraction of energy emitted or absorbed over the IR spectrum will be the same over those common wavelengths (Gilmore, 2002).

A constant non-zero suit surface solar absorptivity (α) is included to provide a more realistic approximation of a physical device. Including a non-zero solar absorptivity also dictates that, in the presence of solar spectrum energy, the effective radiative sink temperature will vary as the electrochromic's emissivity properties are changed. This approximation was not explicitly considered in early evaluations of the architecture on the lunar surface (Metts et al., 2011; Metts and Klaus, 2012). Baseline evaluations throughout this work considered a solar absorptivity of 0.2, near the current space suit's value of 0.18 (Larson and Pranke, 1999; Harris, 2001). A parametric evaluation of different solar absorptivities is included to illustrate the impact of other values on the overall potential system performance.

7.3.2. Internal and External Environments

The internal environment, regarded as heat loads generated within the suit, consists primarily of human metabolic loads and avionics loads (Sompayrac et al., 2009). The avionics load will largely be a function of the suit's final design, which we cannot explicitly consider in this evaluation. During the Apollo lunar landings, metabolic rates ranged from minimums of ~150 W to 15-minute peak maximums of ~725 W and the nominal metabolic rate was ~290 W (HIDH, 2010). These values

129

are largely consistent with the expected metabolic expenditure during Martian EVAs (Pu et al., 2004; Wilde et al., 2004; Jones, 2009). However, additional investigations are required to refine metabolic expenditure estimates of Martian surface EVAs and include actual suit heat loads as the design matures.

The Martian environment has notable differences that must be included in the analysis when compared to the lunar environment. Key differences include the solar day length, seasonal flux variations, soil property values, and the low pressure CO_2 atmosphere (Kaplan, 1988). The lunar sidereal day is approximately 27.3 earth days long, so bulk heat flux variations associated to changes in the solar elevation angle over the duration of an EVA can largely be disregarded (Heiken et al., 1991). The Martian day, on the other hand, is approximately 24.65 Earth hours long, so the resulting change in incident heat flux conditions over the duration of an EVA should be explicitly included (Vasavada et al., 2012). Diurnal results are presented in terms of a local solar time (LST) whereby the Martian day is split into an equivalent 24 hour day (or sol), rather than using the Earth hour standard. The Mars orbital position for a given season is captured in the Solar Longitude (*Ls*).

The surface thermal environment data used in this evaluation were taken from investigations that were completed during the determination of the Mars Science Laboratory's landing site. These data were generated using the Jet Propulsion Laboratory 1-D Surface-Atmosphere Model and the New Mexico State University 1-D Mars General Circulation Model (Vasavada et al., 2012). Diurnal variations in the surface temperature, 1 meter elevation atmosphere temperature,

effective sky temperature, direct solar flux, and diffuse solar flux were all provided by the Vasavada et al. investigation. Seasonal variations in these heat loads were also provided. The atmosphere considered here consisted of pure carbon dioxide at a constant pressure of 7 torr (Waligora and Sedej, 1987; Harris, 2001). The atmosphere imposes some degree of additional convective cooling at sustained wind speeds between 0 m/s (free convection) and of 15 m/s (Campbell et al., 2000; Vasavada et al., 2012). These wind speed limits are used to provide a relevant operational envelope for the expected conditions of each season. A parametric study of wind speed's impact on the theoretically required emissivity setting was also conducted to illustrate the impacts of intermediate wind speeds and high velocity gust conditions. These results provided an indication of emissivity set point variability within expected wind variation limits.

The interaction of the suit with the external environment was modeled through a single thermal node. Fundamentally, the system's thermal balance is described by Eq. 7.1. A summation of IR and solar energies (q_{IR} and q_{sol}) was included to represent the potential for these fluxes to originate from different sources. The participating suit area is assumed to be oriented vertically on an infinite surface plane. This configuration allowed a simple view factor of 0.5 to be assumed for radiative interactions between solar and IR sources (Massina et al., 2014; Massina and Klaus, 2015).

The amount of energy radiated from the suit (q_{rad}) is a function of the current emissivity setting, radiating area, and the radiator's temperature. As

described earlier, the radiator area was set equal to the total nude body surface area of 1.91 m². This configuration is consistent with the thermal architecture's integration into a mechanical counter pressure (MCP) type space suit, and allows desirable skin temperatures to drive the radiator temperature. Additionally, we assumed the MCP garment had a thermal resistance of zero, such that skin temperature comfort guidelines could be used directly as a reasonable approximation of the radiator's temperature (Chambers, 1970; Massina and Klaus, 2015).

$$\Delta q_{stored} = \Sigma(q_{IR} + q_{sol}) + q_{MR,k} - q_{conv} - q_{rad,k} \qquad (7.1)$$

Metabolic rates (q_{MR}) were chosen to be representative of minimum, nominal, and peak rates that may be experienced throughout the space walk. Together, this approach provided a reasonable first-order approximation of the suit and environment interaction, from which the potential performance of the thermal system can be assessed.

7.4. Methods

7.4.1. Overall Heat Balance

The primary data set of this investigation consisted of the steady-state emissivity value theoretically required for the suit system to maintain thermal neutrality as shown in Eq. 7.2. This value was derived from Eq. 7.3 at steady state, where the net energy stored (q_{stored}) equaled zero. Astronaut metabolic rates (q_{MR}) of 100 W, 300 W, 500 W, and 700 W were considered throughout the evaluation. The

radiating temperature of the suit (T_{suit}) was taken directly from the optimal skin temperature comfort guidelines provided by Chambers (1970). The temperatures used were: 305.8 K, 303.8 K, 302.0 K, and 300.6 K from the 100 W to 700 W cases respectively. Note that this radiator temperature variation reduces the blackbody flux capacity by 6.63% between the high and low metabolic rates. Incident infrared radiation was considered to originate from the provided ground and sky temperatures $(T_{IR,i})$. Incident solar radiation consisted of a direct solar flux and a diffuse solar flux $(q''_{sol,i})$. No additional shading or complex geometry interactions were explicitly considered. The 1 meter elevation atmospheric temperature (T_{1m}) data was used as the baseline wind temperature for the convective heat transfer contribution.

$$\epsilon_k = \frac{\sum(\alpha AF_{suit,i}q''_{sol,i}) + q_{MR,k} - \bar{h}A(T_{suit} - T_{1m})}{(\sigma AT_{suit}^4 - \sum(\sigma AF_{suit,i}T_{IR,i}^4))} \tag{7.2}$$

$$q_{stored} = \sum(\epsilon_k \sigma AF_{suit,i}T_{IR,i}^4 + \alpha AF_{suit,i}q''_{sol,i}) + q_{MR,k} - \bar{h}A(T_{suit} - T_{1m}) - \epsilon_k \sigma AT_{suit}^4 \tag{7.3}$$

7.4.2. Determination of Convection Coefficients

Average free and forced convection coefficients were calculated for each of the seasonal environments investigated. Each coefficient is based on an average film temperature in a pure CO_2 atmosphere at a pressure of 7 torr. Table 7.1 provides a list of the coefficients used throughout the evaluation and is included for posterity. These data were extracted from a National Institute of Standards and Technology (2011) web resource, and used to determine relevant Reynolds, Prandtl, and

Rayleigh numbers per their standard definitions for heat transfer from a vertical cylinder (Incropera et al., 2007).

Table 7.1. Thermophysical properties of CO_2 at 7 torr and various film temperatures, from NIST (2011)

	Ave Film Temp [K]	Density (ρ) [kg/m³]	Specific Heat (c_p) [J/kg*K]	Viscosity $(\mu \cdot 10^{-5})$ [kg/m*s]	Thermal Conductivity (k) [W/m*K]
Fall (Ls = 0.06°)	246.7	0.020025	788.02	1.2391	0.012660
Winter (Ls = 90.4°)	235.7	0.020960	775.62	1.1841	0.011890
Spring (Ls = 180.2°)	248.4	0.019888	789.93	1.2476	0.012782
Summer (Ls = 270.0°)	255.0	0.019373	797.31	1.2805	0.013261

Average convection coefficients were calculated for both the operational envelope limit case wind speeds of 0 m/s and 15 m/s. The free convection coefficient was determined from Nusselt number correlation for an isothermal cylinder as described by Popiel et al. (2007), which is found in Eqs. 7.4-7.6. The characteristic length in the free convection case is the cylinder's height (H) considered to be 1.8 m; D is the cylinder's diameter considered to be 0.311 m.

$$\overline{Nu}_H = \frac{\overline{h}H}{k} = ARa_H^n \tag{7.4}$$

$$A = 0.519 + 0.03454 \left(\frac{H}{D}\right) + 0.0008772 \left(\frac{H}{D}\right)^2 + 8.855x10^{-6} \left(\frac{H}{D}\right)^3 \tag{7.5}$$

$$n = 0.25 - 0.00253 \left(\frac{H}{D}\right) + 1.152x10^{-5} \left(\frac{H}{D}\right)^2 \tag{7.6}$$

In the forced convection case, wind velocity of 15 m/s, the conditions of each season exhibit a Reynolds number on the order of 10^3 such that a laminar boundary condition is experienced. The characteristic dimension in this forced case is the

134

diameter of the cylinder. Here we use the comprehensive equation for the Nusselt number described by Eq. 7.7 to determine the average convection coefficient (Incropera et al., 2007).

$$\overline{Nu}_D = \frac{\bar{h}D}{k} = 0.3 + \frac{0.62 Re_D^{\frac{1}{2}} Pr^{\frac{1}{3}}}{\left[1+(0.4/Pr)^{\frac{2}{3}}\right]^{\frac{1}{4}}}\left[1 + \left(\frac{Re_D}{282,000}\right)^{\frac{5}{8}}\right]^{\frac{4}{5}} \tag{7.7}$$

Calculated convection coefficients ranged from 0.276 W/m²K to 0.287 W/m²K in the free convection case and from 1.909 W/m²K to 2.038 W/m²K in the forced convection case. With atmospheric temperatures always being less than the radiating surface temperature, the increase in convective heat transfer resulted in a net reduction in the required radiating power.

7.4.3. Determination of Excess Energy Requirements

The total thermal control power that must be supplied by the life support system in order to maintain thermal neutrality is described in Eq. 7.8. Ideally, the electrochromic radiator architecture would be capable of regulating the overall thermal balance without including additional mechanisms. However, environmental conditions which exceed achievable emissivity limits, 0.19 to 0.9, will require some supplemental thermal control mechanism. Values for the difference in theoretically required dissipation energy and the corresponding high or low limit can then be used to define supplemental heat regulation requirements. When the theoretical emissivity setting is in violation of achievable limits, the supplemental heat regulation guidelines are described by Eq. 7.9. As presented, a positive excess energy requirement correlated to needing some additional heat dissipation

135

mechanism, e.g. an evaporator. A negative excess energy indicated that the astronaut would require additional energy be added to the system or an improved insulation scheme.

$$q = \epsilon_k \sigma A T_{suit,k}^4 \tag{7.8}$$

$$q_{sup} = (\epsilon_k - \epsilon_{lim}) \sigma A T_{suit,k}^4 \tag{7.9}$$

7.5. Results and Discussion

The theoretically required emissivity values needed to maintain thermal neutrality at a 0 m/s wind speed, free convection case, are provided in Fig. 7.1. The corresponding high and low diurnal limits for the required emissivity are provided in Table 7.2. From these data, one can see that in the nominal 300 W metabolic load case, emissivity limits are only violated around the summer noon hours. This tends to suggest that when there are very low winds on Mars, the electrochromic radiator architecture can support the astronaut's thermal condition with little or no contribution from other mechanisms. However, work rates can vary significantly outside of the nominal 300 W range and will tend to require some additional mechanism depending on the time of day the EVA is being conducted. For instance, peak metabolic loads, near 700 W, are not sustainable by the system in any season if they are incurred near the local noon hours because achievable emissivity limits are violated. Nevertheless, peak rates can be accommodated during nighttime and low solar angle hours (early morning and late evening).
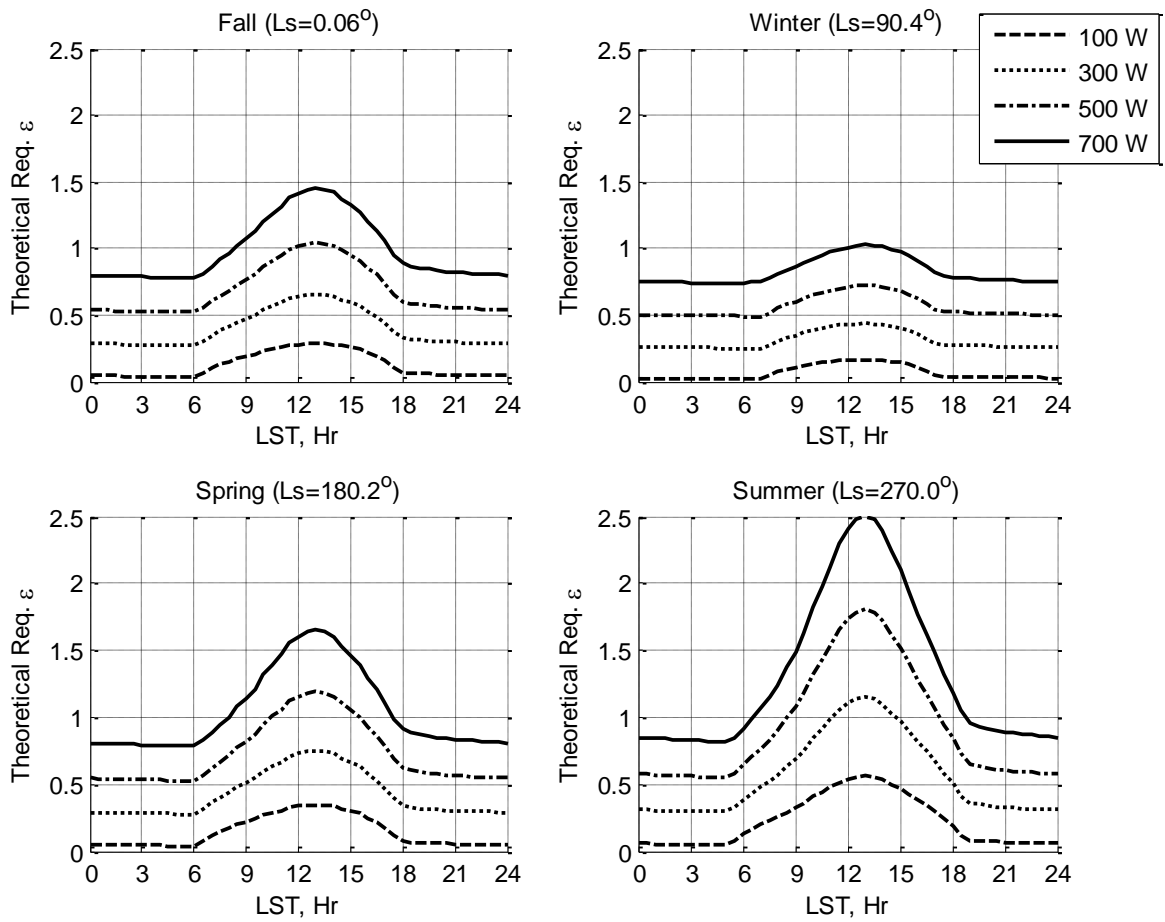
Figure 7.1. Diurnal theoretical emissivity requirements for 0 m/s wind speed for the given season.

Table 7.2. Theoretical diurnal emissivity limits for given metabolic rate and convection conditions

		100 W Free (Forced)	300 W Free (Forced)	500 W Free (Forced)	700 W Free (Forced)
Fall	Min	0.04 (-0.42)	0.27 (-0.18)	0.52 (0.06)	0.78 (0.31)
(Ls = 0.06°)	Max	0.29 (0.01)	0.65 (0.37)	1.04 (0.76)	1.45 (1.16)
Winter	Min	0.02 (-0.48)	0.25 (-0.25)	0.49 (-0.02)	0.74 (0.22)
(Ls = 90.4°)	Max	0.16 (-0.21)	0.44 (0.06)	0.72 (0.34)	1.03 (0.64)
Spring	Min	0.04 (-0.41)	0.28 (-0.17)	0.53 (0.07)	0.79 (0.32)
(Ls= 180.2°)	Max	0.35 (0.09)	0.75 (0.50)	1.19 (0.93)	1.65 (1.39)
Summer	Min	0.05 (-0.39)	0.29 (-0.15)	0.55 (0.11)	0.82 (0.37)
(Ls= 270.0°)	Max	0.56 (0.39)	1.15 (0.98)	1.80 (1.64)	2.51 (2.35)

The theoretically required emissivity values needed to maintain thermal neutrality at the sustained 15 m/s wind speed condition are provided in Fig. 2. Again, corresponding high and low diurnal limits are provided in Table 7.2. Here the sustained wind speeds have the uniform effect of lowering the required emissivity setting to maintain the astronaut's thermal condition. Note that in this case, the 100 W and 300 W overnight theoretical emissivity values are near or below zero, which indicates that additional heat input is required by the system. Alternatively, if EVA was to be conducted in these conditions, additional insulation, such as layers of thermal clothing (a coat, etc.), could be worn in lieu of including a full suit heater system. Again we see that even with the increase in convective cooling, peak metabolic rates near the noon hour cannot be accommodated by the

proposed architecture alone. In these conditions, the additional heat rejection capacity provided by the atmosphere reduces the theoretical high limit for daytime EVAs. However, while the summer case still violates the achievable maximum limit, the supplemental heat rejection requirement is reduced.
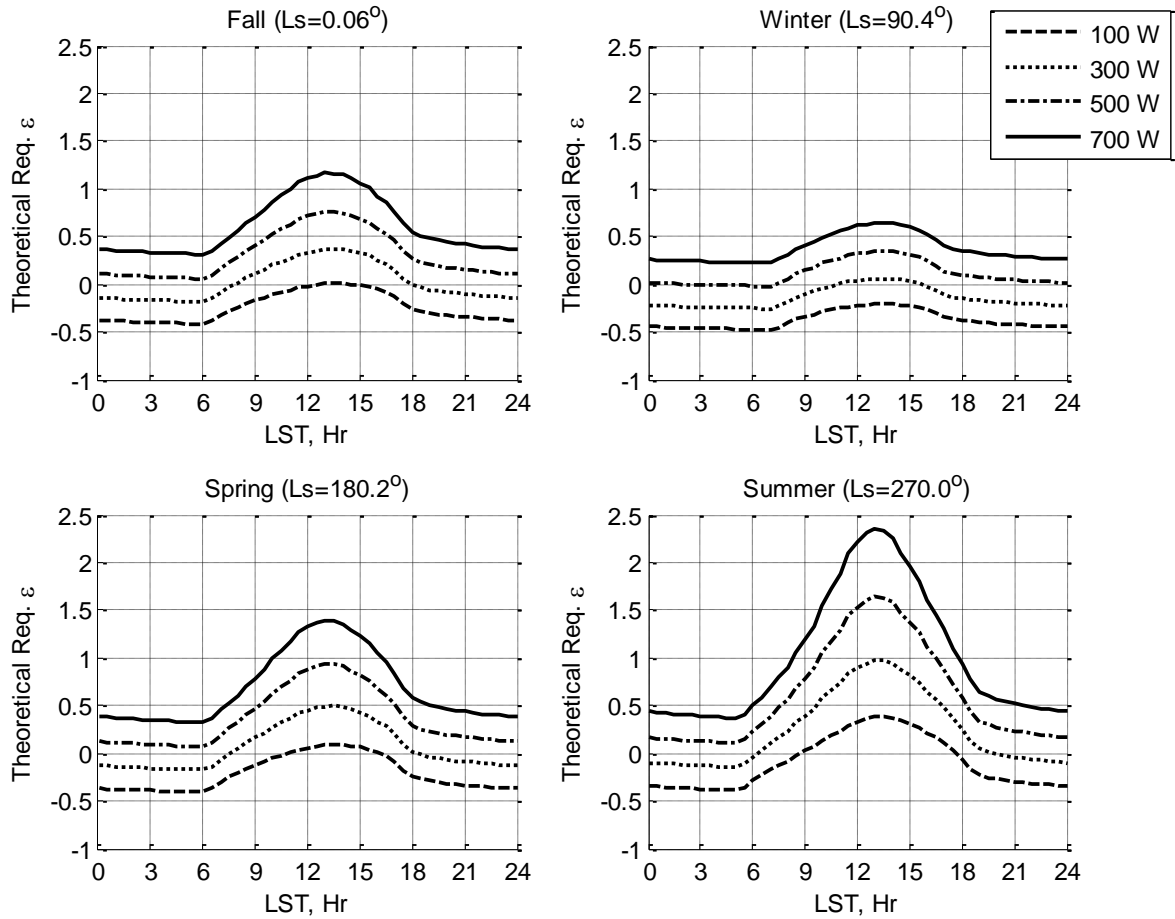
Figure 7.2. Diurnal theoretical emissivity requirements for 15 m/s wind speed in the given season

To further elaborate on the physical and operational limitations which can be extracted from this data set, Fig. 7.3 provides a heavily annotated version of summer conditions with 15 m/s wind speeds. Theoretical emissivity limits of 0 to 1

are included to bound the absolute operational envelope in which a variable emissivity system could function. Additionally, the practical limits of a variable emissivity electrochromic system are included to illustrate the current performance limitations. The space within these limits defines the operational capacity of the proposed system for the given conditions of that time of day. Any metabolic excursion outside of those limits implies an additional supplemental cooling (energy excess) or heating/insulating mechanism (energy deficit) would need to be included to reduce the risk of potential astronaut performance degradation.

These data could also be used to define operational requirements for time of day in which an EVA can be conducted. For instance, assuming the astronaut will maintain a constant metabolic load near the nominal 300 W case, an EVA can be conducted safely between the Martian local solar times of approximately 7:45 to 12:00 and 14:30 to 18:15 without additional thermal control mechanisms.
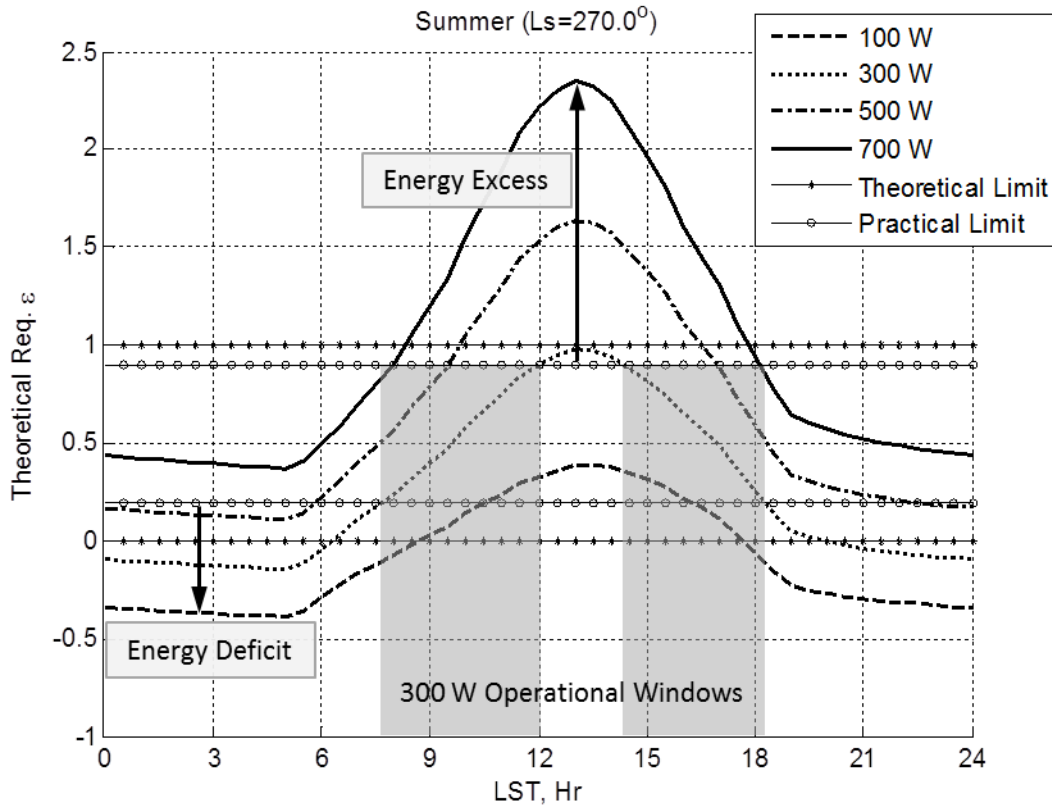
Figure 7.3. Diurnal theoretical emissivity values for summer conditions and sustained wind speed of 15 m/s

As described in Eq. 7.9 the difference of the theoretical emissivity required from Table 7.2 and the corresponding limit describes the power deficiency for a given case. Table 7.3 provides the supplemental thermal control powers required to maintain thermal neutrality under the given conditions. Minimum values come from the worst case cold condition which occurs overnight at the 15 m/s wind speed. Maximum values come from worst case hot condition which occurs just after the local noon hour at the 0 m/s wind speed. Again, negative table values represent a heat input requirement to accommodate an energy deficit, and positive values represent an additional heat rejection requirement to accommodate the energy

excess in the system. As described earlier, these excursion ranges either dictate operational limits or will require some sort of supplemental thermal control scheme.

In either case, even the supplemental energy limits may be prohibitively large, although these limits are over an entire day so shorter EVAs may still be acceptable. As was done in the discussion of Fig. 7.3, daily profiles can be used to define notional EVA excursion limits for the hours in which a spacewalk could be conducted. The addition of some supplemental heat rejection and/or heat supply mechanism would serve to increase the allowable EVA window. While both the heat rejection and supply mechanisms may represent the use of a consumable, heat rejection is typically associated with the loss of a mass consumable (e.g. water) and heat supply with the use of power (or offset by incorporating additional insulating garments to reduce heat loss in this case).

Note that the 300 W metabolic rate case only requires additional cooling in summer conditions. If the supplemental cooling system was sized for summer conditions, it could be designed to offer a modest 250 W of cooling capacity, which is less than half of what the current sublimator system is capable of supplying (Larson & Pranke, 1999).

Table 7.3. Supplemental thermal control power requirements for given season and metabolic rate. Negative values represent a heat input requirement, while positive values represent an additional heat rejection requirement. Limit cases are highlighted.

		100 W	300 W	500 W	700 W
Fall	Min	-573 W	-346 W	-119 W	0 W
(Ls = 0.06°)	Max	0 W	0 W	128 W	487 W
Winter	Min	-631 W	-410 W	-190 W	0 W
(Ls = 90.4°)	Max	0 W	0 W	0 W	111 W
Spring	Min	-564 W	-336 W	-107 W	0 W
(Ls= 180.2°)	Max	0 W	0 W	261 W	662 W
Summer	Min	-546 W	-310 W	-74 W	0 W
(Ls= 270.0°)	Max	0 W	229 W	815 W	1423 W

In addition to the conditions investigated above, here we provide illustrations of the impact of additional variations in solar absorptivity and wind speed. Each of the parametrics are based on a 300 W metabolic rate in the spring environment. The impact of changes to the solar absorptivity on the theoretically required emissivity setting is found in Fig. 7.4. The additional energy absorbed as the absorptivity increases results in an increase in the required emissivity setting. The different profiles overlap during nighttime hours when there are no solar fluxes to influence the thermal balance. While the high practical emissivity limit was not near violation in our nominal $\alpha = 0.2$ case, an additional increase in the absorptivity of less than 0.2 would dictate that additional cooling mechanisms be included. Furthermore, an increase in solar absorptivity to the theoretical limit of 1 would more than double the heat rejection required to maintain the astronaut's thermal condition. This nuance is worth consideration due to the potential impacts of the

inevitable accumulation of Martian dust on the suit's radiator. Dust accumulation was an issue well documented during the Apollo program and may have a significant impact on potential performance of a variable emissivity space suit radiator (Gaier, 2005). Further investigations are required to determine the extent to which surface contamination would affect the potential use of this architecture for surface EVA.
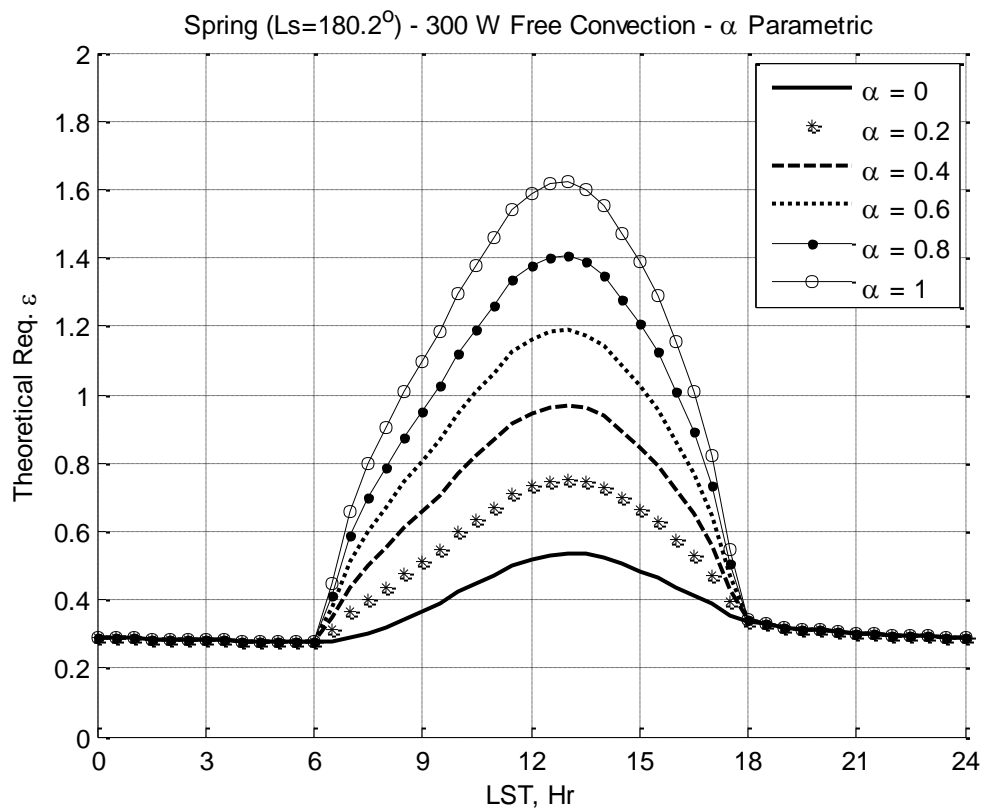
Figure 7.4. Impact of variations in solar absorptivity on the theoretical emissivity required to maintain thermal neutrality. The 300 W metabolic rate case, with free convection, was used to illustrate the relative impact in a spring environment.

The impact of variations in wind speed on the theoretical emissivity requirements is found in Fig. 7.5. A uniform reduction in required emissivity was observed as wind speed is increased due to the added convective cooling component.

These data can be used for a given EVA time to determine the system's capability for coping with wind gusts of different magnitudes or bulk variations in sustained wind speeds. While the required minimum to maximum emissivity range increases in order to accommodate the full spectrum of wind speeds, the high limit for achievable emissivity would not be encountered. With atmospheric temperatures always being lower than the radiator temperature at this location, any relative velocity between the astronaut and atmosphere would increase the dissipation capacity of the architecture. Additionally, if the radiator's solar absorptivity properties begin to degrade as demonstrated in Fig. 7.4, EVAs on windy days will tend to have a positive impact on the amount of heat rejection the suit's thermal control mechanisms will need to supply. That is, less supplemental cooling capacity is needed because the increase in convective cooling can partially compensate for the additional solar energy absorbed.
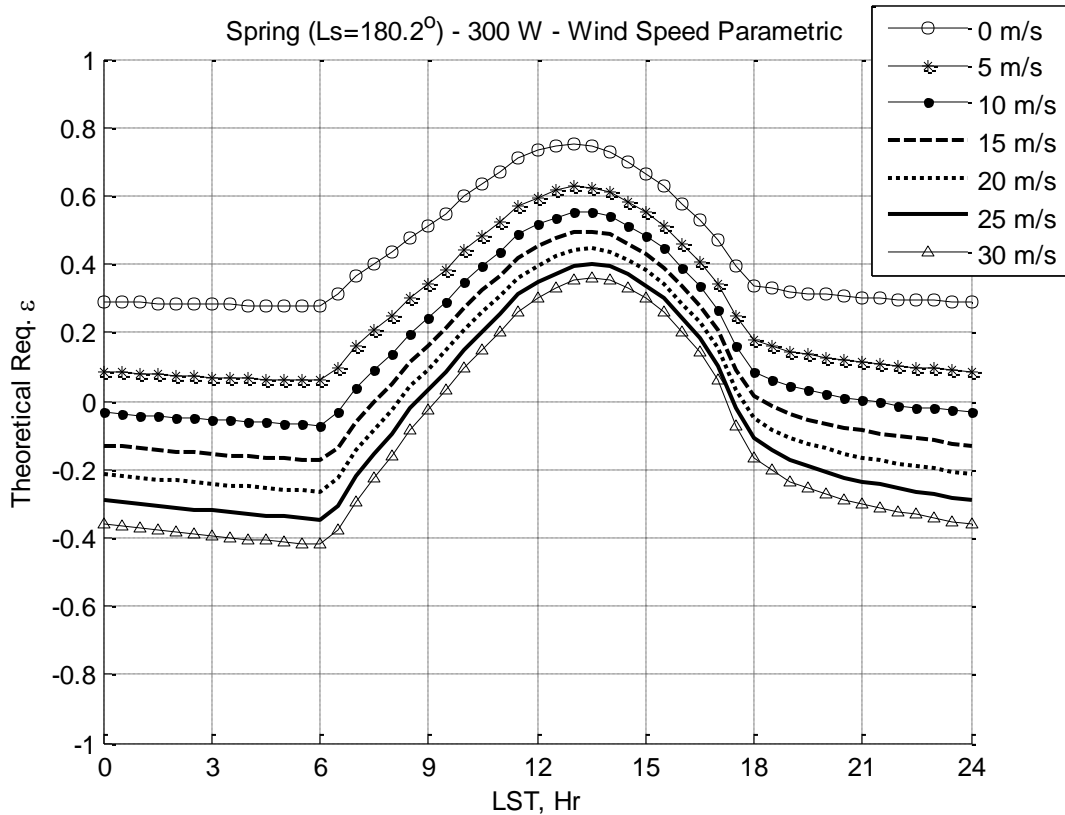
Figure 7.5. Impact of variations in wind speed on the theoretical emissivity required to maintain thermal neutrality. The 300 W metabolic rate case was used to illustrate the relative impact in a spring environment.

All of the provided theoretical emissivity requirements have been for a radiating area consistent with that of the average nude surface area of an EVA astronaut. As previously discussed, integration into a gas pressurized space suit would roughly double the available area for radiator integration, but also adds complexity in transporting heat from the skin to the suit radiator surface. By assuming all other characteristics remain the constant (radiator power, radiator temperature, convection characteristics, etc.), the required emissivity setting would effectively be reduced by half with the doubled area. The general relationship for the area dependence on theoretical emissivity is found in Eq. 7.10. Additional

consideration could be given to the imposed variation in the convection coefficient due to the change in geometry, however, these are considered minimal impacts to the overall trend. While the additional area would reduce the maximum emissivity requirements, it would also act to reduce overall variations observed throughout a diurnal cycle. Overall, a larger area would expand the operational envelope of the full suit electrochromic radiator architecture.

$$\epsilon_2 = \frac{\epsilon_1 A_1}{A_2} \tag{7.10}$$

These results indicate that the use of the full suit variable emissivity radiator architecture would provide a viable means of significant thermal control throughout much of the Martian year. Additionally, thermal control power limits were identified for the stated metabolic rates in each season. These limits could be used to define requirements for any necessary additional thermal control mechanisms that would enable EVA operations with higher metabolic loads and/or over larger portions of the Martian day.

7.6. Conclusions

Implementing a full suit, variable emissivity radiator for EVA thermal control on the Martian surface was evaluated under environmental conditions at a latitude of 27.5 °S using a simplified thermal model where the heat transfer interactions with the suit occurred through a single node. Martian local solar times are identified where the electrochromic radiator architecture can theoretically provide adequate thermal control over a range of metabolic rates. At the evaluated location, the nominal average dissipation case of a 300 W metabolic load could be

accommodated in nearly all daytime hours during any season without the addition of a supplemental thermal control mechanism. Additional heat dissipation for this case was only required near local noon hours in summer conditions, where a supplemental heat rejection mechanism with a capacity of around 250 W would provide sufficient buffer to enable continuous EVA operations throughout the day. The duration of a transient thermal excursion is also a factor, as the human comfort range may tolerate short periods of thermal imbalance (Massina et al., 2015).

The impact of variable wind speeds and solar absorptivity variations were also considered. With the local Martian atmosphere always being at a lower temperature than the space suit, any increase in wind velocity will reduce the net heat dissipation demands on the thermal control system. Alternatively, degradation of the suit's radiator surface properties can result in an increase in the supplemental heat dissipation requirements of the system. These considerations should be included in future investigations aimed at incorporating a full suit radiator architecture for use in the Martian environment.

In summary, the results show that a full suit, variable emissivity radiator thermal control architecture is theoretically capable of providing considerable heat dissipation capacity in the Martian environment, thereby reducing or eliminating consumable mass losses associated with traditional venting systems. Additional investigations are required to determine best practices for incorporating this approach into a space suit design, as well as for adding supplemental cooling and/or heating/insulating mechanisms to further expand the operational envelope.

7.7. Special Acknowledgement

Special thanks to Keith Novak of the NASA Jet Propulsion Laboratory and Kevin Anderson of California State Polytechnic University at Pomona for providing guidance in regards to expected Martian surface environments.

Related Output Publication:

Massina, C.J. and Klaus, D.M. (20XX). Prospects for Implementing Variable Emittance Thermal Control of Space Suits on the Martian Surface, [Under Review].

CHAPTER 8

Summary, Conclusions, and Future Work

8.1. Research Objectives

The work of this dissertation focused on the following research objectives, as provided in Chapter 1.

1. Analytically characterize the steady-state performance envelope and contamination impacts for utilizing flexible radiators in the lunar surface environment

2. Analytically assess the impact of emissivity modulation on sink (equilibrium) temperature

3. Provide a first-order electrochromic pixel resolution metric based on analysis and testing for thermal control in a lunar environment

4. Assess transient impacts of flexible/electrochromic radiator performance on human thermal comfort in a dynamic environment

5. Evaluate integration extensibility potential for Martian surface EVA

8.2. Summary of Chapters

Chapter 1 described the initial motivation for this work. Development of technologies with the ability to reliably reduce EVA consumable burdens is a long standing focus of NASA. However, to date, no zero consumable system has been demonstrated in either a laboratory or space environment. This work focused on the evaluation of a space suit thermal control architecture capable of reducing the consumable losses associated with EVA thermal control.

Chapter 2 provided much of the necessary background information required for analyzing the EVA thermal control problem. Additional justification for the use of a full suit radiator with variable emissivity properties was also provided.

Chapter 3 addressed research objectives 1 and 2 by examining the full suit radiator concept in a lunar EVA environment. In this evaluation, the environment was allowed to dictate the required suit radiator temperatures. By selecting reasonable suit operating temperatures, effective 'Go-No Go' zones for conducting spacewalks on the lunar surface, using only the variable emissivity radiator space suit architecture, were obtained. The identified zones translate to restrictions to exploration latitudes for long duration lunar missions. These results can also be extrapolated to characterization of first-order pressure garment thermal properties for successful architecture integration.

Chapter 4 considered research objective 3 through analytical modeling of a simplified suit geometry in a lunar pole environment. The total area of both mechanical counter pressure and gas pressure space suits was scaled to a cylinder and used to determine the nominal electrochromic pixel coverage (area) and required properties to maintain an astronaut's thermal condition. Two fundamental integration concepts with two unique heat dissipation schemes were identified. Under constant heat flux integration, the suited astronaut will be more sensitive to variations in the environment and requires additional pixel discretization and control authority. In constant temperature integration, heat loads are more effectively mixed, which reduces some integration complexity. Overall, this

investigation provides a best case starting point for pixel quantity determination and illustrates several of the considerations of using the proposed architecture in a suit's thermal control system.

Chapter 5 further elaborated on the work presented in chapter 4 by empirically testing the discretized mixed emissivity state concept. The series of thermal vacuum experiments conducted provide proof-of-concept for the mixing of high and low emissivity states to obtain an effective intermediate state. The use of two different test article substrate materials illustrates the potential performance differences associated to the thermal conductivity of an integrated garment. This is a key consideration for future architecture use, as a low thermal conductivity (high thermal resistance) garment can result in unfavorable thermal gradients, astronaut discomfort, and potentially performance degradation.

Chapter 6 addressed research objective 4 by providing first-order dynamic simulations of the interaction a suited astronaut may have with their local environment. A variable emissivity radiator was implemented with quasi-realistic saturation states. These simulations allowed the effects of unfavorable thermal excursions, were the radiator architecture cannot actively match required dissipation needs, to be identified and evaluated. The evaluated test cases showed potential effects of emissivity saturation on an astronaut's thermal condition but didn't illustrate effects of prolonged exposure or resulting system instabilities.

Finally, Chapter 7 addressed research objective 5 by evaluating the variable emissivity space suit radiator architecture in a Martian surface environment. These

results highlighted the major difference between lunar and Martian EVA; primarily, that in addition to differences in external environment, e.g. radiation loading and atmosphere, one must also consider the diurnal and seasonal environment changes to provide a complete characterization. These results can be used to develop first-order operational constraints, similar to those provided in lunar evaluations, and to define supplementary heat input or output rates required for maintaining thermal equilibrium in the explored Martian surface conditions.

8.3. Conclusions

The investigations completed within this dissertation show that the full suit, variable emissivity radiator EVA thermal control architecture provides the ability to actively maintain an astronaut's thermal condition within specified ranges of metabolic rates and external environments. This capability is consistent across the lunar and Martian surface EVA conditions examined. When the system is constrained within the operational envelopes described throughout, no water sublimation is needed for the purpose of space suit thermal control. Excursions outside of the defined envelopes, however, in either metabolic rate or environmental loading, are possible in both lunar and Martian environments, which introduces the need for supplemental thermal control. A hybrid system that could take advantage of the local environment through the full suit radiator while providing a separate mechanism to additionally heat or cool the suit would enable the space suit to maintain thermal equilibrium across wider operational envelopes. Or, by following

the operational guidelines provided, the need for hybrid system capabilities is reduced or eliminated.

The evaluation methods used to assess the electrochromic based architecture proposed here also have broader applicability to implementing alternative space suit thermal control schemes or to other technologies that could be used in a variety of spacecraft. For example, in the fundamental Stefan-Boltzmann radiation heat transfer equation (Eq. 2.3), other variables could be modified to control heat rejection from a space suit. While only variations in emissivity were explored here, other technologies can similarly leverage changes in radiator temperature or area. The set of evaluations conducted provide a foundation for alternative investigations of non-electrochromic based architectures in the future. Additionally, the use of variable emissivity electrochromics has a similar potential to increase the operational envelope of spacecraft ranging from CubeSats to lunar landers.

The thermal vacuum testing completed during this research provides insight into the impact of heat deposition schemes on radiator performance and verifies that mixing high and low emissivity states of discretized areas provides a predictable net emissivity. The integration of electrochromics into a space suit thermal control system will utilize either a constant heat flux or constant temperature configuration. While both heat input configurations offered the same effective net emissivity, impacts of the thermal conductivity of the substrate material must be considered as large variations in temperature across a surface may be undesirable for a given application.

The initial goal of this research was to advance the technology readiness level (TRL) (Mankins, 1995) of the variable emissivity suit radiator architecture. At the conclusion of Metts' (2010) work, the TRL was considered to be a 3/4, indicating that analytical proof-of-concept and component level validation in a laboratory environment had been completed. At the conclusion of this dissertation, the architecture remains at a TRL 3/4 by definition. However, contributions to guidelines for use in lunar and Martian surface environments, first-order pixelation considerations, and first-order dynamic simulation assessment all represent a significant iteration within this TRL. The results of these evaluations provide further characterization of the architecture and greatly expand the understanding of the capabilities in the proposed application.

Finally, the Martian surface evaluation presented is a significant step forward in the evaluation of EVA thermal control strategies where a convective atmosphere exists. The results show that diurnal and seasonal variations in the local environment should be explicitly considered throughout a systems development, the use of average constant temperatures is generally inappropriate. This is a significant shift in thinking from lunar evaluations where, due to the length of a lunar day, environmental loads are mostly constant for a given surface location.

8.4. Future Work

For this work to continue in the future, additional research and development is required to advance electrochromic devices to the level required by these

architecture studies. Specifically, advances in and verification of electrochromic pixel robustness, reliability, and intermediate state precision and repeatability over the lifetime of the system need to be completed. Any implemented electrochromic devices must be fully compatible with the hostile space environment, where they may be exposed to large thermal swings and potentially damaging radiation. In addition to radiation and thermal concerns, potential electrochromic degradation from coverage and abrasion due to planetary regolith must also be mitigated over the lifespan of the suit.

In addition to advances in electrochromic material performance, many of the investigations here should be further elaborated upon to increase the understanding of the integration requirements and operational limits. Additional modeling and testing can advance the design and optimize the heat transfer process from the human, through the suit, and to the external environment. As the architecture matures and the fidelity of the system increases, it will be more appropriate to include avionics loads and consider how supplemental thermal control mechanisms can be integrated. Additional high fidelity, steady-state and dynamic evaluations can then be completed to refine the operational limits associated with the system's utilization. This research provides a technical foundation for this work to continue and should be considered as a starting point for those continuing to evaluate the electrochromic based architecture and other novel EVA thermal control mechanisms.

REFERENCES

Ashwin-Ushas Corp., 2014, "Variable Emittance Electrochromic Materials for Spacecraft Thermal Control: Our Unique, Patented Technology in a Nutshell," http://www.ashwin-ushas.com/EleHome/SpaceThermal/spacethermal.html   (last accessed Oct. 7, 2014).

ASTM, 2010, *Standard Test Method for Calorimetric Determination of Hemispherical Emittance and the Ratio of Solar Absorptance to Hemispherical Emittance Using Solar Simulation*, ASTM E434-10.

Bannon, E., Iaconimi, C., Bower, C., and Linrud, C., 2010a, "Stagnating Radiator Thermal Model Design and Verification," *AIAA* 2010-4650, 10th AIAA/ASME Joint Thermophysics and Heat Transfer Conference, Chicago, IL, 28 June – 1 July.

Bannon, E.T., Bower, C.E., Sheth, R., Stephan, R., Chandrasekhar, P., and Zay, B., 2010b, "Electrochromic Radiator Coupon Level Testing and Full Scale Thermal Math Modeling for Use on Altair Lunar Lander," AIAA 2010-6110.

Barer, A.S., 1991, "EVA Medical Problems," *Acta Astronautica*, 23, pp: 187-193.

Bessière, A., Marcel, C., Morcrette, M., Tarascon, J.M., Lucas, V., Viana, B., and Baffier, N., 2002, "Flexible electrochromic reflectance device based on tungsten oxide for infrared emissivity control," *J. Applied Physics*, 91(3), pp: 1589-1594.

Brogan, W.L., *Modern Control Theory*, 3rd ed., Prentice Hall, Englewood Cliffs, New Jersey, 1991, Chap. 14.

Buckey, J.C. Jr., 2006, *Space Physiology*, Oxford University Press, Oxford.

Bue, G., Hodgson, E., Izenson, M., and Chen, W., 2013, "Multifunctional Space Evaporator-Absorber-Radiator," AIAA 2013-3306.

Campbell, A.B., 1999, "Thermal Modeling, Analysis, and Control of a Space Suit," Ph.D. Dissertation, University of Missouri-Columbia.

Campbell, A. B., French, J. D., Nair, S. S., Miles, J. B., and Lin, C. H., 2000, "Thermal Analysis and Design of an Advanced Space Suit," *J. Thermophysics and Heat Transfer*, 14(1), pp. 151–160.

Chambers, A.B., 1970, "Controlling Thermal Comfort in the EVA Space Suit," *ASHRAE Journal*, 12, pp: 33-38.

Chandrasekhar, P., Zay, B. J., Birur, G. C., Rawal, S., Pierson, E. A., Kauder, L., and Swanson, T., 2002, "Large, Switchable Electrochromism in the Visible Through Far-Infrared in Conducting Polymer Devices," *Advanced Functional Materials*, 12(2), pp. 95–103.

Chandrasekhar, P., Zay, B. J., Lawrence, D., Caldwell, E., Sheth, R., Stephan, R., and Cornwell, J., 2014, "Variable-Emittance Infrared Electrochromic Skins Combining Unique Conducting Polymers, Ionic Liquid Electrolytes, Microporous Polymer Membranes, and Semiconductor/Polymer Coatings, for Spacecraft Thermal Control," *J. Applied Polymer Science*, 131(19), p. 40850, doi: 10.1002/app.40850.

Chappell, S.P., Norcross, J.R., Abercromby, A.F., and Gernhardt,M.L., 2010, *Life Sciences Implications of Lunar Surface Operations*, NASA/TM-2010-21638, National Aeronautics and Space Administration.

Clark, C. and Conger, B., 2000, "Thermal Analysis Basics and Design Guidelines," Lockheed Martin Space Operations, Houston, TX, Internal Lecture Notes.

Conley, C.A. and Rummel, J.D., 2008, "Planetary protection for humans in space: Mars and the Moon," *Acta Astronautica*, 63, pp: 1025-1030.

Conley, C.A. and Rummel, J.D., 2010, "Planetary protection for human exploration of Mars," *Acta Astronautica*, 66, pp: 792-797.

Crawford, S.S., Mills, W., and Lusignan, B., 2000, "Analysis of a Passive Thermal Control System for use on a Lightweight Mars EVA Suit," SAE Technical Paper 2000-01-2480.

Demiryont, H., and Moorehead, D., 2009, "Electrochromic Emissivity Modulator for Spacecraft Thermal Management," *Sol. Energy Mater. Sol. Cells*, 93(12), pp. 2075–2078.

Eckart, P., 1996, *Spaceflight Life Support and Biospherics,* Space Technology Library, Vol. 5, Microcosm Press, Torrance, CA, & Kluwer Academic Publishers, Boston.

Ephrath, A.R., 1971, *University Role in Astronaut Life Support Systems: Portable Thermal Control Systems*, NASA CR-1852, National Aeronautics and Space Administration.

Farrington, R., Rugh, J., Bharathan, D., Paul, H., Bue, G., and Trevino, L., 2005, "Using a Sweating Manikin, Controlled by a Human Physiological Model, to Evaluate Liquid Cooling Garments," SAE Technical Paper 2005-01-2971, doi: 10.4271/2005-01-2971.

Fullerton, R.K., 2001, "Advanced EVA Roadmaps and Requirements," SAE Technical Paper 2001-01-2200.

Gaier, J.R., 2005, "The Effects of Lunar Dust on EVA Systems During the Apollo Missions," NASA TM-2005-213610, Glenn Research Center, Cleveland, OH.

Gaier, J.R., Siamidis, J., and Larkin, E.M.G., 2010, "Effect of Simulated Lunar Dust on the Properties of Thermal Control Surfaces," *J. Spacecraft and Rockets*, 47(1), pp: 147-152.

Gernhardt, M. L., Jones, J. A., Scheuring, R. A., Abercromby, A. F., Tuxhorn, J. A., and Norcross, J. R., 2009, "Risk of compromised EVA performance and crew health due to inadequate EVA suit systems," In: *Human Health and Performance Risks of Space Exploration Missions*: evidence reviewed by the NASA Human Research Program. Washington, DC: Government Printing Office, pp: 333-358.

Gilmore, D.G. (ed.), 2002, *Spacecraft Thermal Control Handbook – Volume 1: Fundamental Technologies*, 2nd ed., The Aerospace Press, El Segundo, CA.

Granqvist, C. G., 1995, *Handbook of Inorganic Electrochromic Materials*, Elsevier, Amsterdam, Chap. 1.

Griffin, B. N., Spampinato, P., and Wilde, R. C., 1999, "Extravehicular Activity (EVA) Systems," Human Spaceflight: Mission Analysis and Design, W. J. Larson and L. K. Pranke, eds., McGraw-Hill, New York.

Guibert, A. and Taylor, C.L., 1952, "Radiation Area of the Human Body," *J Appl Physiol.,* 5(1), pp. 24-37.

Hager, P.B., 2013, "Dynamic thermal modeling for moving objects on the Moon," Ph.D. Thesis, Technische Universität München.

Hager, P. B., Klaus, D. M., and Walter, U., 2014, "Characterizing Transient Thermal Interactions Between Lunar Regolith and Surface Spacecraft," *Planetary and Space Science*, 92, pp. 101–116.

Hager, P. B., Walter, U., Massina, C. J., and Klaus, D. M., 2015, "Characterizing a Transient Heat Flux Envelope for Lunar Surface Space Suit Thermal Control Applications," *J. Spacecraft and Rockets*, 52(4), pp. 1193-1202.

Hale, J. S., and Woollam, J. A., 1999, "Prospects for IR Emissivity Control Using Electrochromic Structures," *Thin Solid Films*, 339(1–2), pp. 174–180.

Harris, G.L., 2001, *The Origins and Technology of the Advanced Extravehicular Space Suit*. American Astronautical Society History Series, Vol. 24, Univelt, San Diego, CA.

Havenith, G., 1999, "Heat Balance When Wearing Protective Clothing," *Annals of Occupational Hygiene*, 43(5), pp. 289–296.

Hedgeland, R. J., Hansen, P. A., and Hughes, D. W., 1994, "Integrated Approach for Contamination Control and Verification for the Hubble Space Telescope First Servicing Mission," *Proc. SPIE* 2261, pp. 10–21.

Heiken, G.H., Vaniman, D.T. and French, B.M., 1991, *Lunar Sourcebook: A User's Guide to the Moon,* Cambridge University Press, Lunar and Planetary Institute, Houston, TX.

HIDH, 2010, *Human Integration Design Handbook*, National Aeronautics and Space Administration, Washington, DC, Report No. NASA/SP-2010- 3407, Rev. Baseline.-oe23.

Hill, S.A., Kostyk, C., Motil, B., Notardonato, W., Rickman, S., and Swanson, T., 2012, *Thermal Management Systems Roadmap: Technology Area 14*, National Aeronautics and Space Administration.

Hodgson, E., 2001, *A Chameleon Suit to Liberate Human Exploration of Space Environments*, NASA Institute for Advanced Concepts – Phase I, Contract No. 07600-067.

Hodgson, E., Bender, A., Goldfarb, J., Hansen, H., Quinn, G., Sribnik, F., and Thibaud-Erkey, C., 2004, *A Chameleon Suit to Liberate Exploration of Space Environments*, NASA Institute for Advanced Concepts – Phase II, Contract No. 07600-082.

Hodgson, E., Izenson, M., Chen, W., and Bue, G.C., 2012, "Spacesuit Evaporator-Absorber-Radiator (SEAR)," AIAA 2012-3484.

Howell, John R., "A Catalog of Radiation Heat Transfer Configuration Factors," 3rd Edt. Online Resource, http://www.engr.uky.edu/rtl/Catalog/, Retrieved 28 Jan. 2014.

Hurlbert, K., Bagdigian, B., Carroll, C., Jeevarajan, A., Kliss, M., and Singh, B., 2012, *Human Health, Life Support and Habitation Systems: Technology Area 06*, National Aeronautics and Space Administration.

Incropera, F.P., Dewitt, D.P., Bergman, T.L., and Lavine, A.S., 2007, *Fundamentals of Heat and Mass Transfer*, Sixth Edition, John Wiley & Sons, Hoboken, NJ.

Infrared Thermography, "Emissivity Values for Common Materials," http://www.infrared-thermography.com/material-1.htm, Retrieved 8 Nov. 2015.

Izenson, M.G., Chen, W., and Trevino, L., 2005, "Zero-Venting, Regenerable, Lightweight Heat Rejection for EVA Suits," SAE Technical Paper 2005-01-2974.

Izenson, M.G., Chen, W., Phillips, S., and Bue, G., 2011, "Nonventing Thermal and Humidity Control for EVA Suits," AIAA Paper No. 2011-5260.

Izenson, M.G. et al., 2014, "Performance of a Multifunctional Space Evaporator-Absorber-Radiator (SEAR)," ICES-2014-51.

Jones, H., 2009, "Spacesuit Cooling on the Moon and Mars," SAE Technical Paper 2009-01-2418, doi:10.4271/2009-01-2418.

Kaplan, D. (comp.), 1988, *Environment of Mars*, National Aeronautics and Space Administration, NASA Technical Memorandum 100470.

Kislov, N., Groger, H., and Ponnappan, R., 2003, "All-Solid-State Electrochromic Variable Emittance Coatings for Thermal Management in Space," Space Technology and Applications International Forum, American Institute of Physics, Albuquerque, NM, pp. 172–179.

Klaus, D., Bamsey, M., Schuller, M., Godard, O., Little, F., and Askew, R., 2006, "Defining Space Suit Operational Requirements for Lunar and Mars Missions and Assessing Alternative Architectures," SAE Technical Paper 2006-01-2290.

Kuznetz, L.H., 1990, "Space Suits and Life Support Systems for the Exploration of Mars," AIAA Paper No. 90-3732, AIAA Space Programs and Technologies Conference, Huntsville, AL.

Larson, W.J. and Pranke, L.K. (eds.), 1999, Human Spaceflight Mission Analysis and Design, McGraw-Hill, New York.

Mankins, J.C., 1995, "Technology Readiness Levels: A White Paper," Advanced Concepts Office, Office of Space Access and Technology, National Aeronautics and Space Administration.

Massina, C.J., Klaus, D. M., and Sheth, R. B., 2014, "Evaluation of Heat Transfer Strategies to Incorporate a Full Suit Radiator for Thermal Control in Space Suits," 44th International Conference on Environmental Systems, Tucson, AZ, Paper No. ICES-2014-089.

Massina, C.J., Nabity, J.A., and Klaus, D.M., 2015, "Modeling the Human Thermal Balance in a Space Suit using a Full Surface, Variable Emissivity Radiator," ICES-2015-26.

Massina, C.J. and Klaus, D.M., 2015, "Defining a Discretized Space Suit Surface Radiator with Variable Emissivity Properties," *J. Thermal Science and Engineering Applications*, 7(4), 041014-041014-9.

MATLAB, 2014, Software Package, Ver. R2014b, Mathworks, Natick, MA.

Mays, D.C., Campbell, A.B., Nair, S.S., Miles, J.B., and Thomas, G.A., 2001, "Thermal technologies for space suits," *ASHRAE Journal*, 43(1), 25.

Metts, J.G. and Klaus, D.M., 2009, "Conceptual Analysis of Electrochromic Radiators for Space Suits," SAE Technical Paper 2009-01-2570, doi:10.4271/2009-01-2570.

Metts, J.G., 2010, "Assessing Feasibility of Electrochromic Space Suit Radiators for Reducing Extravehicular Activity Water Consumption," PhD. Thesis, University of Colorado, Boulder.

Metts, J.G. and Klaus, D.M., 2011, "Equivalent System Mass Analysis for Space Suit Thermal Control," AIAA 2011-5180.

Metts, J.G., Nabity, J.A., and Klaus, D.M., 2011, "Theoretical performance analysis of electrochromic radiators for space suit thermal control," *Advances in Space Research*, 47(7), pp: 1256-1264.

Metts, J.G. and Klaus, D.M., 2012, "First-order feasibility analysis of a space suit radiator concept based on estimation of water mass sublimation using Apollo mission data," *Advances in Space Research*, 49(1), pp: 204-212.

Montgomery, L.D., 1974, "A Model of Heat Transfer in Immersed Man," *Annals of Biomedical Engineering*, 2, pp. 19-46.

Mychkovsky, A. and Ponnappan, R., 2005, "Calorimetric Measurement of Emissivity in Space Conditions," AIAA 2005-961, 43rd AIAA Aerospace Sciences Meeting and Exhibit, Reno, NV.

Nabity, J., Mason, G., Copeland, R., Libberton, K., Stephan, R., Trevino, L., and Paul, H., 2007, "Space Suit Radiator Performance in Lunar and Mars Environments," SAE Technical Paper 2007-01-3275.

Nabity, J.A., Mason, G., Copeland, R., and Trevino, L., 2009, " A Freezable Heat Exchanger for Space Suit Radiator Systems," *SAE Int. J. Aerospace*, 1(1), pp: 355-363, doi: 10.4271/2008-01-2111.

Newman, D. & Barratt, M., 1997, "Life Support and Performance Issues for Extravehicular Activity," In: *Fundamental of Space Life Sciences*. Vol. 2. Krieger Pub. Co., Chapter 22, pp: 337 – 364.

NIST, 2011, Isobaric Properties for Carbon dioxide, National Institute of Standards and Technology, Material Measurement Laboratory, URL: http://webbook.nist.gov/cgi/fluid.cgi?P=7&TLow=234.5&THigh=256.4&TInc=.1& Applet=on&Digits=5&ID=C124389&Action=Load&Type=IsoBar&TUnit=K&PU nit=torr&DUnit=kg%2Fm3&HUnit=kJ%2Fkg&WUnit=m%2Fs&VisUnit=Pa*s& STUnit=N%2Fm&RefState=DEF, Retrieved, April 2015.

Nunneley, S., 1970, "Water Cooled Garments: A Review," *Space Life Sciences*, 2, pp: 335-360.

Obama, B., 2010, *National space policy of the United States of America.* Executive Office of the President.

Ochoa, D. A., Mirinda, B., Conger, B., and Trevino, L., 2006, "Lunar EVA Thermal Environment Challenges," SAE Paper No. 2006-01-2231.

Ochoa, D.A., Vogel, M.R., Trevino, L.A. and Stephan, R.A., 2008, "Potential of a New Lunar Surface Radiator Concept for Hot Lunar Thermal Environments," SAE Technical Paper 2008-01-1960, doi:10.4271/2008-01-1960.

Olson, J. et al., 2011, *Voyages: charting the course for sustainable human exploration,* Technical Report NP-2011-06-395-LaRC, National Aeronautics and Space Administration, Langley Research Center.

Pater, I. and Lissauer, J.J., 2010, *Planetary Sciences*, 2nd ed., Cambridge University Press, Cambridge, United Kingdom, pp. 77.

Peck, M. et al., 2012, *NASA Strategic Space Technology Investment Plan*, National Aeronautics and Space Administration, NASA Headquarters.

Pitts, B., Brensinger, C., Saleh, J., Carr, C., Schmidt, P., and Newman, D., 2001, "Astronaut Bio-Suit for Exploration Class Missions," NIAC Phase I Report, http://www.4frontiers.us/dev/assets/BioSuit-NIACPhaseIReport.pdf.

Popiel, C.O., Wojtkowiak, J., and Bober, K., 2007, "Laminar free convective heat transfer from isothermal vertical slender cylinder," *Experimental Thermal and Fluid Science*, 32, pp. 607-613.

Pu, Z., Kapat, J., Chow, L., Recio, J., Rini, D., and Trevino, L., 2004, "Personal Cooling for Extra-Vehicular Activities on Mars," AIAA Paper No. 2004-5970.

Race, M. S., Criswell, M. E., and Rummel, J. D., 2003, "Planetary Protection Issues in the Human Exploration of Mars," SAE Paper No. 2003-01-2523.

Richardson, D.L., 1965, "Study and Development of Materials and Techniques for passive Thermal Control of Flexible Extravehicular Space Garments," Aerospace Medical Research Laboratories, Air Force Systems Command, AMRL-TL-65-156.

Siegel, R., and Howell, J., 2002, *Thermal Radiation Heat Transfer*, 4th ed., Taylor & Francis, New York.

Sompayrac, R., Conger, B., and Trevino, L., 2009, "Lunar Portable Life Support System Heat Rejection Study," SAE Technical Paper 2009-01-2408, doi:10.4271/2009-01-2408.

Stolwijk, J.A.J., and Hardy, J.D., 1966, "Temperature Regulation in Man – A Theoretical Study," *Pflügers Archive,* 291, pp. 129-162.

Sunada, E., Birur, G.C., Ganapathi, G.B., Miller, J., Berisford, D., and Stephan, R., 2010, "Design and Testing of an Active Heat Rejection Radiator with Digital Turn-Down Capability," AIAA-2010-6159.

Taylor, J.R., 1997, *An Introduction to Error Analysis The Study of Uncertainties in Physical Measurements*, University Science Books, Sausalito, CA, pp. 75.

Tepper, E., Trevino, L., and Anderson, J., 1991, "Results of Shuttle EMU Thermal Vacuum Tests Incorporating an Infrared Imaging Camera Data Acquisition System," SAE Technical Paper 911388, doi:10.4271/911388.

Trevino, L., Copeland, R.J., Elliott, J.E., and Weislogel, M., 2004, "Freeze Tolerant Radiator for Advanced EMU," SAE Technical Paper 2004-01-2263.

Trevino, L.A. and Lafuse, S.A., 2008, "Minimizing EVA Airlock Time and Depress Gas Losses," SAE Technical Paper 2008-01-2030.

Vasavada, A.R. et al., 2012, "Assessment of Environments for Mars Science Laboratory Entry, Descent, and Surface Operations," *Space Science Reviews*, Vol. 179, Iss. 1-4, pp. 793-835, doi: 10.1007/s11214-012-9911-3.

Waligora, J.M. and Horrigan D.J., 1975b, "Metabolism and Heat Dissipation During Apollo EVA Periods," In: *Biomedical Results of Apollo,* NASA SP-368. Sect. 2, Ch. 4, Pp. 115-128.

Waligora, J.M. and Sedej, M.M., 1987, "Physiological and Technological Considerations for Mars Mission Extravehicular Activity," NASA N87-17798, Johnson Space Center.

Wertz, J.R., Everett, D.F., and Puschell, J.J., 2011, *Space Mission Engineering: The New SMAD*, Space Technology Library, Microcosm Press, Hawthorne, CA, pp: 691.

Wilde, R.C., Abramov, I.P., and McBarron, J.W., 1993, "Extravehicular Individual Life Support: A Comparison of American and Russian Systems," SAE Technical Paper 932223.

Wilde, R., Hodgson, E., and Mumford, R., 2004, "What does it take to Work on Mars? A New Direction in Spacesuit Systems," AIAA Paper No. 2004-5967.

Williams, J.L., Copeland, R.J. and Webbon, B.W., 1972, "Regenerable Thermal Control and Carbon Dioxide Control Techniques for use in Advanced Extravehicular Protective Systems," Proceedings of the Second Conference on Portable Life Support Systems, NASA SP-302, N72-27114, pp: 139-157.

Young, A., 2009, *Spacesuits – The Smithsonian National Air and Space Museum Collection,* powerhouse Books, Brooklyn, NY.

APPENDICES

APPENDIX A: SUMMARY OF PUBLICATIONS AND PRESENTATIONS

2013

Massina, C.J. and Klaus, D.M. (2013). "Considerations for Incorporating Variable Emissivity Radiators into a Space Suit Heat Rejection System," AIAA 43rd International Conference on Environmental Systems, Vail, CO, July 2013, (poster).

2014

Massina, C.J., Klaus, D.M., and Sheth R.B. (2014). "Evaluation of Heat Transfer Strategies to Incorporate a Full Suit Flexible Radiator for Thermal Control in Space Suits," ICES-2014-89, uri: http://hdl.handle.net/2346/59691.

Massina, C.J. (2014), "Evaluation of Heat Transfer Strategies to Incorporate a Full Suit Flexible Radiator for Thermal Control in Space Suits," 44th International Conference on Environmental Systems, Tucson, AZ, July 2014, (presentation).

Massina, C.J. (2014), "Characterization of Dynamic Thermal Control Schemes and Heat Transfer Pathways for Incorporating Variable Emissivity Electrochromic Materials into a Space Suit Heat Rejection System," 1st Annual Aerospace Researchpalooza. University of Colorado, Boulder, CO, 29 August 2014, (presentation).

2015

Massina, C.J. (2015), "Evaluating Thermal Control Technologies and Techniques for Reducing Consumable Losses in Space Suit Heat Rejection Systems," National Renewable Energy Laboratory, Golden, CO, 14 January, (presentation).

Hager, P.B., Walter, U., Massina, C.J., and Klaus, D.M. (2015), "Characterizing a transient heat flux envelope for lunar surface space suit thermal control applications," *J. Spacecraft and Rockets*, 52(4), pp: 1193-1202, doi: 10.2514/1.A33182.

Massina, C.J., Nabity, J.A., and Klaus, D.M. (2015), "Modeling the Human Thermal Balance in a Space Suit using a Full Surface, Variable Emissivity Radiator," ICES-2015-26.

Massina, C.J. (2015), "Modeling the Human Thermal Balance in a Space Suit using a Full Surface, Variable Emissivity Radiator," 45th International Conference on Environmental Systems, Belleview, WA, July 2015, (presentation).

Massina, C.J., Nabity, J.A., and Klaus, D.M. (2015), "Utilization of Variable Emissivity Electrochromic Devices for Space Suit Thermal Control," *NASA Thermal and Fluids Analysis Workshop (TFAWS),* TFAWS15-AT-06, Silver Spring, MD, August 2015.

Massina, C.J. (2015), "Utilization of Variable Emissivity Electrochromic Devices for Space Suit Thermal Control," NASA Thermal and Fluids Analysis Workshop, Silver Spring, MD, August, 2015, (presentation).

Massina, C.J. and Klaus, D.M. (2015). "Defining a Discretized Space Suit Surface Radiator with Variable Emissivity Properties." *J. Thermal Science and Engineering Applications,* 7(4), 041014-041014-9, doi:10.1115/1.4031132.

Under Review/In Prep

Massina, C.J. and Klaus, D.M. (20YY), "Prospects for Implementing Variable Emittance Thermal Control of Space Suits on the Martian Surface," [Under Review]

Massina, C.J., Nabity, J.A., and Klaus, D.M. (20YY), "Evaluation of Radiators with Discretized Emittance Properties.," [Working Title – In Prep]

 "Life Support Mass Reduction Strategies for Martian Surface EVA – Thermal Control System," [Working Title – In Prep].

 "Interaction of Variable Emissivity Space Suit Radiators with Dynamic Environments," [Working Title – In Prep]

APPENDIX B: GENERAL EVENTS SCHEDULE

Activity or Milestone	Estimated Date
Research	
Complete first order thermal model and preliminary assessment of control properties	Dec. 2012 (Completed)
Determine first-order interaction of variable emissivity electrochromics with lunar and asteroid environments	June 2013 (Completed)
Develop first iteration of LabView DAQ architecture and perform thermal vacuum testing- JSC	Aug. – Oct. 2013 (Completed)
Define space suit radiator surface temperature bounds on performance for lunar environments	Jan. 2014 (Completed)
Complete background literature investigation and compile comprehensive exam materials	April 2014 (Completed)
TherMoS paper writing for assessing flux dynamics on the lunar surface	March – May 2014 (Completed)
Perform pixel sizing analysis for first journal article	May – Oct. 2014 (Completed)
Development of Laboratory investigations of thermal control and atmosphere revitalization systems (course work relevant to thesis)	Aug. – Dec. 2014 (Completed)
1st **Journal Article Submission** – Pixel area considerations (printed)	21 Feb. 2015 (Completed)
Complete transient human simulations for ICES 2015 paper and presentation	Dec. 2014 – March 2015 (Completed)
Investigations of prospects for full suit, electrochromic radiator architecture use for Martian surface EVA	Feb. – May 2015 (Completed)
Mixed emissivity test article definition	May – June 2015 (Completed)
Summer 2015 work (ICES conference, TFAWS conference, and NREL – human thermal comfort tools [ongoing])	May – Aug. 2015 (Completed)
2nd **Journal Article Submission** – Martian environment extension (in review)	22 Sept. 2015 (Completed)
Mixed emissivity test article construction	Sept. – Oct. 2015 (Completed)
Mixed emissivity thermal vacuum testing	Oct. – Nov. 2015 (Completed)

		Start Date	End Date
Written dissertation completed		Dec. 2015 (completed)	
3rd Journal Article Submission – Mixed Emissivity Test results		Feb. – April 2016	
Additional publication of applicable extensions is TBD but includes human transient evaluations and Mars thermal control schemes		Jan. – June 2016	
Academic / Degree			
Ph.D. Preliminary Exam (Qualifying Exam) - Passed		Sept. 2012	
Ph.D. Comprehensive Exam		May 2014	
Ph.D. Thesis Defense		Jan. 2016	
Graduation		May 2016	
On-Site Experience (Visiting Technologist) – NASA Center or R&D Lab		*Start Date*	*End Date*
JSC – Phase Change Material work (non-thesis thermal control technology)		3/25/2013	4/26/2013
JSC – Variable emissivity radiator environment interaction		6/3/2013	6/28/2013
JSC – Electrochromic Thermal Vacuum		8/19/2013	9/12/2013
JSC – Thesis work & PCM Demo assistance		6/8/2014	7/2/2014
National Renewable Energy Laboratory (NREL) – Human Thermal Comfort Tools Assessment (Part-Time)		5/18/2015	10/16/2015
Conference	*Location*	*Start Date*	*End Date*
43rd International Conference on Environmental Systems	Vail, CO	7/14/2013	7/18/2013
44th International Conference on Environmental Systems	Tucson, AZ	7/13/2014	7/17/2014
45th International Conference on Environmental Systems	Bellevue, WA	7/12/2015	7/16/2015
NASA Thermal & Fluids Analysis Workshop	Silver Spring, MD	8/3/2015	8/7/2015

APPENDIX C: CORE TEMPERATURE RANGE LIMITS AND ASSOCIATED PERFORMANCE DECREMENTS

From HIDH, 2010

Core Temperature °C (°F)	Equivalent Heat Storage kilojoules (BTU)	Medical Condition
37.7–38.2 (99.9–100.8)	317–422 (300–400)	Onset of decrement in performance of cognitive tasks Decreasing manual dexterity Discomfort Hyperthermia (or heat stress)
38.2–39.2 (100.8–102.6)	422–633 (400–600)	Slowed cognitive function Increased errors in judgment Loss of tracking skills 25% risk of heat casualties Possible heat exhaustion
39.2–39.6 (102.6–103.3)	633–844 (600–800)	Functional limit of physical tasks 50% risk of heat casualties Probable heat exhaustion Possible heat stroke
>40 (>104)	>844 (>800)	100% risk of heat casualties Probable heat stroke

APPENDIX D: MARTIAN SEASONS AND SOLAR LONGITUDE

The following is an excerpt from the following website and pertains to definition of the Martian solar longitude; used to define seasonal variations in surface thermal characteristics. Season designations are reversed for sites in the southern hemisphere. For instance, Ls = 0 is the fall equinox for sites below the Martian equator; such as Gale Crater and MSL's landing site.

http://www-mars.lmd.jussieu.fr/mars/time/solar_longitude.html

> *The solar longitude Ls is the Mars-Sun angle, measured from the Northern Hemisphere spring equinox where Ls=0. Ls=90 thus corresponds to summer solstice, just as Ls=180 marks the autumn equinox and Ls=270 the winter solstice (all relative to the northern hemisphere).*